GEORGIA INSTITUTE OF TECHNOLOGY
Engineering Experiment Station

PROJECT TERMINATION

Date 8/25/71

PROJECT TITLE: Aids to Navigation Radar Requirements

PROJECT NO: A-1277

PROJECT DIRECTOR: Mr. W. K. Rivers

SPONSOR: U. S. Coast Guard

TERMINATION EFFECTIVE: 8/2/71*

CHARGES SHOULD CLEAR ACCOUNTING BY: 8/31/71

*Final Report due date - submitted 8/25/71.

Contract Closeout Items Remaining:

Final Invoice w/Closing Documents
Final Report of Inventions
Government Property Inventory and
Certificate.

Electronics (Sensor Systems) Division

COPIES TO:

Project Director
Director
Associate Director
Assistant Directors
Division Chief
Branch Head
Accounting
Engineering Design Services

General Office Services
Photographic Laboratory
Purchasing
Report Section
Library
Security
Rich Electronic Computer Center

EES 402 (R10—62)

GEORGIA INSTITUTE OF TECHNOLOGY
Engineering Experiment Station

PROJECT INITIATION

Date: __9/1/70__

Project Title: **Aids to Navigation Radar Requirements**

Project No.: **A-1277**

Project Director: **Mr. W. K. Rivers**

Sponsor: **U. S. Coast Guard**

Effective **August 1, 1970**　　Estimated to run until: **December 1, 1970**

Type Agreement: **Contract No. DOT-CG-10657-A**　　Amount: $7,283.00

Reports Required:　Interim Letter Report
Final Technical Report

Sponsor Contact Person:　LCDR Lawrence Graham
Commandant (FSP-2)
U.S.C.G. Headquarters
400 Seventh Street, S. W.
Washington, D. C. 20591

Assigned to **Electronics (Sensor Systems)** Division

COPIES TO:

- ☐ Project Director
- ☐ Director
- ☐ Associate Director
- ☐ Assistant Director(s)
- ☐ Division Chiefs
- ☐ Branch Head
- ☐ General Office Services
- ☐ Engineering Design Services

- ☐ Photographic Laboratory
- ☐ Research Security Officer
- ☐ Accounting
- ☐ Purchasing
- ☐ Report Section
- ☑ Library
- ☐ Rich Electronic Computer Center
- ☐ _____

RA-62(12-66)

AIDS-TO-NAVIGATION RADAR REQUIREMENTS

by

Wayne Rivers

31 January 1971

Technical Report No. 1

on

Georgia Tech Project A-1277

Prepared For
United States Coast Guard
Washington, D. C. 20591
Contract DOT-CG-10657-A

Engineering Experiment Station
GEORGIA INSTITUTE OF TECHNOLOGY
Atlanta, Georgia

GEORGIA INSTITUTE OF TECHNOLOGY
Atlanta, Georgia 30332

AIDS-TO-NAVIGATION RADAR REQUIREMENTS

by

Wayne Rivers

31 January 1971

Technical Report No. 1

on

Georgia Tech Project A-1277

AIDS-TO-NAVIGATION RADAR REQUIREMENTS

by

Wayne Rivers

Abstract

The specifications of a stereotype maritime radar are assembled from a concensus of currently deployed radars for use with models of radar performance to define desired radar properties of a new series of navigation buoys. Model elements considered include detection thresholds in noise and clutter backgrounds, diffraction and duct propagation modes near the sea surface, and shadowing by sea waves. Recommended buoy cross sections and estimates of detection ranges and probability of detection are given.

TABLE OF CONTENTS

LIST OF FIGURES

LIST OF TABLES

I INTRODUCTION

A. Background

The U.S. Coast Guard is considering a new family of navigation buoys in which advanced materials technologies will be used. The purpose of this study is to provide data concerning the requirements on buoys in maritime radar navigation for use in the buoy design. The classes of buoys and their design-goal parameters are listed in Table 1.

Table 1. Radar Navigation Buoys

	Class	Reflector Height	Min. Range Visible	Max. Sea State
1.	Exposed	8 Feet	5.5 nmi	5*
2.	Semiexposed	6	4.5	3
3.	Sheltered	3	3.0	2
4.	River	2	1.0	1
5.	Emergency	1.8	1.0	3

*Max. sea state for small craft. Larger ships expect to use Class 1 up to Sea State 6.

For purposes of this study, parameters of a stereotype radar were specified, which represent the characteristics of the more common basic maritime radars. The detailed specifications of this radar and the baseline data from which they were chosen are given in Section C of this chapter. The radar is anticipated to be used either on small craft with a typical antenna mounting height of 10 feet or on a larger ship at a height of 65 feet. It is required of the buoy that it have sufficient radar cross section for the return to be detectable by the stereotype (typical) radar at the design range, and that the reflector be visible in the design sea state. Therefore, information leading to selection of buoy cross sections and reflector heights to assure that the navigation goals are achieved is a primary output of this study.

B. Organization of Report

The questions of visibility of the buoy reflector from the radar as limited by sea-wave shadowing or by inadequate signal-to-noise ratio (range too great or power too low or cross section too small) are considered independently in this report. The effects of shadowing by wave crests are studied in Chapter II, energy spreading and other propagation losses in Chapter IV, and the results are combined and interpreted in Chapter V. The important results are summarized in the last section of this chapter. Recommendations are included with the summary.

C. Definition of a Stereotype Radar

Specifications of a number of currently available marine radars were assembled to serve as a basis for defining a stereotype to be used in the analytic models; these specifications are listed in Table 2. Those tabulated entries which are shown in parentheses were not available explicitly in the source literature but were inferred from other information or assumed for purposes of calculation. Thus, only those entries which are not parenthesized are validated by source traceability. In addition many optional variations have been ignored in preparing this table. Because all of the options improve radar performance, the stereotype derived from the tabulated data represents a minimum performance, lowest cost, basic radar. Where entries have been left out, the specification was not given and no value was assumed, because it was believed not necessary or hazardous for derivation of the stereotype.

Almost all the radars conform to a formula employing X-band pulsed transmitters, fan-beam antennas, multiple pulse lengths and display ranges, and (apparently) single-crystal-mixer receivers. However, the various combinations of specifications of these elements as well as transmitter power result in substantial variation in performance. The difference between the best and worst is a factor of five in the ranges at which a target of given cross section can be detected (based on free-space propagation losses), which corresponds to an equivalent difference in effective power of about 28 dB. The distribution of performance factors, which are tabulated in the column

2

Table 2. Marine Radar Specifications

Mfg.	Model	Freq GHz	Ant Gain dB	Az bw Deg	El bw Deg	Pol	Scan Rate r.p.m.	p.r.f. Hz	Peak Power kW	Pulse Length μs	N.F. dB	IF band MHz	Displ dia inch	Displ range nmi	Phosphor	Video Det	An Input W	R'_o dBnmi
U.S. Coast Guard	SPS-57	9.4	(26.0)	1.9	25-30	HH	25	2k/1kHz	3	0.1/0.5	12.5	(10/2)	7	.5,1,2,4,8, 16 nmi	P19A	Lin & Log	450	1.1/2.8
Sperry (3)	SPS-53	9.4	(27.2)	1.6	20		15	1.5k/750	35	0.1/0.5	11	12/4		0.5 - 32	P7A		600	4.9/6.1
Kelvin Hughes (1)	17R	9.45	27	1.2	25	HH	24	2.2k/1.1k	3	.05/.2/.5	13	30 MHz	4 or 9	.3,.6,.9,1.2, 1.5,2.5,5,10		Lin	350	0.7
Kelvin Hughes(1)	14/9R2us	9.4	27 or 30	1.2 or 0.7	25	HH	24	1.1kHz	60	.05/.3	(12)	20 MHz	9	.25,5,1,1.5, 3,6,12,24,48		Lin	1000	4.6
Kelvin Hughes(1)	19/9 or 12	9.45	31 or 32	1.0 or 0.75	18	HH	24	3.2/1.6/0.8k	25	.05/.25/.75	11	25/15/5MHz	12	.25,.5,.75, 1.5,3,6,12, 24,48		Lin		5.7/6.4/7.4
Decca (3)	D-202	9.4	(25.2)	1.9	27		24	1k	3	0.1/0.5	12.5	(10/2)	7.5	0.5 - 24			450	1.1/2.8
Decca (3)	D-101	(9.4)	(25.2)	1.9	27		24	3k	3	.08/.25	(12)	(12.5/4)	7	0.5,1.5,5,15			200	1.1/2.4
Decca (2)	RM316	9.4		1.2				2k/1k	10	.05/.15/.5			9	0.5,.75,1.5,3 6,12,24,48				
Decca (2)	RM326	9.4		1.2				2k/1k/500	25	.05/.15/.5/1.2			9	do				
Decca (2)	TMS2400	3.4		2.0				1k	75	.1/.5			16.5	.75,1.5,3,6, 12,24,60				
Raytheon (3)	1500	(9.4)	(26.6)	2.2	17		20	1.5k/750	7	0.2	(12)	(5)	10	0.5,1,2,4,8,16			600	3.6
Raytheon (2)	1640	9.4		.6				4k/1k	40	.05/.5			16.5	.5,1,2,4,8, 20,50				

NOTES: (1) Source; Manufacturer's Specifications
(2) Reference 1
(3) Reference 2

3

Table 2. Marine Radar Specifications (Continued)

Mfg.	Model	Freq GHz	Ant Gain dB	Az bw Deg	El bw Deg	Pol	Scan Rate r.p.m.	p.r.f. Hz	Peak Power kW	Pulse Length μs	N.F. dB	IF band MHz	Displ dia inch	Displ range nmi	Phosphor	Video Det	An Input W	R'_o dBnmi
Raytheon (2)	1650A	3.4		1.9				4k/1k	60	.05/.5			16.5	do				
Raytheon (3)	1900	(9.4)	(23.2)	3.0	27		20	2k	35	0.14	(12)	(7)	7	0.5,2,6,12			350	0.7
Raytheon (3)	2502	9.4	(26.6)	1.6	23		80	6k/2k/1k	20	.05/.5/1	12	8	10	0.5 - 48,24, 1.5,3,6,12	P19A		350	4.2
Bendix (3)	MR4	9.4	(23.4)	2.6	30		21	1.2 kHz	5	0.25	(12)	8	7	0.5 - 16	P14A		500	1.1
Bendix (3)	MR5	9.4	(23.4)	2.6	30		21	1.6k/625	7.5	.1/.4	(12)	(10/2.5)	7	0.5,2,4,8,16			450	1.2/2.8
RCA (3)	N3B3	9.4	(24.2)	3.2	20		25	2.3/1.1k	3	0.1/0.25	(12)	8		0.5 - 18	P7A			1.0
RCA (3)	N6A-10	(9.4)	(25.8)	1.8	25		20	800	1	.1/.6	(12)	10	7	0.5,1.5,4,12, 32			225	0.3
Phillips (3)	8GR260/00	9.4	(32.2)	0.6	17		40	2.5k	20	0.04	(12)	40		.3 - 2.5			500	5.3
Canadian Marconi(3)	LN-55	9.4	(24.7)	2.6	22		22	1.5 k	6	0.2	12	5	10		P7A		200	2.5
USSR (2)	Lotsiya	9.4		1.5				1.6k/800	6	0.1/0.3			5	0.5,1,2,4,8,16				
USSR (2)	Okean	9.4/3.4		0.75/2.3				2.55k/850	80	0.1/1.0			18	1,2,4,8,16,32, 64				
Japan Radio (2)	JMA123	9.4		1.8				800	8	0.1/0.6			7	1,3,8,15,30				
Japan Radio (2)	JMA131	9.4		1.0				2.5k/500	40	0.1/0.8			12	0.5,1,2,4,8,20, 60		Lin & Log		
Stereotype		(9.4)	(25)	(1.5)		(HH)	(20)	(1k)	(3)	(0.1)	(12)	(10) MHz	(7)	(2,8)	(P7A)	(Lin)		(1.1)

labeled R_o'(dBnmi), is shown in Figure 1. This performance factor is the range (expressed in dB with respect to 1 nmi) at which a 1-m^2 target will be detected, assuming free-space propagation. This factor was calculated from:

$$R_o' = 2.5 \log \left\{ \frac{P_T \ G^2 \ \lambda^2 \ 10.76}{kT \ F_n \ (4\pi)^3 B \ V \ L} \right\} -37.8 \text{ dB}, \tag{1}$$

where P_T, G, λ, FN, and B were obtained from the appropriate table entry, and values of 3 and 6 dB were used uniformly for the loss L and the visibility V, respectively. The factor of 37.8 dB converts the reference units from feet to nautical miles. Factors for both the shorter and longer range scales have been tabulated where receiver bandwidth changes are specified to occur with change in pulse length. Most of the lower performance radars are close to the value R_o' = +1 dB nmi, and this is the performance chosen for the stereotype.

A complete list of the stereotype parameters chosen is given in Table 3. It should be noted that by assembling this model no approval or endorsement is given to the resulting formula, but it appears that this stereotype represents the consensus of basic radars built in the not-too-remote past for small craft.

D. Summary

Two types of maritime microwave propagation modes are identified, surface-layer trapping and diffraction, which prevail about 70 and 30 percent of the time, respectively, near the sea surface at X-band. Propagation losses associated with these two modes are used with the specifications of a stereotype radar to calculate buoy reflector signal returns. Minimum detectable signal-to-noise and signal-to-clutter ratios are calculated and used with noise and clutter levels to derive noise and clutter background thresholds that signals must exceed for satisfactory detection. The comparison of signal levels with thresholds at design ranges yields the necessary buoy cross sections. Consideration of the effect of surface roughness on the statistical variation of diffraction losses and on shadowing qualifies the meaning of detection by assigning a probability level not easily exceeded by increasing cross section alone.
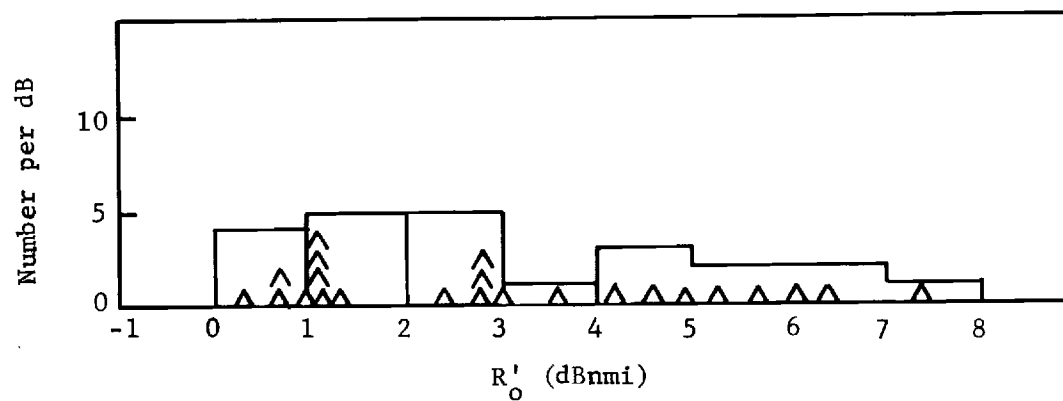
Figure 1. Distribution of performance index. Ordinate is number of radars per dB interval of performance index. R_o'(dBnmi) is the range for detecting a $1-m^2$ target expressed in dB with respect to 1 nmi.

Table 3 Specifications of Stereotype Radar

Frequency	9.4 GHz
Antenna height	10 feet
Antenna gain	25 dB
Scan rate	20 rpm
Azimuth beamwidth	1.5 degree
Elevation beamwidth	22 degree
Polarization	HH
Pulse repetition frequency	1 kHz
Peak transmitted power	3 kW
Pulse length	100 ns
Dissipative loss	3 dB
Receiver noise figure	12 dB
IF bandwidth	10 MHz
Envelope detector	Linear
Display	7"-dia. PPI
Displayed ranges	2, 4, 8 nmi
Phosphor	P7
Spot size	0.02 inch
Focus type	Magnetic

It is concluded that reflectors of reasonable size can enable detection at the design ranges and heights under favorable propagation conditions (trapping), but that no reasonably sized reflector would allow detection at design ranges under unfavorable (diffraction) conditions. With reflector sizes adequate for favorable conditions, the range reduction under unfavorable conditions is about a factor of two. The range at which median propagation losses apply to give signals equal to threshold defines the maximum range for detection, and of course at that range the probability of detection is 0.5 at best. One buoy, the Class 5 unit, is so short as to further limit the probability of its being visible to only 0.3.

Because of the smaller expectation of unfavorable propagation conditions with primary penalty of reduced range by about a factor of two, it is recommended that cross sections of buoy reflectors be set at levels adequate for favorable conditions, +25 dBsm for Classes 1 and 2, +21 dBsm for Class 3 and +10 dBsm for Classes 4 and 5. Because the visibility of the Class-5 buoy in its design sea state could be improved substantially be increasing its reflector height, it is recommended that the possibility of increase to a minimum of 3 feet above the water line be considered.

II. SHADOWING BY SEA WAVES

A. Diffraction by an Obstacle

The concept of shadowing must be treated with caution when applied in the microwave region, because effects can be appreciably different from the geometric model intuitively applied as a useful approximation at optical wavelengths. One outstanding characteristic of shadows behind obstacles is that the edges are "soft" as opposed to abrupt in the geometric limit. The "softness" increases at longer wavelengths and when the obstacle (sea-wave crest) is at greater distances from the microwave terminal (antenna or buoy reflector).

It is reasonable to consider the concept of shadowing as applicable only if one obstacle protrudes high above all others nearby or if it is relatively close to the field point. This is because a large number of wave crests at a distance from the field point have diffraction effects which combine to form a composite diffraction field of a curved average earth surface. At radar ranges less than the effective horizon distance, this composite diffraction field is approximately described by the interference field reviewed in Section III-A.

The effect of individual wave crests near the terminal is considered here in a deterministic sense, and in the next two sections from a statistical point of view. Consider an obstacle a distance d_2 from the terminal, where $d_2 \ll R$, the radar range, and assume that the obstacle is prominent with respect to its neighbors; an example is a high crest close to the terminal. When the crest height is near the geometric line of sight between terminals, a loss is introduced which is described in Figure 2 in terms of a normalized height difference v, defined by

$$v = \delta h \left\{ \frac{2}{\lambda d_2} \right\}^{1/2} , \qquad (2)$$

where δh is the distance the obstacle lies below the line of sight. One important feature is that when $\delta h = v = 0$, there is 12 dB diffraction loss. One v-unit (equivalent to $h = 1.9$ feet for $d_2 = 67$ feet, which would be typical for Sea State 5) each side of $v = 0$ can decrease this loss to zero or raise it to about 30 dB. Compared to a

9

sea-surface roughness for Sea State 5, which implies a standard deviation of over 2.5 feet, this transition from illuminated to shadowed condition is fairly well defined and one might designate the boundary of the shadow as occurring for the line of sight about one foot above a wave crest.

B. Geometric Shadowing Probabilities

In this section there is calculated the probability that the line of sight between antenna and buoy is clear. The results of this calculation are applicable to the visual case but not to microwave propagation, and are only of interest to explore the relative effects of various factors.

The geometry considered in this calculation of shadowing probabilities is shown in Figure 3. The radar antenna is represented at Point A and the buoy reflector at B. The curved line represents the effective mean water surface, having a radius of a_e. Points A and B are separated by range R and lie at instantaneous heights h_a and h_b above this mean surface. A line tangent to the mean surface exists which is offset from the line of sight by h_r. At a point which is at a distance from the antenna the line of sight is at a height h_z above the mean surface.

The rough sea surface is represented by a Gaussian-distributed random function. Cartwright [3] gives the cumulative distribution of the normalized height $z = h_z/\sigma_z$ of maxima (crests in terms of the height z and a bandwidth parameter, ε). The cumulative probability that a given wave crest will be higher than z is

$$q_1(z) = (1/2) \left\{ 1 - \mathrm{erf}\left(\frac{\sqrt{2}z}{\varepsilon}\right) + (1-\varepsilon^2)^{1/2} \exp\left(-\frac{z^2}{2}\right) \left[1 + \mathrm{erf}\left\{\frac{\sqrt{2}z}{\varepsilon}(1-\varepsilon^2)^{1/2}\right\}\right] \right\}. \quad (3)$$

The probability that a given wave crest will be lower than z is $1-q_1(z)$. It is assumed here that adjacent wave crests are independent; under this assumption, the probability that N wave crests are jointly below their individual heights z_i is
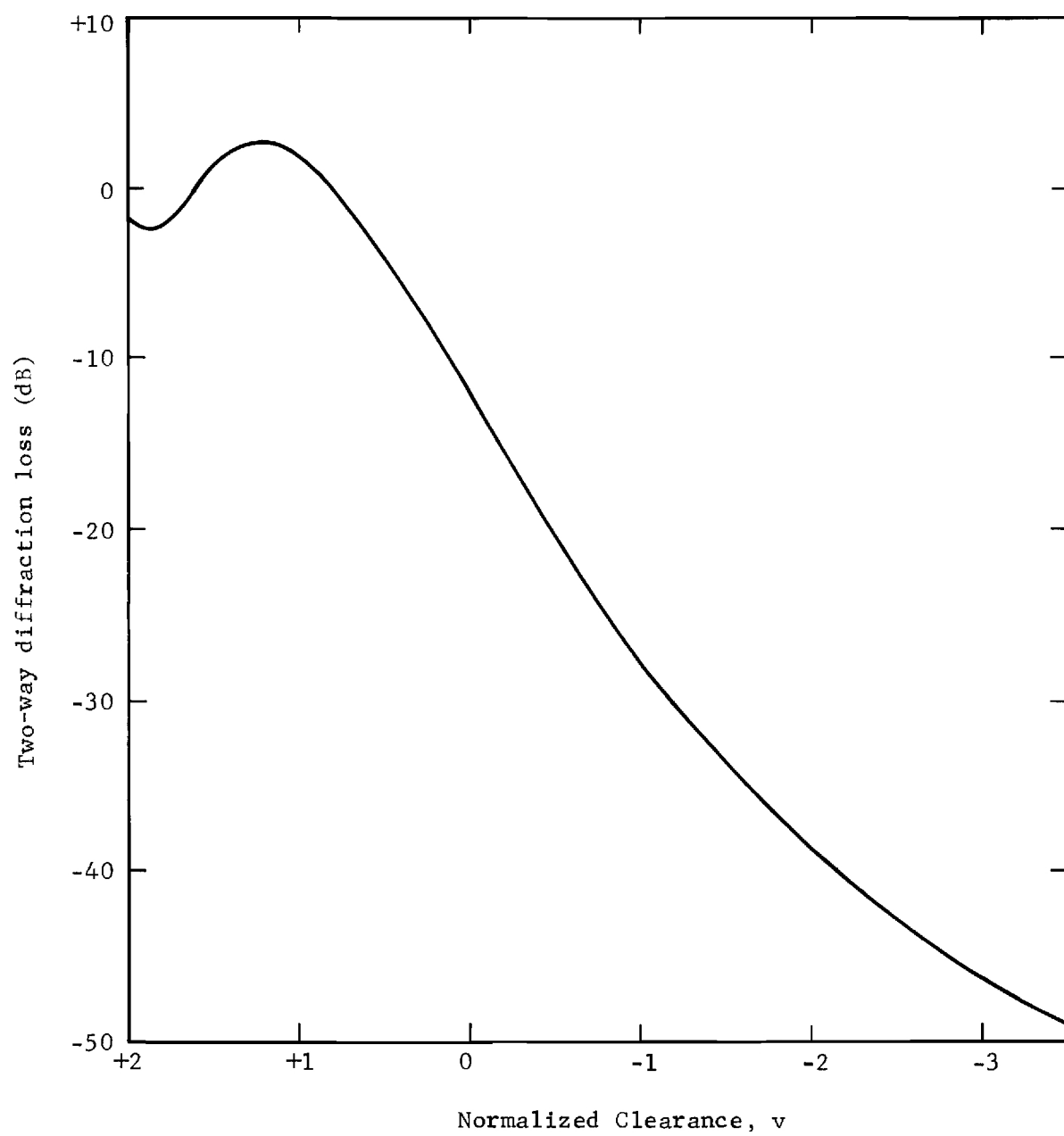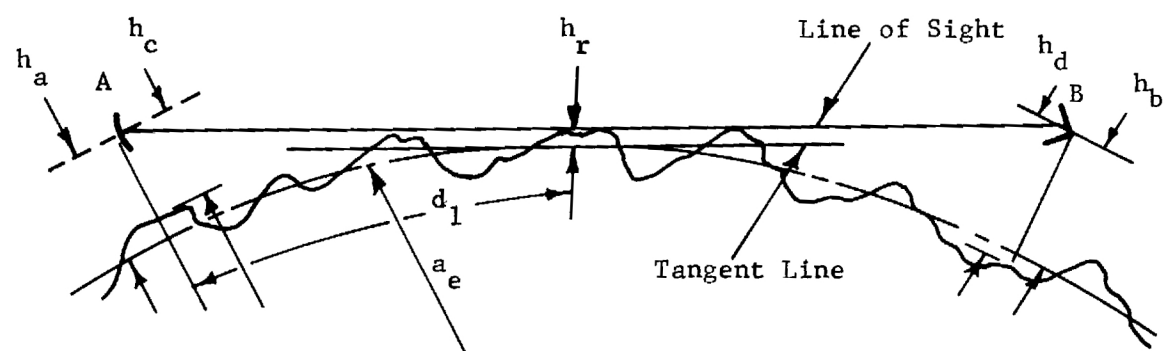
Figure 2. Two-way knife-edge diffraction loss.

Figure 3. Geometric shadowing profile

$$P_U = \prod_{i=1}^{N} \{1-q_1(z_i)\}. \tag{4}$$

Thus, P_U is the probability that the line of sight from A to B is clear (unobstructed). Using the definitions of the ln and exp functions, Equation 4 can be written:

$$P_U = \exp\left\{\sum_{i=1}^{N} \ln\{1-q_1(z_i)\}\right\}. \tag{5}$$

The summation can be approximated by an integral in which the unit dN is replaced by $dN=dX/\overline{\lambda}$, where $\overline{\lambda}$ is the average wavelength of the sea surface structure. This integral form is

$$P_U \simeq \exp\left\{\int_0^R \ln\{1-q[z(x)]\}\frac{dx}{\overline{\lambda}}\right\}. \tag{6}$$

Because both the boat and the buoy are heaving up and down with the sea, h_a and h_b are Gaussian random functions, which implies that P_U is conditional upon the instantaneous values of h_a and h_b. The conditional nature is removed by averaging over h_a and h_b,

$$P_C = \frac{1}{2\pi\sigma_z^2} \int_{\infty}^{\infty} \int_{\infty}^{\infty} P_U \exp\left\{-\frac{(h_a-h_c)^2}{2\sigma_z^2} - \frac{(h_b-h_d)^2}{2\sigma_z^2}\right\} dh_a dh_b, \tag{7}$$

where h_c and h_d are the respective heights of the antenna and reflector above the local instantaneous water line.

The above-described computations were implemented with the algorithm described in Tables 4, 5 and 6. Table 4 lists the variables, their definitions and computer program symbol. Table 5 lists the mathematical form of the algorithm used, and Table 6 lists the computer program. The program is written in the language FOCAL used on small machines made by the Digital Equipment Corporation [4].

Probabilities of clear line of sight were calculated for the principal combinations of variables derived from Table 1 and listed here in Table 7.

13

Table 4 Variables for Shadowing Calculation

Variable	Units	Definition	Focal Symbol
h_c	Feet	Antenna height above water line	HC
h_d	Feet	Buoy reflector height above water line	HD
h_a	Feet	Instantaneous antenna height above mean water level	HA
h_b	Feet	Instantaneous reflector height above mean water level	HB
R	nmi	Range	RA
σ_z	Feet	Standard deviation of sea surface	SZ
$\overline{\lambda}$	Feet	Average sea wave length	LA
ε	----	Bandwidth parameter	EP
a_e	Feet	Effective earth radius	AE
ε_f	----	Derived bandwidth factor	EF
d_1	Feet	Distance from A to tangent pf.	D1
h_r	Feet	Offset between loss and tangent line	HR
z	----	Normalized height of line of sight (LOS)	ZA
X	Feet	Distance from A to calculation point	XI
q_1	----	Probability crest is above z	Q1
P_U	----	Probability LOS (h_a, h_b) is unobstructed	PU
P_C	----	Probability LOS_{av} is unobstructed	PC

14

Table 5 Computation of Geometric Shadowing Probabilities

1. Input h_c, h_d, R, σ_z, $\overline{\lambda}$.

2. Set values for ε, a_e. Calculate $\varepsilon_f = (1 - \varepsilon^2)^{1/2}$.

3. Calculate $d_1 = R_f = 6076$ R; $d_1 = \dfrac{R_f}{2} + \dfrac{a_e(h_a - h_b)}{R_f}$

$$h_r = \frac{h_a - h_b}{2} - \frac{R_f^2}{8a_e} - \frac{a_e(h_a - h_b)^2}{2 \cdot R_f^2}$$

4. Calculate $z = \left(h_r + \dfrac{(X - d_1)^2}{2a_e}\right) / \sigma_z$

$$q_1 = \frac{1}{2}(1 - \mathrm{erf}(\sqrt{2}z/\varepsilon) + \varepsilon_f \exp(-z^2/2)(1 + \mathrm{erf}(\sqrt{2}z\varepsilon_f/\varepsilon))$$

5. Integrate: $P_U = \exp\left\{\displaystyle\int_0^{R_f} \ln(1 - q_1)\, dX/\overline{\lambda}\right\}$, by stepping X in 4 above.

6. Integrate: $P_C = \dfrac{1}{2\pi} \displaystyle\int_{-3\sigma_z}^{3\sigma_z}\int_{-3\sigma_z}^{3\sigma_z} P_U \exp\left\{- \frac{(h_a - h_c)^2}{2\sigma_z^2} - \frac{(h_b - h_d)^2}{2\sigma_z^2}\right\} \dfrac{dh_a}{\sigma_z}\,\dfrac{dh_b}{\sigma_z}$,

by stepping h_a and h_b in 3 above.

15

Table 6. Program for Shadowing Calculation

```
C-FOCAL S 1/71

01.01 C SHDOWING A LA CARTWRIGHT
01.02 C RA IS IN NMI; OTHERS IN FEET
01.03 C FOR SINGLE HA,HB:D 1;D 2
01.04 C TO AVERAGE OVER HA,HB:D 1;D 6
01.10 A ?HC HD RA SZ LA ?
01.20 S EP=.7; S PI=3.1415923; S R2=FSQT(2)
01.30 S EF=FSQT(1-EP*EP)
01.35 S NX=8; S AE=3.14E7
01.40 S DX=RA*6076/NX; S HA=HC; S HB=HD
01.50 S PE=.3275911; S E1=.25482959; S E2=-.28449674
01.55 S E3=1.4214137; S E4=-1.453152; S E5=1.0614054

02.40 S RU=DX*NX
02.50 S D1=RU/2+AE*(HA-HB)/RU
02.60 S HR=HA-D1*D1/2/AE
02.70 S XI=0; S SM=0; S IX=0; D 3

03.01 C CALC Q1 AND SIMP(XI)
03.05 S ZA=(HR+(XI-D1)†2/2/AE)/SZ
03.07 I (ZA-5)3.10,3.10,S ZA=5
03.10 S XE=ZA*R2/EP; D 5
03.15 S Q1=1-ER
03.20 S ZE=XA*R2*EF/EP; D 5
03.25 S Q1=(Q1+EF*(1+ER)*FEXP(-ZA*ZA/2))/2
03.28 I (Q1-1)3.29,3.29;S Q1=1
03.29 C
03.30 I (XI)1.10,3.40,3.33
03.33 I (XI-RU)3.46,3.40,3.40
03.36 I (IB-3)3.46,3.46,3.43
03.40 S IB=1; G 3.50
03.43 S IB=2; G 3.50
03.46 S IB=4
03.50 S SM=SM+IB*FLOG(1-Q1+2E-7); S IX=IX+1; S XI=IX*DX
03.55 I (XI-RU)3.05,3.05
03.58 I (-SM-16)3.60,3.60; S SM=-16
03.60 S PU=FEXP(DX*SM/3/LA)
03.70 T ! %5.03,?HA,HB,PU ?
```

16

Table 6. Program for Shadowing Calculation (continued)

```
04.10  I  (HA-SZ*3-HC)4.15,4.22,4.15
04.15  I  (HA-HC+3*SZ)4.20,4.22,4.20
04.20  I  (IC-3)4.26,4.22,4.24
04.22  S  IC=1;G  4.30
04.24  S  IC=2;G  4.30
04.26  S  IC=4
04.30  I  (HB-HD-3*SZ)4.35,4.42,4.42
04.35  I  (HB-HD+3*SZ)4.42,4.42,4.40
04.40  I  (ID-3)4.46,4.42,4.44
04.42  S  ID=1;G  4.50
04.44  S  ID=2;G  4.50
04.46  S  ID=4
04.50  D  2
04.55  S  PA=PA+IC*ID*PU*FEXP(-((HA-HC)↑2+(HB-HD)↑2)/SZ↑2)

05.01  C  ERF(XE); ERF(2)=.995322
05.02  I  (FABS(XE)-5)5.10,5.10,5.04
05.04  S  XE=5*FSGN(XE)
05.10  S  TX=1/(1+PE*FABS(XE))
05.20  S  ER=TX*(E1+TX*(E2+TX*(E3+TX*(E4+TX*E5))))
05.30  S  ER=FSGN(XE)*(1-ER*FEXP(-XE*XE))

06.05  S  PA=0;T  ! %4.03,?HA, HC,  HD,  SZ,  LA ?
06.10  F  HA=HC-3*SZ,SZ,HC+3*SZ;D  6.20
06.15  G  6.30
06.20  F  HB=HD-3*SZ,SZ,HD+3*SZ;D  4
06.30  S  HA=HC;S  HB=HD;S  PC=PA/18/PI
06.40  T  !  ?  PC  ?  ;T  !;T  !;G
*
```

Table 7. Results for Geometric Shadowing Over Total Path

Buoy Class	h_c	h_d	R	SS	σ_z	$\overline{\lambda}$	P_c
1	10'	8'	5.5nmi	5	2.56'	134'	.045
2	10	6	4.5	3	1.0	65	.958
3	10	3	3	2	.56	40	.989
4	10	2	1	1	.16	12	.999
5	10	1.8	1	3	1.0	65	.457
1	65	8	5.5	6	3.84	188	.495

In the calculations for P_c in Table 7, values of a_e = 1.5 times the geometric earth radius and ε = 0.7 [3]* were used. It is noted that the geometric visibilities of the Class-5 buoy from the 10-foot platform and the class 1 buoy from the 65 foot platform in their maximum design sea states are marginal, and that for the 10-foot platform and Class-1 buoy is submarginal.

The effects of buoy height, sea state, earth radius, and range were explored in detail for a few cases, and the results are listed in Table 8. In Section A of the table it is seen that increasing the height of the Class-1 buoy improves the probability of unobstructed view in Sea State 5 rapidly at first but the improvement slows as height increases above about 10 feet. Above that level it is the height of the antenna that principally controls the shadowing. As the sea state is reduced in Section B of Table 8, the Class-1 buoy quickly becomes visible. The same result is seen when the effective earth radius is extended. Thus, it is concluded that the visibility of a buoy is very sensitive to the rms surface roughness and the propagation conditions that exists, and can be improved somewhat for the design sea conditions and standard propagation conditions by increasing the reflector height.

*References referred to in the text are enclosed by brackets.

18

Table 8. Shadowing of Class-1 Buoy as a Function
of Wave Height, Earth Radius, and Buoy
Reflector Height

	Ant Ht.	Refl. Ht.	rms Roughness	a_e/a	P_{clear}
A.	10 ft	8	2.56	1.5	.04
		10			.31
		12			.70
		14			.90
		16			.96
B.	10 ft	8	2.7	1.5	.003
			2.4		.10
			2.1		.50
			1.8		.90
			1.5		.99
C.	10 ft	8	2.56	1.33	.01
				1.77	.13
				2.35	.47
				4.16	.83
				9.79	.94
				∞	.99

C. Near-Field Shadowing

Although the effect of the large number of wave crests between the radar and the reflector is accounted for by the curved-earth diffraction theory, it is possible for a large nearby wave to produce significant departure from the curved-earth diffraction prediction. Here the statistical description of the rough surface of the preceeding section has been applied to predict the probability that a high crest does not obscure the radar antenna when the boat is in the deep trough adjacent to the crest. The results of these calculations are shown in Figure 4 for those cases which have appreciable probability of shadowing. In that figure the probability that greater than a given clearance is afforded is plotted against the clearance for the boat with 10-foot antenna height in a State-5 sea, the Class-1 buoy in State-5 and -6 seas and the Class-5 buoy in a State-3 sea. It is seen that the boat antenna in SS 5 is predicted to have one foot or more clearance 85% of the time, but that the Class-5 buoy is effectively obscured 50 to 70% of the time in Sea State 3. The interpretation of these calculations is that for these cases arbitrarily high probability of detection on a single scan in the higher sea states will not be achievable with any practical buoy cross section. For example, the maximum probability of detection under the stipulated conditions of a Sea State 5, a 10-foot antenna height and a Class-1 buoy is approximately $0.85 \times 0.72 = 0.61$.
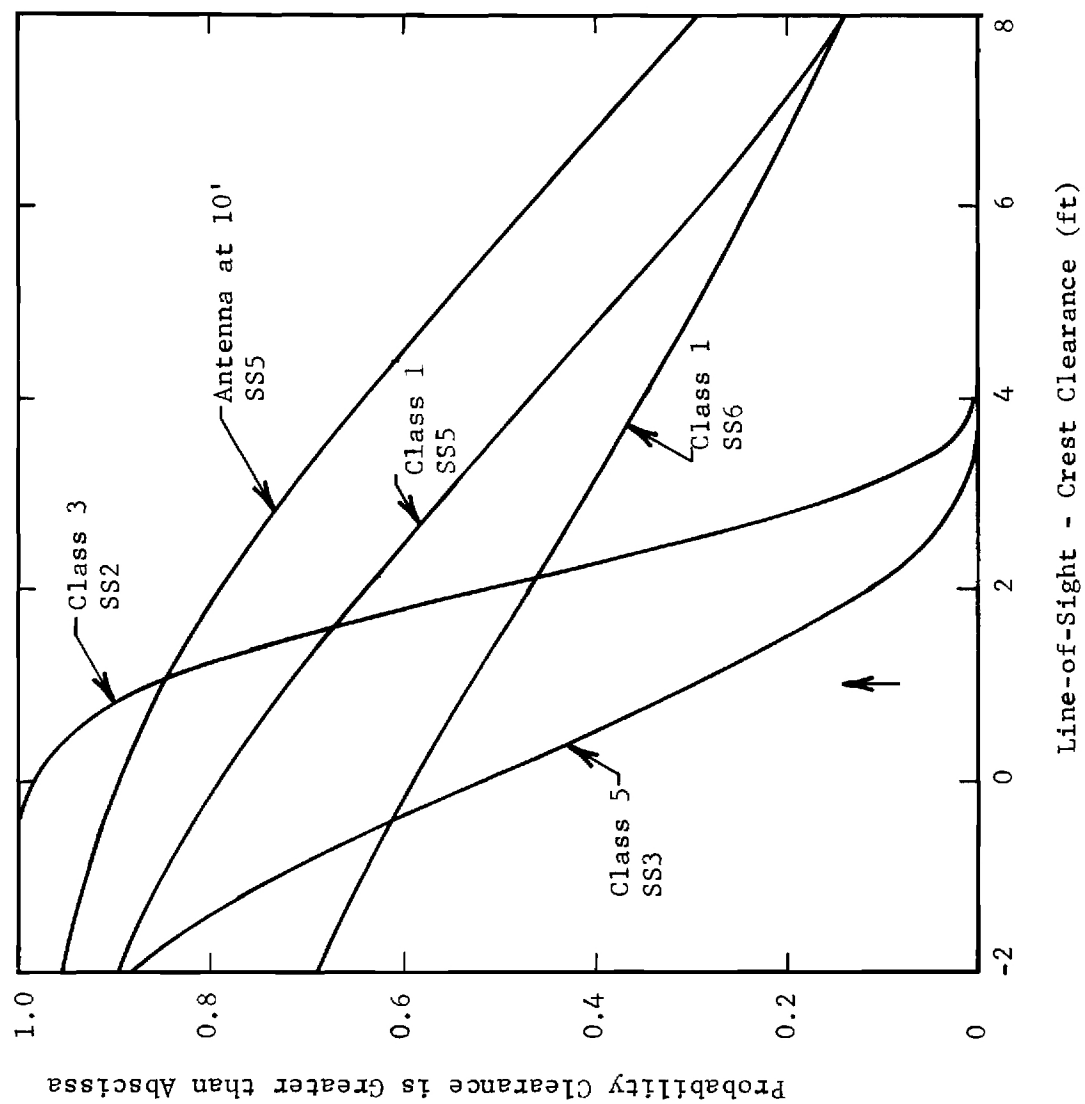
Figure 4. Probability of antenna or reflector being above a nearby crest

21

III VISIBILITY OF RADAR TARGETS

A. Visibility of Target Signals in Noise

A substantial, and definitive study of the capability of a human operator detecting targets on the PPI display of a noncoherent radar was performed by Ruby Payne-Scott [5] during WWII. The data from that study were presented in graphical and nomograph forms. From them a set of equations and a computer program were derived earlier [6] and are used here with the assigned specifications of the stereotype radar to compute minimum-detectable target-to-noise ratios for the present study. The algorithm is expressed in Tables 9, 10 and 11; Table 9 lists and defines the variables of the calculation, Table 10 the equations, and Table 11 the computer program implementing them in the language, FOCAL [4].

The results of the calculations are listed in Table 12. In addition to the explicit specifications of Table 3, the following values were assumed:

k_1 = 3 (corresponding to magnetic focus)

k_2 = 2 (corresponding to a linear envelope detector)

a = .15
b = 1.2 } (corresponding to P7 phosphor)

I = 0.1 ft-Lambert

D_o = 12 inch

D = 3 inch

In Table 9, LP is the minimum detectable signal-to-noise ratio in dB for 0.5 probability of detection. It is seen to vary from a minimum of -1 dB to a maximum of + 2.7 dB for wise choices of displayed range, given the design range of the buoys. It should be noted that these figures and the Payne-Scott model apply to an alert, undistracted operator, and hence represent limiting levels of performance.

Probability of detection improves rapidly with increasing signal-to-noise ratio. Thorough study of probability of detection for the

22

Table 9. Input Variables for PPI Model

Symbol	Units	Definition	FOCAL Symbol
B	MHz	Bandwidth of Receiver (IF)	BW
τ	μs	Pulse Length	TP
θ_a	deg	Azimuth Antenna Beamwidth	TA
D	in.	Length of Display Trace	LD
d	in.	Diameter of Beam Spot	SP
D_o	in.	Distance of Observer's Eye from Screen	OD
R	nmi	Range to Target	RA
R_D	nmi	Display Range	RD
f_r	Hz	Pulse Repetition Rate	RP
S	rpm	Antenna Scan Rate	SC
k_1		C-R-T Grid-Transfer-Law Exponent	K1
k_2		$\begin{cases} = 1 \text{ for square-law detector} \\ = 2 \text{ for linear detector} \end{cases}$	K2
a	s^{-1}	Decay Rate of C-R-T Phosphor	DE
b		Exponent of Decay Factor	QB
I	ft-Lambert	Brightness of Noise Background on C R T Screen	IN
P_{min}/P_n	dB	Minimum detectable target-signal-to-average-noise ratio referred to receiver input	LP

23

Table 10.   PPI Model Equations

1.
$$G_{BandP} = \frac{1}{\left(1-e^{-2B\tau}\right)^2}$$

2.
$$G_{Trans} = \frac{k_2}{k_1}$$

3.
$$s = \frac{D}{R_D \cdot 12.35}$$

$$h_s = \left| \left\{1 + \left(\frac{\tau s}{d}\right)^2\right\} \left\{1 + \left(\frac{\theta_h R D \pi}{d R_D 180}\right)^2\right\} \right|^{1/2}$$

$$G_{Exc} = h_s \left\{\frac{1}{\dfrac{\tau s}{d} \cdot \dfrac{\theta_a R D \pi}{d R_D 180}}\right\}$$

4.
$$\phi = h_s \cdot \frac{\pi}{4} \frac{d^2}{D_o^2}$$

$$\phi_c = 5 \times 10^{-6} \frac{1 + I^{0.55}}{I^{0.55}}$$

$$q = (0.08 \ln \phi_c)^2$$

$$G_{Contr} = 1.27 \phi_c^{1/2} \frac{\left(1 + \left(\frac{\phi}{\phi_c}\right)^q\right)^{1/q}}{\dfrac{\phi}{\phi_c}} = G_{Contr}(\phi, I)$$

24

Table 10.   (Continued)

5. $$\phi_s = \frac{\pi}{4} \; \frac{d^2}{D_o{}^2} \left[1 + \left(\frac{s}{2Bd}\right)^2 \right]^{1/2}$$

$$n_s = \frac{7.5 \; f_r dR_D}{S \; D \; R} \left[1 + \left(\frac{2Bd}{s}\right)^2 \right]^{1/2}$$

$$n = n_s \; \frac{1 + \left(1 + \frac{60a}{S}\right)^{-b}}{1 - \left(1 + \frac{60a}{S}\right)^{-b}}$$

$$G_{RepP} = \left[1 + \frac{1}{n \cdot G^2{}_{Contr} \; (\phi_s, \; I) \cdot G^2{}_{Trans}} \right]^{1/2}$$

$$C_P = 5.2$$

$$P_{min}/P_n = C_P \cdot G_{BandP} \cdot G_{Trans} \cdot G_{Exc} \cdot G_{RepP} \cdot G_{Contr}$$

25

Table 11. Program for Visibility in Noise on PPI Display

```
C-FOCAL  S  2/71

01.01  C PPI MODEL.  TO INPUT VARIABLES, G 1.22.
01.10  S PI=3.14159
01.20  S CP=5.2
01.21  G 1.30
01.22  A ? BW TP TA LD SP OD RD RA RP SC K1 K2 DE QB IN ?
01.23  G 1.1
01.30  F RA=RD/10,RD/10,RD;D 2;D 1.40
01.35  QUIT
01.40  T ! %5.02, ?RD, RA, LP ?


02.10  S GB=1/(1-FEXP(-2*BW*TP))↑2
02.20  S GT=K2/K1
02.31  S SM=LD/RD/12.35
02.32  S T1=TP*SM/SP
02.33  S T2=LD*TA*PI*RA/180/SP/RD
02.34  S SA=FSQT((1+T1*T1)*(1+T2*T2))
02.35  S GE=SA/T1/T2
02.37  S SE(00)=SA*PI*((SP/OD)↑2)/4
02.39  S J=0;D 3
02.41  S KR=FSQT(1+(2*BW*SP/SM)↑2)
02.43  S SE(01)=SP↑2*PI*FSQT(1+(SM/2/BW/SP)↑2)/4/OD↑2
02.55  S NS=KR*7.5*RP*SP*RD/SC/LD/RA
02.57  S T3=FEXP(FLOG(1+60*DE/SC)*(-QB))
02.59  S NN=NS*(1+T3)/(1-T3)
02.61  S J=1; D 3.4;D 3.5
02.63  S GR=FSQT(1+1/NN/GC(01)↑2/GT↑2)
02.70  D 4


03.10  S T4=FEXP(.55*FLOG(IN))
03.20  S ST=5E-6*(1+T4)/T4
03.30  S QE=(.08*FLOG(ST))↑2
03.40  S GC(J)=FEXP(FLOG(1+FEXP(QE*FLOG(SE(J)/ST)))/QE)
03.50  S GC(J)=GC(J)*1.27*ST*FSQT(ST)/SE(J)


04.10  S LP(I)=10 *FLOG(GB*GT*GE*GC(00)*GR*CP)/FLOG(10)
*
```

Table 12. Minimum Detectable Target Signal-to-Noise Ratios

Displayed Range RD	Range RA	$(S/N)_{LP50}$	$(S/N)_{90}$	$(S/N)_{99}$
2 nmi	1 nmi	−1 dB	+1.0 dB	+2.5 dB
4	3	0	2.0	3.5
8	4.5	2.7	4.7	6.2
8	5.5	2.2	4.2	5.7
2 nmi	2 nmi	−2.0 dB		
	1.5	−1.6		
	1.0	−1.0		
	0.5	+0.5		
4 nmi	4 nmi	−0.4 dB		
	3	0		
	2	+0.8		
	1	+2.5		
8 nmi	8 nmi	1.5 dB		
	6	2.0		
	4	2.9		
	2	4.9		
	1	7.4		

"automatic detector" incorporating an ideal integrator of noncoherent video has been performed by Marcum [7] and repeated by others [8]. The use of these calculations to describe human operator performance has been partially validated [9, 10]. The curves of Reference 8 were used to relate the baseline results presented in Table 12 (which apply to probability of detection, $P_D = 0.5$) to other values of P_D, and the results are also shown in Table 12. The offsets were derived from Reference 8, page 353, Figure 10.4-5 for $n' = 10^3$.

Average noise power referred to the receiver input is given by $P = kTBF_n$, where k is Planck's constant, T the reference temperature, B the receiver noise bandwidth and F_n the noise figure. For the stereotype radar, with B = 10 MHz and $F_n' = 12$ dB, the receiver noise power is -121.8 dBw.

B. Clutter-Limited Visibility

Radar sea-return signals differ from receiver noise signals in two important ways: the sea return signal at video is distributed over a greater dynamic range than the Rayleigh distribution which describes ideal noise at video, and signal voltages corresponding to specific radar cells vary more slowly in time than noise, which is completely independent from one pulse to the next. Associated with this temporal correlation is a spatial correlation which is related to the morphology of the sea-surface waves. The result of these differences is that human operators behave differently when detecting targets in clutter than when noise is the only background, and their performance tends to be poorer for the clutter case.

For the noncoherent radar with conventional PPI display and an antenna scan time of a few seconds per revolution or more, an experienced operator will tend to adjust receiver and video gain controls and display bias so that about 3 per cent of the time the larger-magnitude clutter spikes are visible [11]. This condition results from an as yet unspecified combination of desires to see as far down below the upper clutter levels as possible but still retain sensitivity of the brightness and apparent angular size of returns to the signal magnitude. The compromise is forced because of the large dynamic range of the clutter signals, the narrow dynamic range of the display brightness, and the limited sensitivity of the eye to changes in brightness.

28

Clutter distributions are approximately lognormal; that is, the logarithm of the video signal is approximately Gaussian distributed. The standard deviation of this distribution depends on sea state, pulse length, beamwidth, and grazing incidence angle or range. For the parameters and geometry of the stereotype maritime radar, a standard deviation for sea return of 6 or 7 dB would be expected when clutter is appreciable. For a 7 dB standard deviation, 3 percent of the clutter signal is more than 8.5 dB above the average clutter power. However, this level is an appropriate threshold only if no integration existed. For the stereotype radar there are 12.5 pulses per beamwidth which span a period of 12.5 ms (derived from a beamwidth of 1.5 degrees, a scan rate of 20 rpm, and prf of 1 kHz). The rapidly decorrelating component of the autocovariance function of sea return signal has a width (decorrelation time) of about 4 ms [12], and for linear video detectors comprises about 75% of the variance of the video signal. Thus, there are only about $12.5 \div 4 \simeq 3$ independent samples of the sea-return signal which can be integrated, but this is sufficient to make the threshold level exceeded 3% of the time by the integrated intensity only about 5 dB above the average clutter power [13].

In experiments with operators watching PPI displays of real fluctuating targets in a background of sea return, it has been found that a ratio of target signal to clutter spike power of 10 dB is sufficient to enable detection on a single scan. The plausibility of this level can be tested by realizing that the apparent width of the antenna beam at the -10 dB level is about twice as great as at the -3 dB level, and the width of the pip on the diplay presented to the eye for the stronger signal is wider by the same factor, even if the brightness is increased negligibly because of limited phosphor dynamic range. Thus, it is concluded that when appreciable clutter is received by the radar, high probability of detection of a target may require a 10 + 5 = 15 dB ratio of target signal to average clutter power for the type of radar stipulated here and when properly used.

Parenthetically, this minimum detectable ratio of signal to back-
ground power can be reduced substantially by changes in radar parameters.
The research and applications of Croney [14] on clutter signal processing
techniques involving primarily the use of rapid scanning antennas, optimum
choice of polarization, and logarithmic video detectors demonstrate that
appreciable improvements are possible for target detection in the mari-
time case.

C. Sea-Return Cross Sections

The average radar cross section per unit area of sea return σ° [15],
has been modeled as a deterministic function of those independent variables
which can be identified as influencing sea return [16]. The model equa-
tion was obtained by fitting data from experiments in which care was ex-
ercised in control of these variables and which span a wide enough varia-
tion to show trends (e.g., Reference 17). The equations expressing σ°
are listed in Table 14, the variables are deinfed in Table 13, and the
program is listed in Table 15.

Radar sea return has been calculated using the data-based model for
antenna heights of 10 and 65 feet and Sea States 1 through 6. Results
of this calculation are listed in Table 16. Three measures of sea clutter
are listed: The average cross section per unit area, which is the prin-
cipal modeled quantity; the average cross section for the clutter, which
is computed using the cell size of the stereotype radar; and the average
received clutter power predicted for the stereotype radar. The average
received power is used with the clutter visibility figures discussed in
the previous section to derive the minimum detectable target signal in
a clutter background for that system.

Two factors affecting interpretation of the results should be noted.
The range dependence of sea return is assumed to be dominated at longer
ranges by diffraction in the presence of the curved earth surface, and
the effects of the atmosphere are included only by the choice of effective
earth radius (see Chapter V). When surface evaporation-duct trapping
exists, these figures calculated for σ°, clutter cross section, and aver-
age power quantities, and peak values, on which detection thresholds must
be based in many circumstances, are substantially higher.

In conditions when trapping is dominant, the range dependence of the peaks of the clutter is different from that of the average clutter. In other words, the amplitude distribution of clutter signals is not independent of range, for although the average clutter power will have a range function which is markedly different in the plateau and low-angle regions [18], the peak values of received power will fall off approximately like R^{-4}, which implies a cross section of the clutter scatterers that is constant. At X-band this cross section of clutter spikes is about 1 m^2 [19]. This spike cross section represents the background with which a buoy reflector must compete under conditions of surface trapping.

Table 13 Variables of Clutter Model

Symbol	Units	Definition	FOCAL Symbol
λ	feet	Wavelength	LW
V_W	knot	Wind speed	VW
ϕ	degree	Angle between boresight and upwind direction	PH
h_a	feet	Height of antenna	HA
R	nmi	Range	RA
σ_z	feet	rms surface roughness	SZ
θ_a	degree	Azimuth beamwidth	TA
τ	μs	Pulse width	TP
a_e	feet	Effective earth radius	AE
σ°	dB	Average cross section per unit area	SO
σ_c	dBsm	Average clutter cross section	CC
P'_c	dBw	Average received clutter power	PS

32

Table 14 Horizontal Polarization Clutter Model

1. Input: λ, V_w, σ_z, ϕ, h_a, R, θ_a, τ

2. Set: a_e

3. Calculate: $h_1 = h_a - \dfrac{(R.6076)^2}{2\,a_e}$

$\psi = \dfrac{h_1}{R.6076}$

$\sigma_\phi = \dfrac{12.5\,\psi\,\sigma_z}{\lambda}$

4. Calculate:

$$G_I = 1 - \frac{4}{3}\exp\{-1.23\,\sigma_\phi^2\} + \frac{1}{3}\exp\{-4.92\,\sigma_\phi^2\}$$

$$G_U = \exp\{0.415 \cos \phi\; \lambda^{-0.44}(1 - 1.4\psi)\}$$

$$G_W = V_W^{1.59}\,\lambda^{-0.35}$$

5. Calculate:

$$\sigma^\circ = 10\,\log\{9 \times 10^{-7}\lambda\,\psi^{\,0.4}\,G_W\,G_U\,G_I\}$$

$$\sigma_c' = \sigma^\circ + 10\,\log\left\{\frac{\theta_a\,R\,\tau\,492\,.\,6076}{57.3\,\sqrt{2}}\right\}$$

$$P_c' = -111.5 + \sigma_c' - 40\,\log R$$

Table 15. Program for Sea Return Calculation


```
C-FOCAL S 1/71

01.01 T ! "    HORIZ. POL. SEA RETURN MODEL"
01.03 C RA,RI,DR,RO IN NMI; LW,HA,SZ IN FEET; VW IN KTS; TU IN MICROS
01.04 C PH IN DEG, 0 IS UPWIND; TA IS IN DEG
01.20 S CA=9E-7
01.23 S AE=3.14E7
01.26 S R2=FSQT(2)
01.30 A ! ?LW VW SZ PH HA TA TU ?
01.40 A ! ?RI DR RO ?


02.05 T ! ! %4.03,? VW, SZ, PH, LW, HA ?;T !
02.07 T ! "  RANGE   SIGMA ZERO   CROSS SECT   REC. PWR."
02.08 T ! "   NMI        DB          DBSM         DBW"
02.10 F RA=RI,DR,RO;D 3;D 2.20;D 2.21
02.15 G 2.90
02.20 T ! %3.01,RA;T "    ";T %4.01,SO;T "    ";T %4.01,CC
02.21 T "    ";T %4.01,PS
02.90 C


03.10 S RU=RA*6076
03.15 S H1=HA-RU↑2/2/AE
03.17 I (H1)3.18,3.18,3.20
03.18 T ?RA ?;S RA=RA-DR/2;D 3;D 2.20;G
03.20 S PS=H1/RU;S SS=12.5*PS*SZ/LW
03.25 S GI=1-FEXP(-1.23*SS↑2)*4/3+FEXP(-4.92*SS↑2)/3
03.30 S TS=.415*FCOS(PH/57.3)*FEXP(-.44*FLOG(LW))*(1-1.4*PS)
03.35 S GU=FEXP(TS)
03.40 S GW=FEXP(1.59*FEXP(-.35*FLOG(LW))*FLOG(VW))
03.45 S CS=CA*LW*FEXP(.4*FLOG(PS))*GW*GU*GI
03.50 S AC=TA*TU*RU*492/R2/57.3
03.55 S CC=4.34*FLOG(CS*AC*.093)
03.60 S SO=4.34*FLOG(CS)
03.65 S PS=-111.5+CC-17.36*FLOG(RA)
*
```

Table 16 Radar Sea Return for Buoy Reflection Comparison

Sea State   6
Wind Speed   26 kts
rms Roughness   3.84'
Upwind Look
Antenna Height 65'

Range nmi	σ° dB	σ'_c dBsm	P'_r dBw
0.5	-22.7	1.4	- 98.1
1.0	-23.8	3.3	-108.2
1.5	-24.5	4.3	-114.2
2.0	-25.1	5.1	-118.5
2.5	-25.6	5.5	-121.9
3.0	-26.2	5.7	-124.9
3.5	-27.1	5.4	-127.8
4.0	-28.3	4.8	-130.7
4.5	-29.7	3.9	-133.7
5.0	-31.5	2.7	-136.8
5.5	-33.4	1.1	-140.0
6.0	-35.7	-0.8	-143.4

Sea State   5
Wind Speed   22 kts
rms Roughness   2.56'
Upwind Look
Antenna Height 10'

Range nmi	σ° dB	σ'_c dBsm	P'_r dBw
0.2	-26.8	- 6.7	- 90.2
0.4	-29.0	- 5.8	-101.4
0.6	-32.4	- 7.5	-110.2
0.8	-36.2	-10.0	-117.7
1.0	-39.8	-12.7	-124.2
1.2	-43.2	-15.3	-129.9
1.4	-46.4	-17.8	-135.2
1.6	-49.5	-20.3	-140.0
1.8	-52.5	-22.8	-144.5
2.0	-55.4	-25.3	-148.9

Table 16   Radar Sea Return for Buoy Reflection Comparison
(Continued)

Sea State   3
Wind Speed   15 kts
rms Roughness   1'
Upwind Look
Antenna Height 10'

Range nmi	σ° dB	σ'_c dBsm	P'_r dBw
0.2	-34.9	-14.8	- 98.4
0.4	-43.6	-20.4	-116.0
0.6	-50.4	-25.5	-128.2
0.8	-55.9	-29.7	-137.3
1.0	-60.3	-33.2	-144.7
1.2	-64.3	-36.4	-151.0
1.4	-67.8	-39.2	-156.6
1.6	-71.1	-41.9	-161.6
1.8	-74.2	-44.6	-166.3
2.0	-77.3	-47.2	-170.7

Sea State   2
Wind Speed   12 kts
rms Roughness   .56'
Upwind Look
Antenna Height 10'

Range nmi	σ° dB	σ'_c dBsm	P'_r dBw
0.2	-44.2	-24.0	-107.6
0.4	-55.7	-32.6	-128.2
0.6	-63.3	-38.4	-141.0
0.8	-69.0	-42.8	-150.5
1.0	-73.6	-46.5	-158.0
1.2	-77.6	-49.7	-164.3
1.4	-81.1	-52.6	-169.9
1.6	-84.5	-55.3	-175.0
1.8	-87.6	-58.0	-179.7
2.0	-90.6	-60.5	-184.1

IV PROPAGATION LOSSES OVER THE SEA

Microwave propagation between two distant points just above the sea surface is affected by the atmosphere and by reflections from the sea surface, so that the free-space model of radar propagation must be substantially modified to predict the losses that may be expected. The propagation loss tends to be dominated either by atmospheric effects or by interference of waves reflected in or diffracted by the sea surface. For, when there exists above the surface a negative gradient of refractive index of sufficient magnitude and vertical extent to trap microwaves, propagation losses are low, in some cases lower than in free space. When the strength of this surface evaporation duct is weak, the interference theory adequately describes propagation losses, provided an appropriate value of effective earth radius is used. These limiting cases will be briefly described separately before joint discussion of them is continued.

A. Free-Space Spreading Loss

The standard or baseline performance of the stereotype radar can be expressed in terms of the signal power received from a target as a function of range, assuming that the energy spreads as in free space. The equation describing this received power is

$$P_r = P_t \frac{G^2 \lambda^2 \sigma}{(4\pi)^3 R^4 L} \quad , \qquad (8)$$

where L is the dissipative system losses and λ, σ, and R are of course given in compatible units. Using the parameters of Table 3 in this equation one finds:

$$P_r = 0.7 \cdot 10^{-11} \cdot R^{-4} \cdot \sigma \quad \text{watts,} \qquad (9)$$

Where R is in nmi and σ in m^2. In logarithmic units, Equation 9 becomes.

$$P_r' = -111.5 + \sigma' - 40 \log R(nmi) \qquad \text{dBw,} \qquad (10)$$

where σ' is in dBsm. Thus, the performance potential of the radar is expressible as a single constant, the power received from a 1-m^2 target at 1 nmi, in this case -111.5 dBw.

B. Curved-Earth Diffraction in the Interference Region

Neglecting the atmosphere, propagation from antenna to target can occur both by a direct path and by a path reflected in the surface. Waves arriving at the target by the two paths interfere with a resultant field which depends on their relative magnitudes and phases. The magnitude of the surface-reflected component is less than that of the direct ray because of the dielectric absorption (a minor effect for horizontal polarization) and because of random scattering by the surface roughness. Near grazing incidence, for antenna and target at low heights and separated appreciably in range, the reflection coefficient approaches -1, so that there is cancellation between the direct and surface-reflected fields. This interference reduces the illumination of targets near the earth compared to free space and introduces a propagation loss, expressed by the factor F, which is the ratio of field strength with and without the surface interference.

The two-way propagation loss caused by the interference effect is plotted in Figure 5 for the Class-1 buoy parameters of Table 1. The curves in that figure were calculated from equations derived from Reference 20, and the effects of earth curvature are included explicitly as a parameter of the family. The ordinate is the factor (in dB) by which the power received from a point target is modified by reflection in the rough sea surface. The equations used in the calculation are listed in Table 18 in algorithmic form, the variables in Table 17, and the computer program in Table 19.

It is seen in Figure 5 that the interference effect introduces substantial propagation loss in addition to the free space spreading losses. At the design range of 5.5 nmi the additional two-way loss might be expected to be as great as about 45 dB for the Class-1 buoy when the effective earth radius is 1.33 times geometric. The marine environment is more likely to have a larger effective earth radius, even when trapping in the surface evaporation duct is not dominant.

38

Table 17. Variables for Curved-Earth Diffraction Calculation

Symbol	Units	Definition	FOCAL Symbol
h_a	feet	Height of Antenna	HA
h_b	feet	Height of Reflector	HB
σ_z	feet	R.M.S. Surface Roughness	SZ
λ	feet	Wavelength (Radar)	LW
ρ_{max}	--	Saturation Value of Reflection Coefficient	RM
R	nmi	Range	RA
a_e	feet	Effective Earth Radius	AE
F_r	dB	2-Way Diffraction Loss	CF

Table 18. Equations for Diffraction Calculation

Input: h_a, h_b, σ_z, λ, ρ_{max}, R

Set: a_e

Calculate: $R_f = 6076 \cdot R$

$$p = 2\left\{\frac{1}{3}\left[a_e(h_a + h_b) + R_f^2/4\right]\right\}^{1/2}$$

$$X = \sin^{-1}\left\{\frac{2\,a_e\,R_f(h_b - h_a)}{p^3}\right\}$$

$$d_1 = \frac{R_f}{2} - p\,\sin(X/3)$$

$$a_t = \frac{R_f^2}{2\,a_e(h_a + h_b)^2}$$

$$h_1 = h_a(1 - h_a a_t)$$

$$\Gamma = \rho_{max}\,\exp\left\{-(4\pi\,\sigma_z\,h_1/\lambda d_1)^2\right\}$$

$$\Delta R = \frac{2\,h_a h_b}{R_f}\left(1 - \frac{d_1^2}{2\,a_e h_a}\right)\left(1 - \frac{(R_f - d_1)^2}{2\,a_e h_b}\right)$$

$$\delta = 2\pi\,\Delta R/\lambda$$

$$F_R = 20\,\log\left\{1 + \Gamma^2 + 2\Gamma\,\cos\delta\right\}$$

40

Table 19. Program for Curved Earth Diffration Loss

```
C-FOCAL S 1/71

01.01 T ! "CURVED EARTH PROP; POINT TARGET "
01.10 S AE=3.14E7; S PI=3.1415923
01.20 T ! "  RANGE IN NMI; OTHERS IN FEET; RM IS NEG ! " !
01.30 A ?  HA, HB, LW, RM, SZ, RI, RO, DR ?

02.05 T ! %4.03, ? HA, HB, SZ, LW, RM ?
02.10 F RA=RI,DR,RO; D 3

03.05 S RU=RA*6076
03.10 S PA=2*FSQT(((AE*(HA+HB)+(RU/2)↑2)/3)
03.15 S AR=2*AE*RU*(HB-HA)/PA↑3
03.20 S XI=FATN(AR/FSQT(1-AR*AR))
03.30 S D1=RU/2-PA*FSIN(XI/3)
03.35 S AT=RU↑2/2/AE/(HA+HB)↑2
03.40 S H1=HA*(1-HA*AT)
03.45 S H2=HB*(1-HB*AT)
03.50 S GA=RM*FEXP(-(4*PI*SZ*H1/LW/D1)↑2/2)
03.52 S G1=1-D1↑2/2/AE/HA
03.54 S G2=1-(RU-D1)↑2/2/AE/HB
03.60 S DD=HA*HB*2*G1*G2/RU
03.62 I (G1)3.68,3.68
03.64 I (G2)3.68,3.68,3.70
03.68 S CF=-250; G 3.90
03.70 S DL=2*PI*DD/LW
03.75 S AQ=1+GA*GA+2*GA*FCOS(DL)
03.80 S CF=8.68*FLOG(AQ)
03.90 T ! %3.03, ?RA, CF ?, "DB"
*
```

Figure 5. Two-way curved earth diffraction loss.
Antenna height = 10'; Class-1 buoy;
sea state 5.
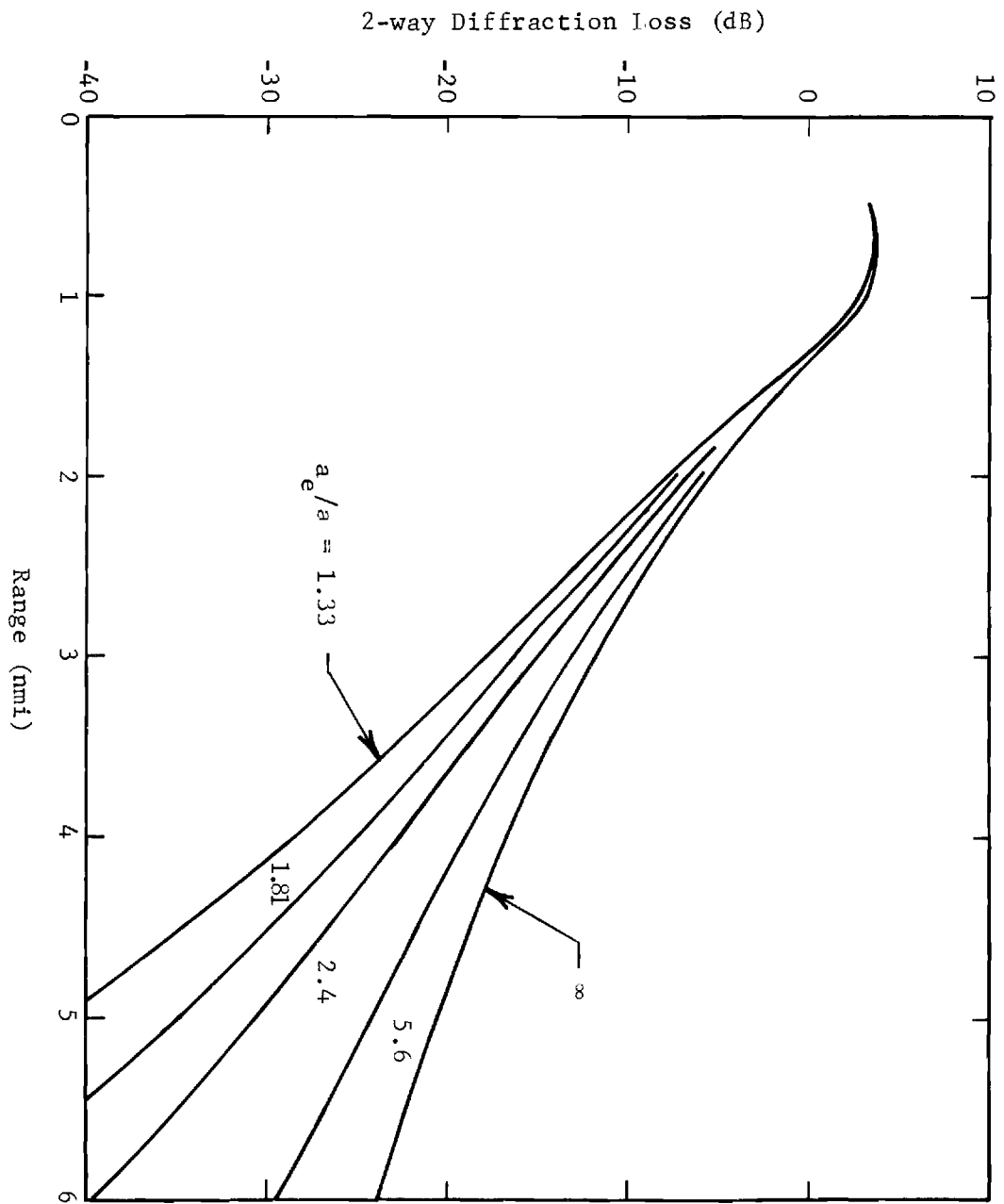
Losses produced by curved earth diffraction are plotted in Figure 6 for the other cases of interest here. It is seen that losses for the Class-1, -2 and -3 buoys are large at their design ranges but those for the Class-4 and -5 buoys are moderate. In both Figures 5 and 6 the median antenna and buoy heights apply, and surface roughness has been included only in its effect on the surface reflection coefficient.

The effect of sea waves raising and lowering the buoy and boat on the diffraction loss has been calculated for the Class-1 and Class-5 buoys in State-5 and -3 seas, respectively, and the results are presented in Figure 7. They apply for an antenna height of 10 feet above the water line, a range of 5.5 nmi and a Gaussian distributed sea-surface height. It is seen that the median losses are equal to the values at design ranges in Figure 6. Curves like those of Figure 7 can be used with a minimum acceptable loss calculated from radar predicted performance, free-space loss and assumed target cross section to predict a net probability of detection, and this is done for marginal cases in Chapter V.

C. Propagation in Surface Evaporation Ducts

The following brief summary is abstracted from the more detailed material of Reference 21. The surface ducts important to this study are formed by a negative gradient of atmospheric refractive index with altitude produced either by decreasing water vapor or by increasing temperature with altitude. The condition of negative gradient will trap microwave energy provided the gradient is strong enough and its height extent is great enough. Lower frequencies require greater height extents (or much greater gradients) than do higher frequencies for a given amount of duct leakage. When strong trapping exists, energy is bound in the vertical plane to a layer of constant altitude, and spreading occurs only in the horizontal plane. For the typical surface evaporation duct, field strengths tend to be a maximum about 10 feet above the surface at X band and 20 feet for S band. The exact height is variable and depends on the shape of the refractive gradient curve and antenna altitude and range. Coupling to a duct is strongest when

43
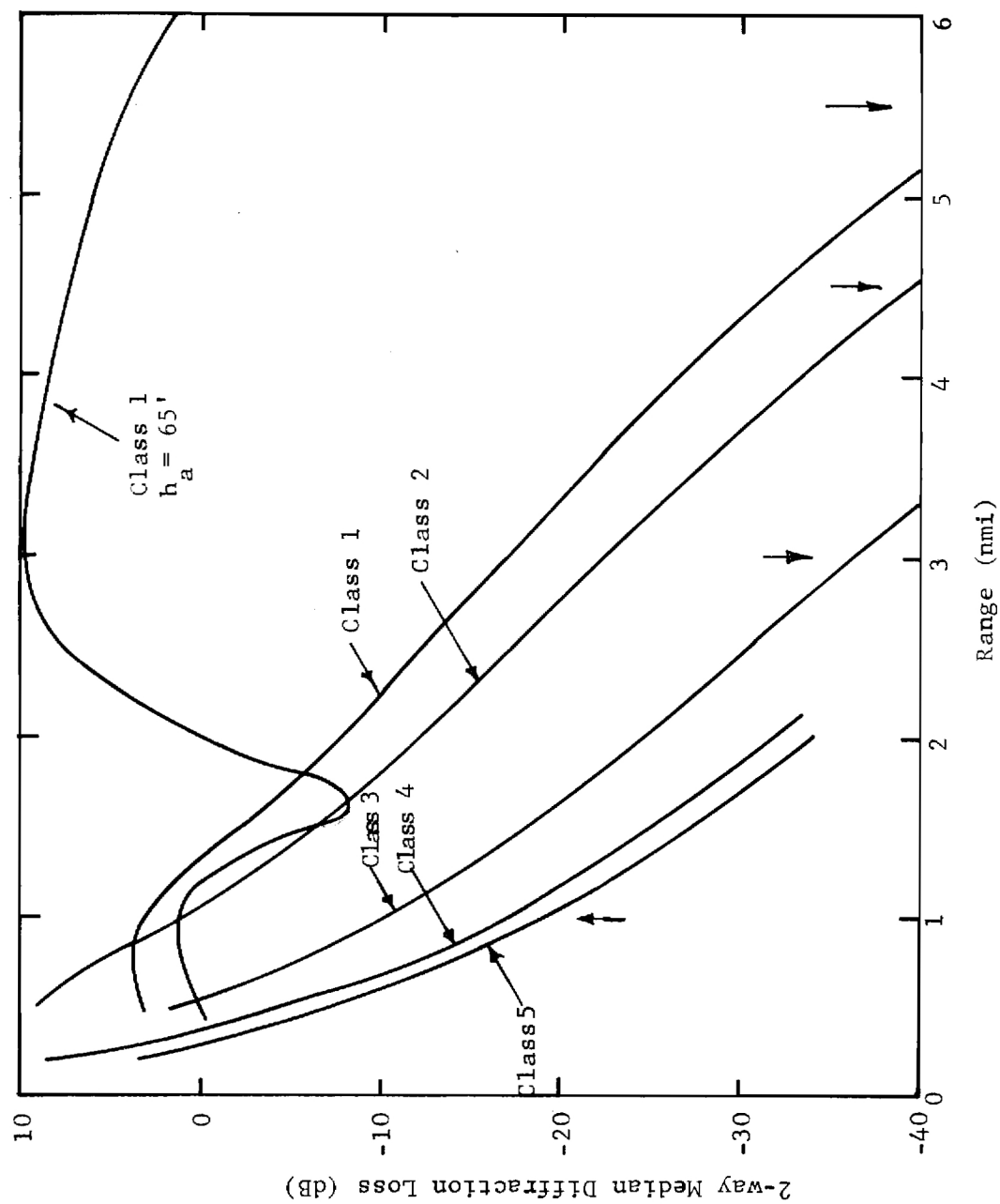
Figure 6. Two-way median curved earth diffraction loss.
Design-goal parameters of Table 1, $a_e = 1.5a$.

44

Figure 7. Cumulative probability of 2-way curved earth diffraction loss. Antenna height = 10 feet; ranges as in Table 1.

Probability that Loss Factor is Less than Abscissa
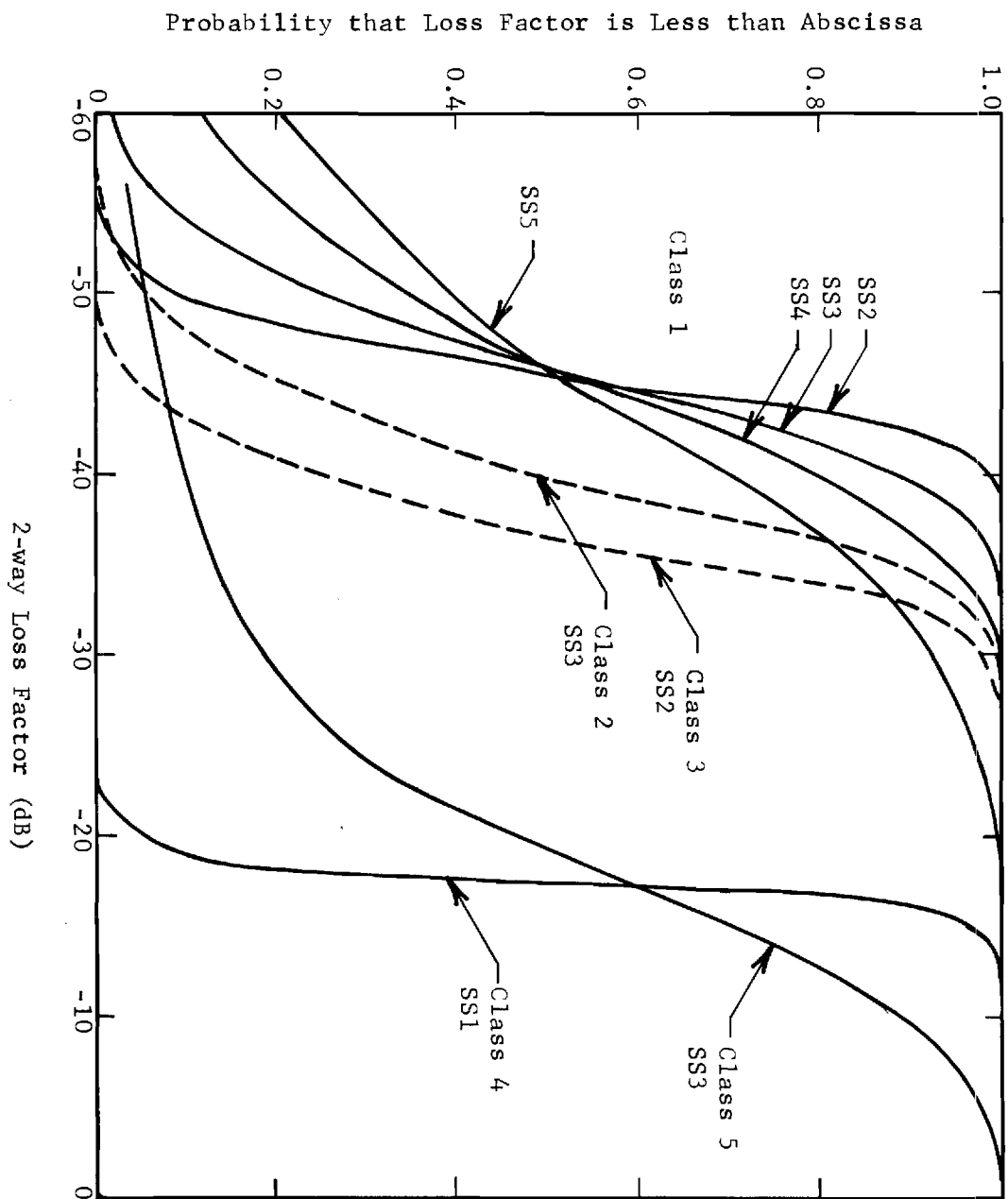
antennas and targets are located at the heights of the maximum field strengths.

When surface trapping exists, signal strengths at a few tens of miles are typically equal to free space or stronger by as much as 10 dB. When the duct conditions are weakened so that energy is not trapped, signal strengths are described by the curved earth diffraction theory, perhaps with a modified earth radius to account for the refraction that does exist. Ducts tend to exist or not; that is, the time spent in either the trapped condition or the diffraction state is long compared to the duration of transition between the two states.

Some rules for the information of surface ducts can be stated [22, 23]. Trapping occurs for conditions in which warm dry air passes over cooler water as from over land, or for the condition of a sea breeze or low wind sustaining layered flow and minimum vertical mixing. When very dry air from land blows over warm water, high wind speeds can still allow negative refraction gradients [24]. Air cooler than water is allowed if of short duration and preceeded by trapping conditions, as overnight. Standard diffraction conditions exist whenever vertical homogeneity of the atmosphere is achieved, as by turbulence. Such a condition of vertical mixing is produced by high or gusty winds, strong surface heating, or a frontal zone. Indifferent gradients can also exist for conditions when the air has travelled over the water for a considerable distance, at speeds of about 15 kts or greater achieving saturation and mixing in the process, or when the air temperature is substantially lower than that of the water and has been so for several hours. Substandard conditions of positive gradient with altitude can be created by fog or by warm moist air flowing over cool water, as from tropical maritime regions.

It is important to note in the above rules the influence of the history of the air mass over the water, the conditions which affect vertical mixing and transfer of water vapor from the surface, and the role of land in determining the boundary conditions for the maritime air mass. Because the conditions for trapping are directly related to the meterological conditions, the durations of trapping or diffraction or substandard periods tend to be from hours to days.

The percentage of time one expects to experience each of the propagation modes is important but difficult to predict at present. It is known that the probability of surface trapping is different for different frequencies (more likely at higher frequencies) and at different times of the year (more likely in summer than in winter) and of the day (more likely in the afternoon and evening than in the morning). Reference 22 presented an analysis of experience at S-band in the Massachusetts Bay area. For observations in that band in the months of August through October, the percentages of 6-hour periods in which each of the three conditions were observed were as shown in Table 20. The total is more than 100% because

Table 20. Distribution of Propagation Conditions
(from Reference 23, for S-band)

| Month | Fraction of 6-Hour Periods Experiencing | | |
	Trapping	Diffraction	Substandard
August	50%	85%	5 - 10%
September	35	90	
October	30	85	10 - 15

in many 6-hour periods more than one propagation condition was observed. These data were from S-band observations and relate to X-band use only by implying that frequency of observation of trapping should be increased over the entries of Table 20.

Although a large body of direct experimental evidence is available for analysis, most of the observations in X-band have been made using antenna heights substantially greater than 10 feet, thus reducing the pertinence of the data for description of the evaporation-duct trapping phenomenon. One recent experiment series with appropriately low antenna

heights [24, 25, 26] indicated that, out of 11 days of operation in three locations on the U.S. east coast, on 8 days ($\sim$75%) strong trapping was experienced at X-band or lower frequencies with signal strengths and range dependence of the order of free-space propagation.

V. MINIMUM DETECTABLE CROSS SECTIONS

The results of the calculations of Chapters III and IV are com-
bined in Figures 8 through 13 to allow comparison of predicted target
signal levels with background levels as a function of range and tar-
get cross section. The figures are graphs of power at the receiver
input in dBw as functions of range in nmi.

The background thresholds plotted were derived from the data in
Chapter III, and only those curves applicable to a 0.9 probability of
detection on a single scan (assuming that the given target signal power
is actually received) have been plotted. Curves for other probability
levels (not plotted) are offset vertically by appropriate constant
amounts from those plotted. The clutter threshold curves apply under
propagation conditions when the curved-earth diffraction effect domi-
nates. When propagation is dominated by surface evaporation-layer
trapping, the appropriate clutter threshold corresponds approximately
to the free-space curve for a cross section of +10 dBsm. The noise
threshold is a function of the choice of displayed range and hence
varies among the figures as the design range changes.

Target signal levels are plotted for free-space spreading loss
and for curved-earth diffraction conditions. Only curves for two cross
sections (0 and +20 dBsm) are plotted so as to minimize the total number
of curves to be represented. Curves for other values of cross section
would lie offset along the ordinate by the appropriate number of dB.
The free-space curves are also to represent minimum signal levels when
surface trapping is dominant. The diffraction curves apply to the
median terminal heights, and thus if the range is such that a diffrac-
tion signal curve intersects the noise threshold level, a net probability
of detection of about 50% would be observed. This is because half of
the time either the buoy or boat or both is lower than median height
and greater diffraction loss is experienced than the curve plotted.

Each of the figures applies to a buoy of a given class in its
design configuration and maximum sea state as specified in Table 1.
All are for an antenna height of 10 feet except Figure 8, which depicts

49
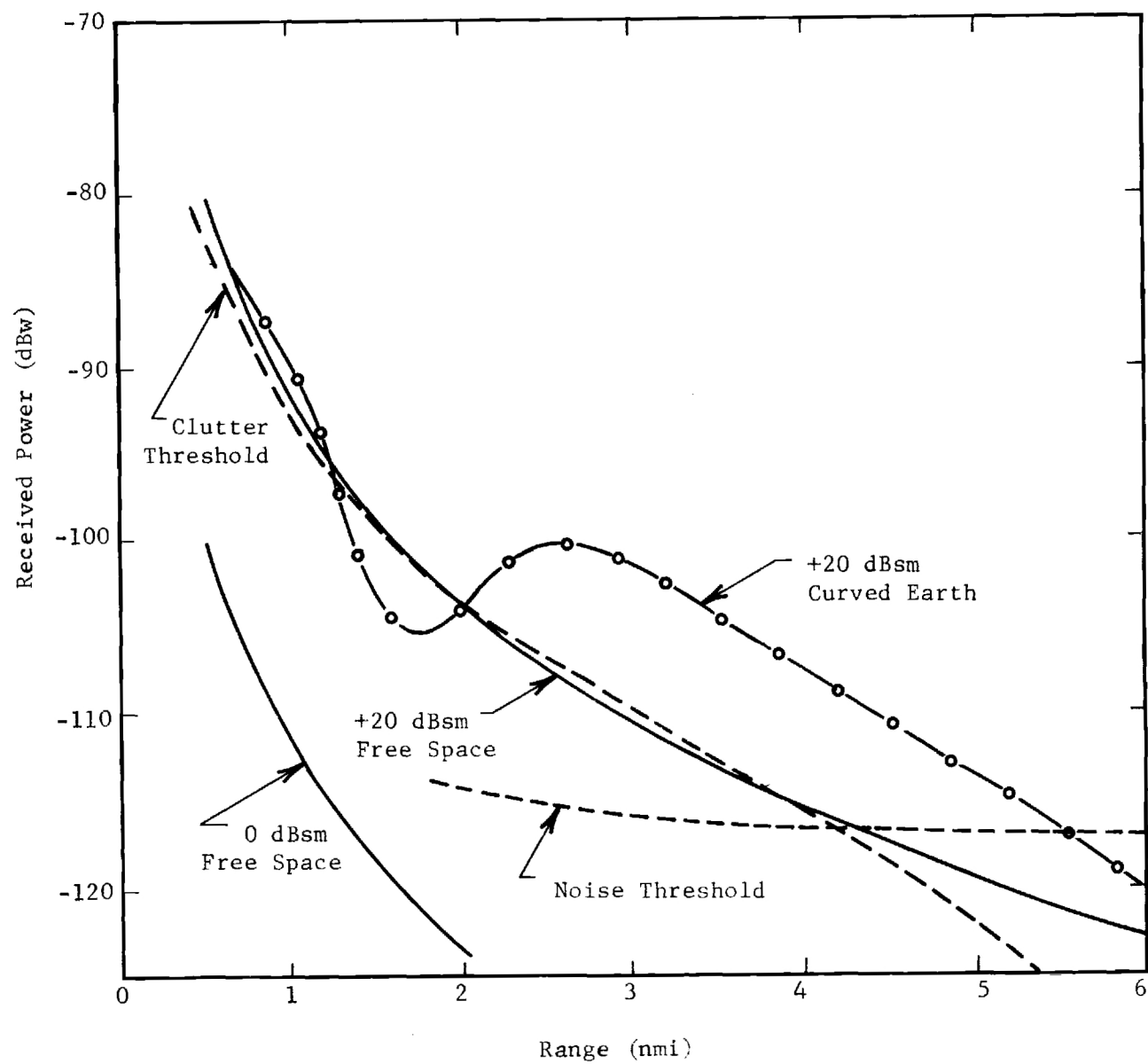
Figure 8. Signals and background thresholds. Class-1 buoy, Sea State 6, antenna height 65 feet.

50
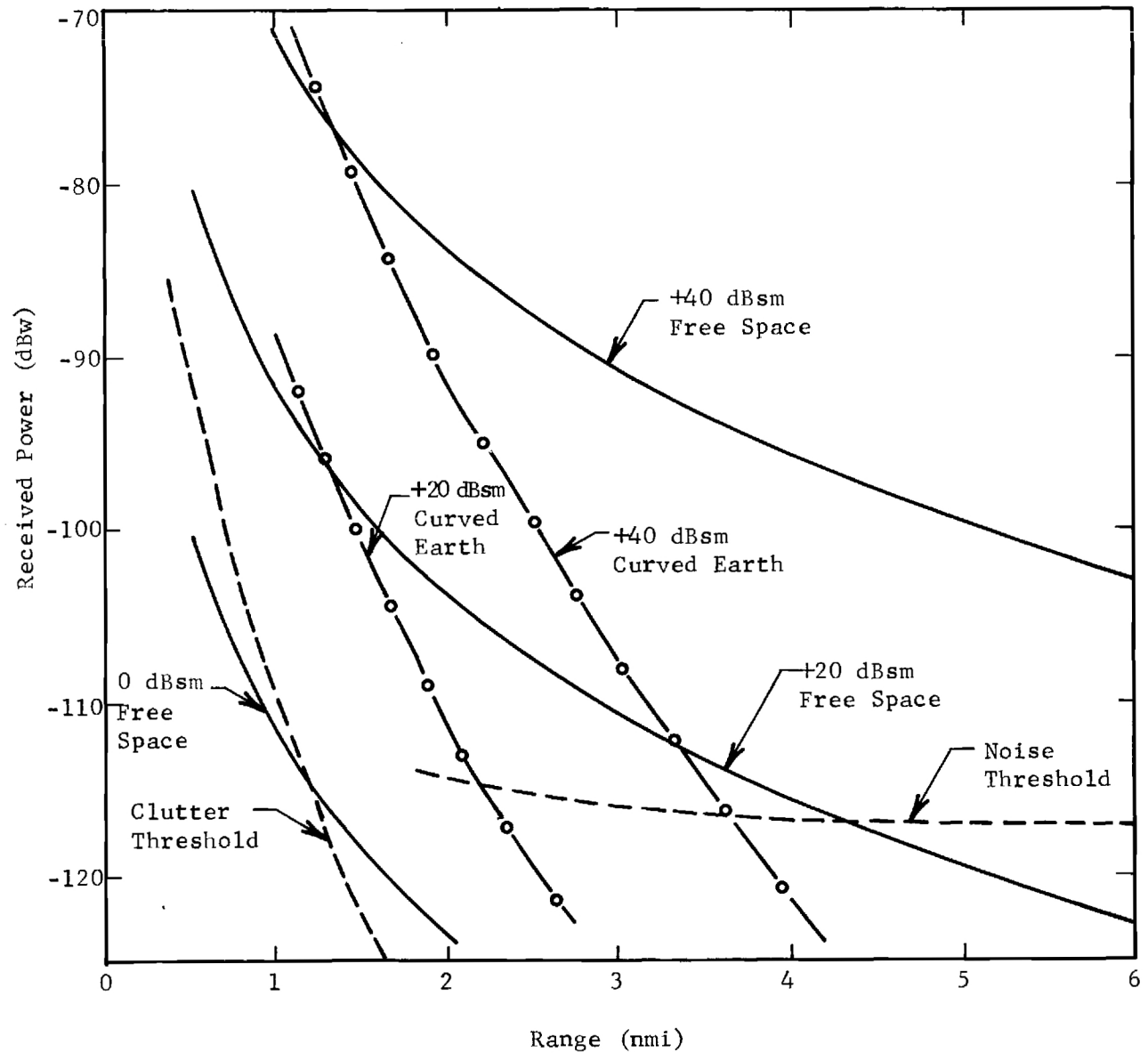
Figure 9. Signals and background thresholds. Class-1 buoy, Sea State 5, antenna height 10 feet.

51
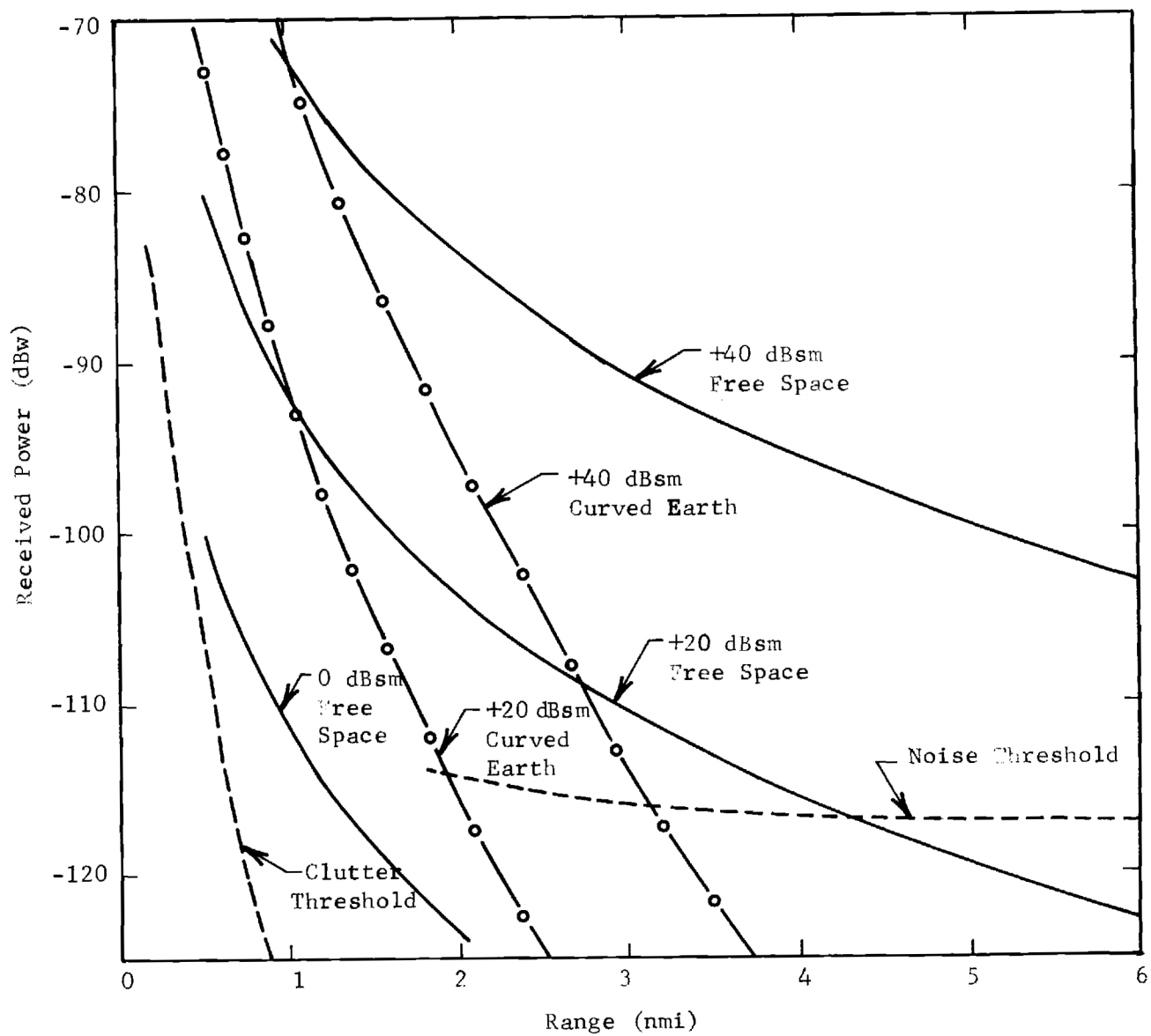
Figure 10. Signals and background thresholds. Class-2 buoy, Sea State 3, antenna height 10 feet.

52
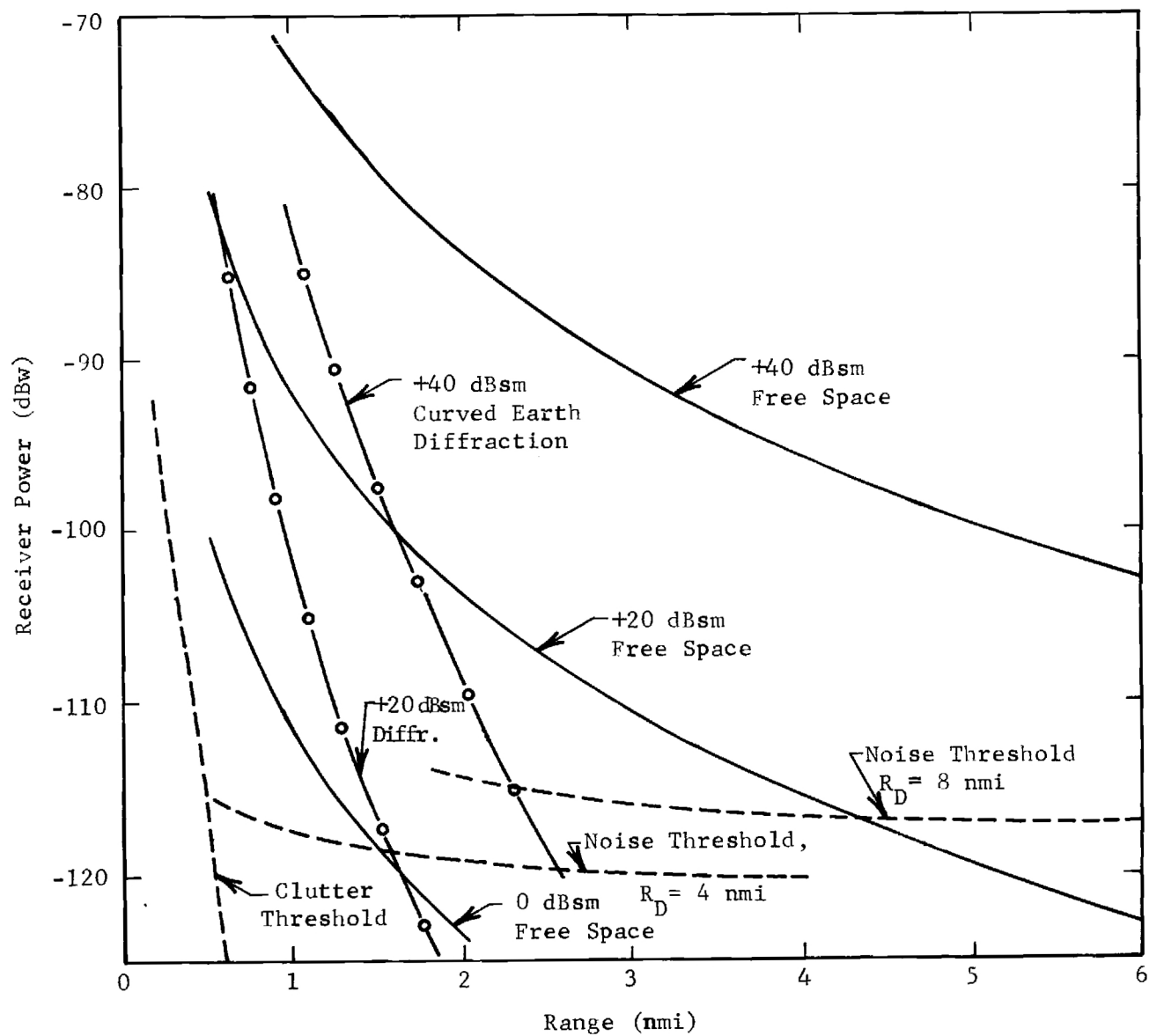
Figure 11. Signals and background thresholds, Class-3 buoy, Sea State 2, antenna height 10 feet.

53
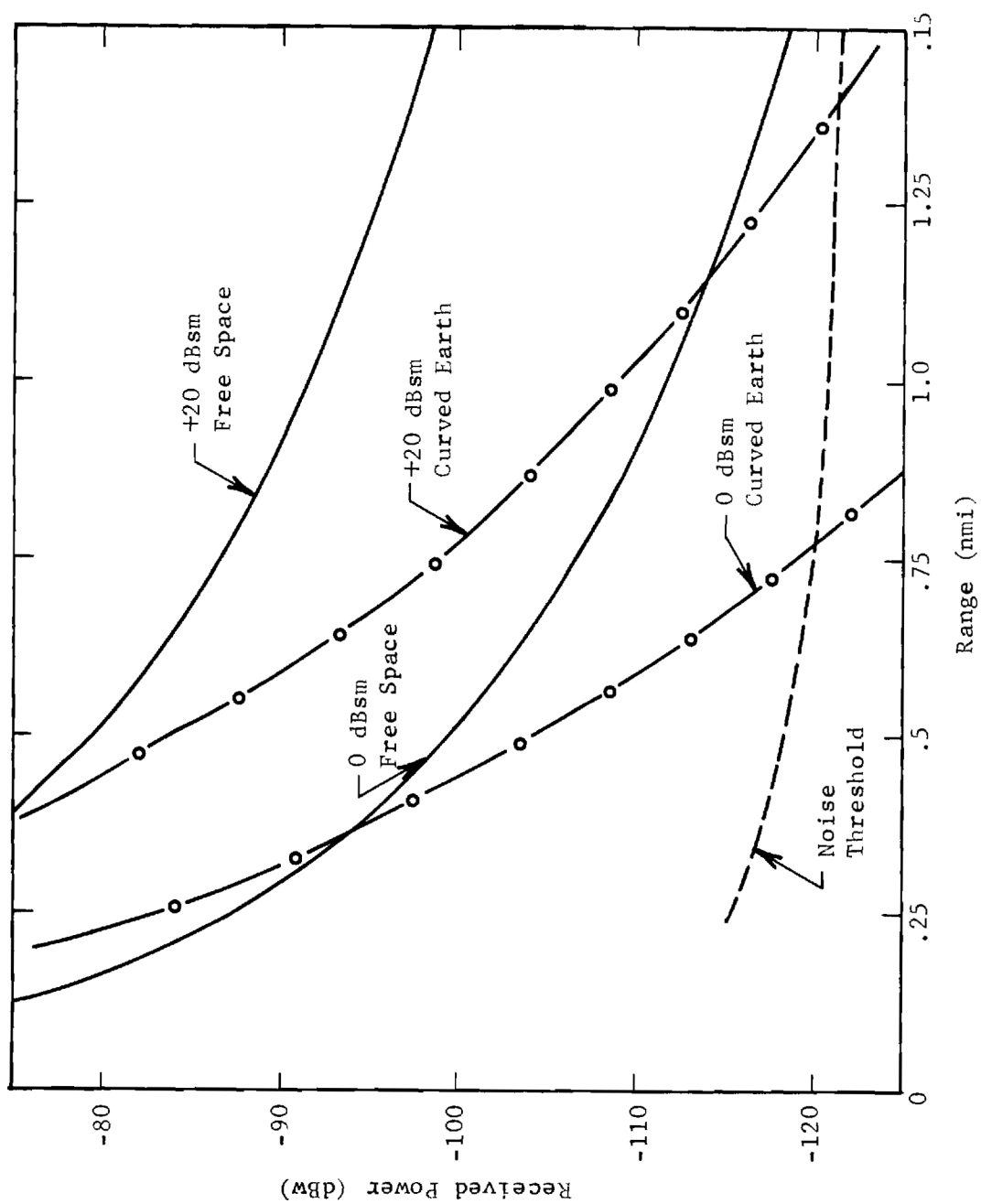
Figure 12. Signals and background thresholds. Class-4
buoy, Sea State 1, antenna height 10 feet.

54
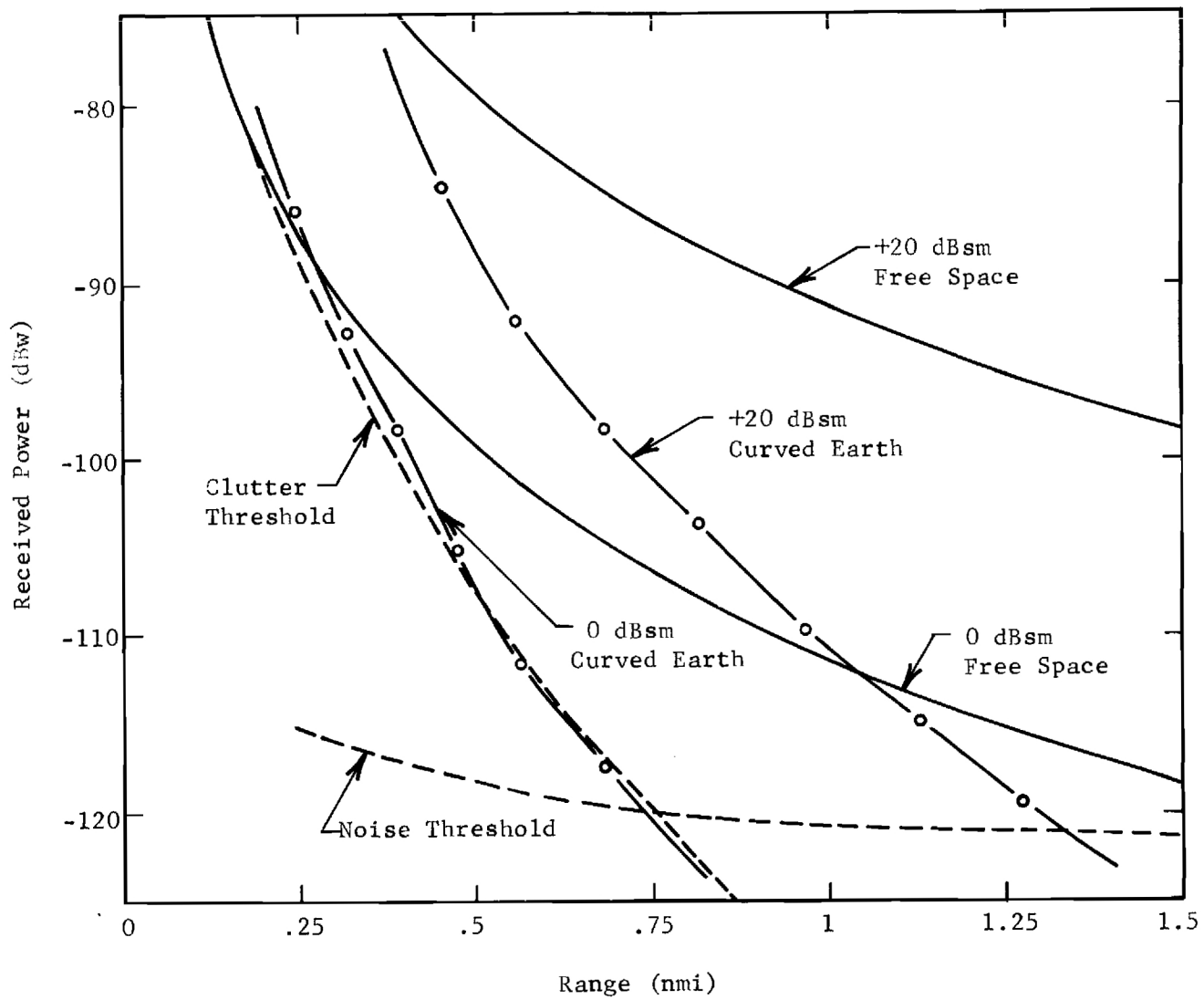
Figure 13. Signals and background thresholds. Class-5 buoy, Sea State 3, antenna height 10 feet

signals for an antenna height of 65 feet and a Class-1 buoy. In all those cases with low antennas, maximum range for detection of a given cross section target under diffraction conditions is about half that under trapping conditions. The slopes of the curves for the extreme conditions are quite different. Whereas a slight change in design cross section can substantially alter detection range under trapping conditions, a very large change in cross section is required to appreciablly alter detection range under diffraction conditions. It is clear from examination of the graphs that for a given class of buoy the cross section which will give marginal operation at the design range under favorable propagation conditions (estimated to occur 70% of the time at X-band) can be too small by several orders of magnitude to give desired performance under unfavorable conditions. Furthermore, the sizes of reflectors required to assure design-goal detectable ranges under unfavorable conditions are too large physically for practical marine buoy systems. For example, a radar cross section of about +60 dBsm would be required in unfavorable circumstances to give 5.5 nmi range detection of a Class-1 buoy; this reflector has a physical projected area of more than 9 m^2!

In Table 21 are listed the cross sections of the various classes of buoys which will give the desired performance under favorable conditions existing more than half the time. Also listed are the reduced ranges at which the buoys will be seen during unfavorable conditions. The fraction of time that reflector will be clear of near obstructions in its maximum design sea state is listed also as it affects the ultimate probability of detection.

Table 21 Minimum Detectable Buoy Reflector Cross Sections (h_a = 10 ft)

Class	Design Range	σ' (dBsm)	Limitation	Worst/Best Range	P_D/Limitation
1	5.5 nmi	+25	Noise	2.5/5.5 nmi	0.5/Surface Roughness
1*	5.5	+25	Noise & Clutter	5.5	0.5/Surface Roughness
2	4.5	+21	Noise	2.0/4.5	0.9/Surface Roughness
3	3	+10	Noise**	1.2/3.0	0.8/Surface Roughness
4	1	+10	Noise**	1.0	0.9+/Cross Section
5	1	+10	Noise**	1.0	0.3/Surface Roughness

*h_a = 65 ft, SS-6

**Clutter, when surface trapping is dominant

The justification for and consequencies of the choices of the buoy reflector cross section values listed in Table 21 require discussion. Propagation conditions close to the sea surface tend to be characterized either by wave trapping in the surface evaporation duct or by diffraction by the reflecting sea surface. In the former case propagation losses are about equal to free-space spreading or less by up to 10 dB. In the latter case the losses can be greater than free space by 20 to 40 dB depending on the specific antenna and buoy heights and range. In the cases of the low antenna height considered (10 feet), the Class-1, -2 and -3 buoy returns experience about 40 dB of diffraction loss under unfavorable conditions, whereas the 20-dB figure applies to the Class -4 and -5 buoy geometries. The reflector cross section required for each detection in trapping conditions (listed in Table 21) can be provided by corner-cube reflectors of practical size; however, reflectors with 20 to 40 dB-greater cross section are likely to be excessive in size for buoy use. Thus, a consequence of choosing the size adequate in favorable propagation conditions is a reduction in range of detection by about a factor of 2 for Class-1, -2 and -3 buoys. However, propagation experience indicates that this reduction will be suffered about 30% of the time (more often in winter than in summer).

Under diffraction conditions clutter is critical as the background limiting detection only in the case of the 65-ft-high antenna in Sea State 6. However, the cross section necessary to allow detection of the Class-1 and 2 buoys at their design ranges with free-space loss levels against a noise background also gives adequate signal-to-clutter ratio under diffraction conditions. Under trapping conditions clutter spike cross sections are expected to be of the order of 1 m^2 (0 dBsm), so that a lower limit of reflector cross section of +10 dBsm is advisable. This reflector size is adequate to provide design-goal range for detection of both Class-4 and -5 buoys even under unfavorable propagation conditions.

Probability of detection is limited by three principal factors:

(a) Signal-to-noise or signal-to-clutter ratio

(b) Sea-wave-produced height variations in diffraction fields

(c) Shadowing by near wave crests

The first contribution is easily countered by slightly increased buoy cross section or by decreased range or losses. An increase of 2 dB in signal-to-noise ratio increases probability of detection from 0.5 to 0.9 an additional 1.5 dB to 0.99. Slighting greater increases are required for the same effect in clutter background. In neither of the other two factors does the probability of detection respond rapidly to changes of cross section. The second case responds moderately to decreased range but very slowly to increased height; the applicable range law is approximately R^{-8}, whereas the height law is about h^{+4}. In the third factor the probability of detection can be improved by slight increases of reflector height. For example the probability of shadowing of the Class 5 buoy by waves in a State-3 sea can be reduced from about 0.7 for a height of 1.8 feet to less than 0.5 by increasing the reflector height to 3 feet (see Figure 4). The critical factor here is the ratio of reflector height to the rms surface roughness. A ratio of greater than 3 is desirable to keep the probability of clear visibility of the order of 0.7 or more.

The rule for combining the probabilities from above is: when the events are independent, the overall probability of detection is

$$P_D = P_1 \, P_2 , \qquad\qquad (11)$$

where P_1 and P_2 are the independent-event frequencies of occurrence. In the present situation, the signal-to-background-controlled probability is likely to be independent of the other contributors, but the probability of shadowing is highly correlated with the condition of increased diffraction loss. The combination of these events is complicated, but a practical rule is to use the worst case of the two unmodified by the other. Thus, the probability of detection corresponding to the diffraction-limited curves of Figures 8 through 13 is 0.5 except for the Class-5 buoy in Sea State 3, where it is 0.3. The curves of Figures 4 and 7 can be used to explore further the tradeoffs between range and probability of detection. The effects of shadowing and increased diffraction loss at the boat and at the buoy should be considered as independent; thus, for example, in the worst case condition of a Sea State 5, the probability of a clear 10-ft antenna of 0.85 must multiply the probability of

a clear Class-1 buoy reflector of 0.72 to give a net probability that both are clear of 0.6.

It appears that in the higher sea states the effects of sea roughness on diffraction loss (trapping is not expected to exist often in Sea State 4-6) and terminal shadowing limit practically achievable probabilities of detection on a single scan to about 0.5. Cumulative probabilities of detection on a sequence of scans can be quite high, however. For example if independent positions of the boat and buoy are experienced on the average of one half a wave period, then in Sea State 5 with a wave period of ∿9 seconds, a cumulative probability of detection of 0.9 would be expected in 5 scans (15 seconds at 20 scans per minute) for a 0.5 probability on a single scan. It would appear that no serious operational disadvantage would be experienced by small craft, and this is fortunate in view of the difficulty of achieving higher single-scan probabilities or longer range for detection under conditions of high winds and sea leading to high propagation losses.

On the basis of the above-discussed rationale, the cross sections listed in Table 21 are those recommended for use on the respective buoys. The safety factor included in these figures is distributed between the specification of the stereotype radar and the marginal loss assumed for the most-frequently encountered propagation condition, both of which are considered to be conservative.

VI REFERENCES

1. P. J. Stahnke, "Small Boat Radar Evaluation," Technical Memorandum Naval Electronics Laboratory Center, 18 Oct 1968

2. R. N. Chernyayev and I. U. Lyubchenko, "Prospects for Developing Shipborne Radar," Sudostroyeniye _ 229 (1968)

3. D. E. Cartwright, "On Estimating the Mean Energy of Sea Waves from the Highest Waves in a Record," Proc. Roy. Soc A239 22 (1958)

4. Introduction to Programming, Digital Equipment Corp. (1969)

5. R. Payne-Scott, "The Visibility of Small Echoes on Radar PPI Displays," Proc. IRE 36 180 (1948)

6. W. Rivers, "Models for Radar Displays," Technical Memorandum on Contract N00024-70-C-1219, Georgia Institute of Technology, 17 Jul 1970

7. J. I. Marcum, "A Statistical Theory of Target Detection by Pulsed Radar," IRE Trans. IT-6 59 (Apr 1960)

8. J. V. DiFranco and W. L. Rubin, Radar Detection, Prentice Hall Inc. (1968)

9. D. G. Tucker, "Detection of Pulse Signals in Noise: Trace-to-Trace Correlation in Visual Displays," J. Brit. IRE 17 319 (1957)

10. M. I. Skolnik, "Discussion: Trace-to-Trace Correlation in Visual Displays," J. Brit. IRE 17 705 (1957)

11. Unpublished data, Contract N00024-70-C-1219, Georgia Institute of Technology

12. J. G. Boring, et al, "Sea Return Study," Final Report on Contract NObsr-49063, Georgia Institute of Technology, 1 Aug 1957, AD 246180

13. S. F. George, "The Detection of Nonfluctuating Targets in Log-Normal Clutter," NRL Report 6796, Naval Research Laboratory, 4 Oct 1968

14. J. Croney and A. Woroncow, "Radar Polarization Comparisons in Sea-Clutter Suppression by Decorrelation and Cosntant False Alarm Rate Receivers," Radio and Electronic Eng. 38 187 (1969)

15. H. Goldstein in D. E. Kerr, Propagation of Short Radio Waves, McGraw-Hill (1957); Sec 6.6

16. W. K. Rivers, S. P. Zehner, and F. B. Dyer, "Modeling for Radar Detection," Final Report on Contract N00024-69-C-5430, Georgia Institute of Technology, 31 Dec 1969

17. J. C. Daley et al., "Sea-Clutter Measurements on Form Frequencies," NRL Report 6806, Naval Research Laboratory, 29 Nov 1968

18. M. Katzin, "On the Mechanisms of Radar Sea Clutter," Proc. IRE 45 (1957)

19. M. Skolnik, "A Review of Radar Sea Echo," NRL Memorandum Report 2025, Naval Research Laboratory, Jul 1969

20. N. I. Durlach, "Influence of the Earth's Surface on Radar," Technical Report 373, Lincoln Laboratory, MIT, 18 Jan 1965, AD 627635

21. C. R. Burrows and S. S. Atwood, Radio Wave Propagation, National Defense Research Committee on Propagation, Academic Press (1949)

22. R. L. Smith-Rose and A. C. Strickland, "An Experimental Study of the Effect of Meterological Conditions Upon the Propagation of Centimetric Radio Waves," Meterological Factors in Radio Wave Propagation The Physical Society (London) 18 (1946)

23. P. J. Rubenstein, et al., "Microwave Transmission Over Water and Land under Various Meterological Conditions," Report 547, Radiation Laboratory, MIT, 13 Jul 1944

24. R. F. Jones, "Low Level Atmospheric Ducts," Nature 163 (1949)

25. V. W. Pidgeon, "Frequency Dependence of Radar Ducting," Technical Memorandum, Applied Physics Laboratory, JHU, 9 Jun 1969

26. G. D. Smith, "Preliminary Report on Results Obtained from the Radar Ducting Experiment at Wallops Island, Va.," Technical Memorandum, Applied Physics Laboratory, JHU, 6 Apr 1970

27. V. W. Pidgeon, "X-band Height-Gain Profiles with an Oceanic Duct," Technical Memorandum, Applied Physics Laboratory, JHU, 24 Jul 1970

DOCUMENT CONTROL DATA - R & D

(Security classification of title, body of abstract and indexing annotation must be entered when the overall report is classified)

1. ORIGINATING ACTIVITY *(Corporate author)*	2a. REPORT SECURITY CLASSIFICATION
Engineering Experiment Station Georgia Institute of Technology Atlanta, Georgia 30332	Unclassified
	2b. GROUP

3. REPORT TITLE

Aids-to-Navigation Radar Requirements

4. DESCRIPTIVE NOTES *(Type of report and inclusive dates)*

Technical Report No. 1

5. AUTHOR(S) *(First name, middle initial, last name)*

Wayne Rivers

6. REPORT DATE	7a. TOTAL NO. OF PAGES	7b. NO. OF REFS
31 January 1971	v + 62	27

8a. CONTRACT OR GRANT NO.	9a. ORIGINATOR'S REPORT NUMBER(S)
DOT-CG-10657-A	
b. PROJECT NO.	
c.	9b. OTHER REPORT NO(S) *(Any other numbers that may be assigned this report)*
d.	

10. DISTRIBUTION STATEMENT

None

11. SUPPLEMENTARY NOTES	12. SPONSORING MILITARY ACTIVITY
Georgia Tech Project A-1277	U.S. Coast Guard Washington, D. C. 20591

13. ABSTRACT

The specifications of a stereotype maritime radar are assembled from a concensus of currently deployed radars for use with models of radar performance to define desired radar properties of a new series of navigation buoys. Model elements considered include detection thresholds in noise and clutter backgrounds, diffraction and duct propagation modes near the sea surface and shadowing by sea waves. Recommended buoy cross sections and estimates of detection ranges and probability of detection are given.

14 KEY WORDS	LINK A		LINK B		LINK C	
	ROLE	WT	ROLE	WT	ROLE	WT
Buoy	8					
Navigation	4					
Maritime	5					
Radar	10					
Mathematical Models	1					
Propagation	6					
Diffraction	6					
Ducting	6					
Sea Clutter	6					
Cross Section	2					

ELECTRICAL DESIGN DATA FOR NAVIGATION BUOYS

by

Gene K. Huddleston and Wayne Rivers

15 June 1971

Technical Report No. 2

on

Georgia Tech Project A-1277

Prepared For
United States Coast Guard
Washington, D. C. 20591
Contract DOT-CG-10657-A
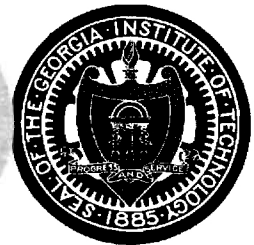
1971

Engineering Experiment Station
GEORGIA INSTITUTE OF TECHNOLOGY
Atlanta, Georgia

GEORGIA INSTITUTE OF TECHNOLOGY
Atlanta, Georgia   30332

ELECTRICAL DESIGN DATA
FOR
NAVIGATION BUOYS

by

Gene K. Huddleston

and

Wayne Rivers

15 June 1971

Technical Report No. 2

on

Georgia Tech Project A-1277

Prepared for

ELECTRICAL DESIGN DATA FOR NAVIGATION BUOYS

Gene K. Huddleston and Wayne Rivers

ABSTRACT

The electrical design of plastic buoys containing passive radar reflectors for use in radar navigation is discussed. The specific buoy configuration considered consists of a cylindrical homogeneous wall of uniform thickness (Radome) enclosing an octahedral radar reflector with the internal space filled with a low-density dielectric foam. Design data are presented to aid in the determination of optimum wall thicknesses and thickness tolerance for a number of candidate buoy wall materials. Computed performance data showing the reduction in radar cross section of the enclosed reflector due to the radome and filling for three orientations of the buoy are presented. A simplified flat-panel model of the radome/reflector system is developed which predicts with acceptable accuracy the wall transmission loss as a function of thickness and dielectric properties of the materials.

TABLE OF CONTENTS

LIST OF FIGURES

LIST OF TABLES

I. INTRODUCTION

Plastic buoys with internal radar reflectors are being developed by the U.S. Coast Guard. The transmission loss of the buoy wall for microwaves affects the buoy performance as a radar aid to navigation, and therefore this loss must be considered in buoy design. It is the purpose of this report to present design data to allow the selection of optimum buoy wall thicknesses and the estimation of acceptable tolerances and consequent radar signal loss.

The buoy design contemplated consists of a cylindrical homogeneous wall (shell) of uniform thickness enclosing the radar reflector. The reflector is octahedral, formed by three square or elliptical plates intersecting at right angles. The reflector is to be inserted with two opposite faces normal to the (vertical) cylinder axis and, therefore, with six faces visible in the horizontal plane. The interior of the buoy is to be filled with low density plastic foam, hereafter referred to as the core. Wall materials being considered include ABS, acrylic, Nylon 6, polyethylene, glass reinforced polyester, and polyvinylchloride. The filling material is anticipated to be polyurethane foam with a density of 3 to 5 $\#/ft^3$. The combination of shell and filling core are referred to in this report as the radome.

Radar signal loss of a dielectric shell is determined by the relative dielectric constant, ϵ_{rs}, and loss tangent, $\tan \delta_s$, of the shell and by the geometric variables, the shell thickness , d, the incidence angle, θ, and polarization angle, α_p. (The subscript s denotes shell parameters; later the subscript c will be used to denote core parameters.) Relative maxima and minima of transmission loss occur as wall thickness is increased, which leads to the concept of optimum wall thickness. This concept is discussed quantitatively in Chapter II. The values of ϵ_{rs} and $\tan \delta_s$ typical of the candidate materials are summarized as well as the impact of variations of wall thickness from the optimum value. In Chapter III, the average radar signal loss is discussed, where the averages are taken over the buoy geometry for various azimuth, tilt and radar polarization angles. Appendix A includes the equations

1

used in wall loss calculations and graphs of the one-way transmission factors useful in thickness tolerance estimation. Appendix B comprises an analysis of the corner reflector cluster enclosed in a cylindrical radome which yields a measure of the reduction in radar cross section of the reflector due to the radome.

The results of this study of buoy electromagnetic design can be summarized as follows. Homogeneous cylindrical shell thicknesses are recommended which are multiples of a half-wavelength, calculated using Equation (1) on Page 4. A value for n, the number of half wavelengths, of 1 is recommended, but a value of 2 is also feasible electrically for some materials. The value of θ used in Equation (1) should be 0 degrees, which represents an acceptable approximation to the best average effective incidence angle. The values of relative dielectric constant and loss tangent are highly variable among the various materials and even among the formulations of a given plastic family, so that it is necessary to measure ϵ_r and tan δ of the particular materials being considered at the microwave band of interest before a design is finalized (see Section II-B). Tolerance assignment on the nominal wall thickness can be made using the curves of Appendix A and interpolation techniques; deviation of wall thickness from nominal should be controlled as discussed in Section II-C.

Exploration of the average radar signal loss of the buoy radome was performed considering the various incidence angles, buoy tilt, azimuth and polarization angles. These figures were compared with the loss estimated for a plane dielectric wall with foam backing, and it was concluded that the plane-sheet formulas predicted the transmission loss within about 0.2 dB. This plane-wall model results in considerable simplification in the procedure required for estimation of average loss compared to the exact equations and tedious integrations required. The loss mechanisms are ranked as follows, beginning with the most serious:

1. Mismatching of the reflection coefficients of the shell at the front and rear surfaces. This loss is controlled primarily by $\sqrt{\epsilon_{rc}}$ of the core foam material.

2. Dissipation in the foam core. This loss is controlled by the product $\sqrt{\epsilon_{rc}} \cdot$ tan δ_c.

3. Dissipation in the shell material. This loss is controlled by the product $\sqrt{\varepsilon_{rs}}\tan \delta_s$.

4. Defocussing by the curved shell and cylindrical core lens.

The principal design compromise available to offset the radar signal loss of the buoy radome is reflector size. It is estimated that only small increases in size (< 10%) over that of an open reflector will offset the radome loss with careful designs for materials which have loss tangents less than 0.01; materials with the higher loss tangents may require reflector size increases of up to 20% to offset the radome loss. From the standpoint of electrical properties alone, the materials are loosely ranked beginning with the best as follows:

1. ⌠Polyethylene
2. ⌡ABS
3. Acrylic
4. ⌠PVC
5. ⌡Nylon
6. Glass reinforced polyester

This ranking corresponds roughly to the order of increasing loss tangent, which dominates the resulting radome loss.

II. OPTIMUM WALL THICKNESS

A. Criteria for Choice of Wall Thickness

The concept of an optimum wall, or shell, thickness is useful because for some thicknesses the reflection of a electromagnetic wave from the front surface of a dielectric panel is cancelled in part by the reflection from the rear surface. The thickness at which the cancellation is greatest is a function of the free space wavelength (λ_o), the relative dielectric constant (ϵ_{rs}), and the angle of incidence between the ray and the surface normal (θ). The optimum thickness is given by equation (1) for a plane, homogeneous dielectric sheet surrounded by free space [1].

$$d_{opt} = \frac{n\lambda_o}{2\left[\epsilon_{rs} - \sin^2\theta\right]^{\frac{1}{2}}} \quad , \quad 0 \leqq n \tag{1}$$

Clearly, there is no unique best thickness for a given wavelength and dielectric constant when the wall is cylindrical, because a range of incidence angles is encountered. The value of thickness chosen, therefore, must represent a compromise giving the lowest average loss over the incidence angles which are important.

The index, n, in equation (1) corresponds to the number of half wavelengths in the wall thickness. The lowest loss occurs for n = 1 (except for the impractical case of n = 0), and for n $\geqq$ 2 greater minimum losses will be experienced because of dielectric dissipation. However, structural considerations may make the choice of n = 2 attractive, and its use should be considered practical. Some values of d_{opt} are plotted in Figures 1 and 2 against incidence angle and dielectric constant. Values of d_{opt} are obtained from Figures 1 and 2 for n > 1 by multiplying d_{opt} read by n. It is seen that the optimum thicknesses vary more slowly with angle for the higher dielectric constants than for lower ones. The graphs indicate the dependences of thickness, but a precise choice of best thickness requires knowledge of the dielectric

4
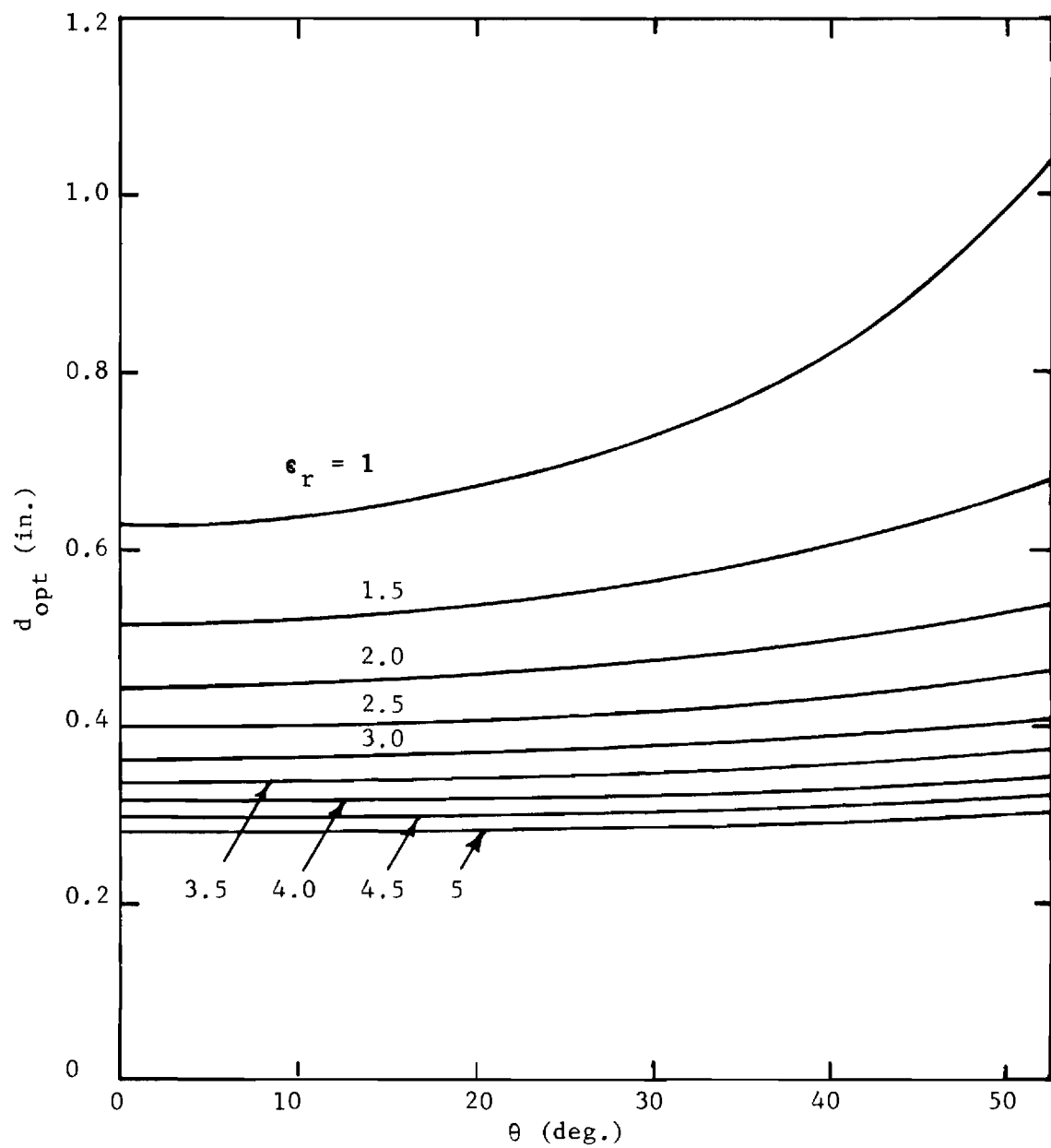
Figure 1. Optimum Wall Thickness at Various Incidence Angles.
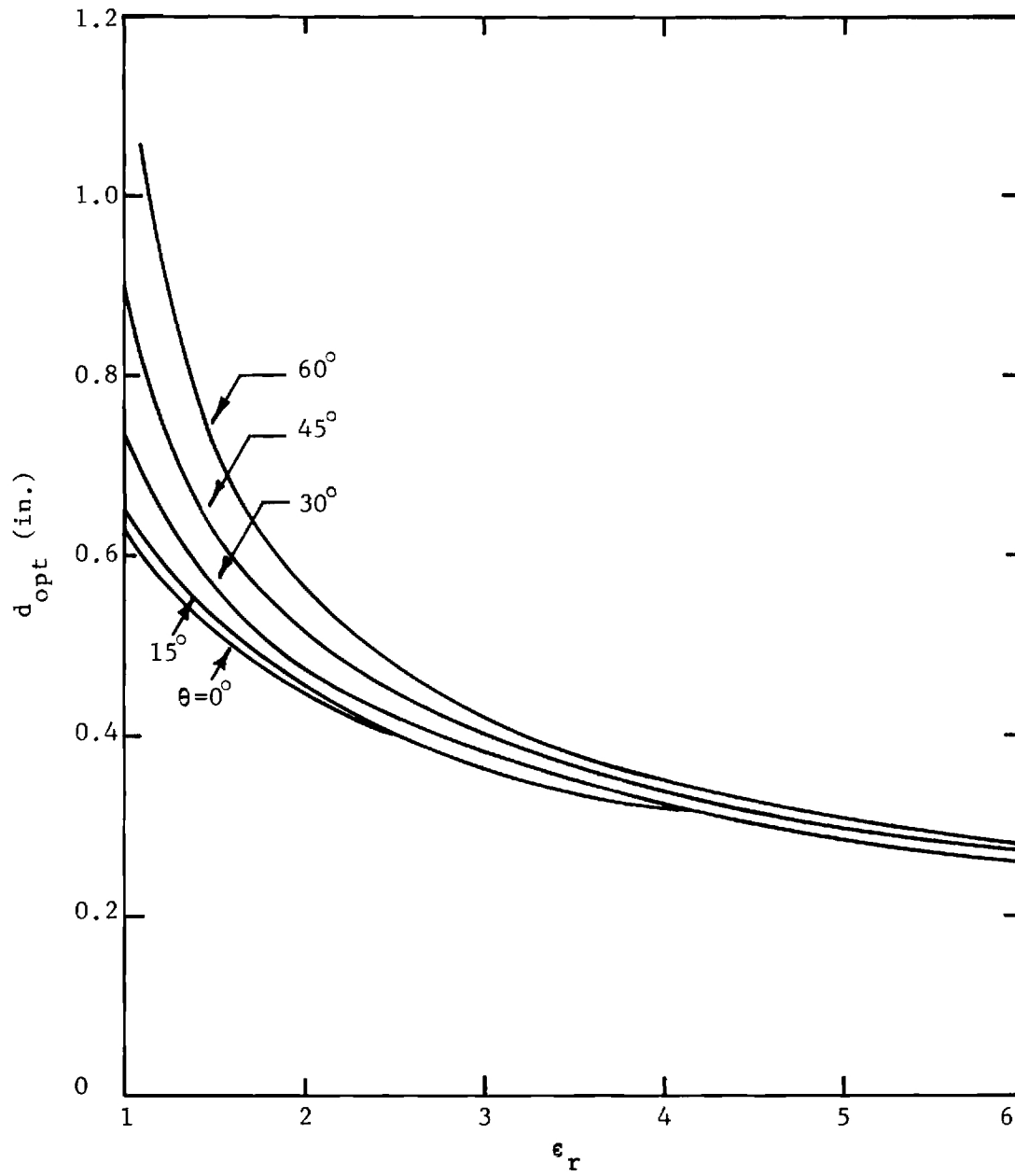
Figure 2. Optimum Wall Thickness as a Function of Dielectric Constant.

constant of the material being considered and definition of a weighted average incidence angle. Dielectric properties are discussed in the next section.

The appropriate value of θ to use in equation (1) is not at all intuitively obvious. However, the data presented in Figure 3 provides a sound basis for concluding that $\theta = 0$ degrees is the appropriate value to use to obtain the optimum thickness, d_{opt}, of the shell. In Figure 3, the reduction in the radar cross section of the corner reflector cluster due to the radome is plotted as a function of θ used in equation (1) for the two combinations of relative dielectric constant and loss tangent of the shell shown under each graph. The method used to compute the data in Figure 3 is discussed fully in Chapter III and Appendix B. For later reference, it is noted that the computations were carried out for a cylindrical shell of outer radius $\rho_1' = 22.5$ inches and a core dielectric specified by $\varepsilon_{rc} = 1.07$, $\tan \delta_c = 0.0002$. The cylindrical buoy was oriented to present the largest radar cross section under static sea conditions (referred to later as Orientation #1). The microwave frequency of 9.350 GHz (X-band) was used in these and all computations made during this study.

It is concluded that $\theta = 0$ leads to a value of optimum thickness which gives a loss which is effectively as low or lower than for other values near zero. This conclusion represents a useful simplification for this buoy design problem, but it should not be generalized without testing. For, in radome designs in which large incidence angles are encountered an appreciable fraction of the time, setting $\theta = 0$ may not be appropriate.

B. Microwave Properties of Candidate Materials

Radar signal loss is most strongly affected by the two primary electrical parameters, the relative dielectric constant, ε_{rs}, and the loss tangent, $\tan \delta_s$, of the radome wall material [1,2]. These two parameters control the optimum wall thickness, the loss for a given thickness, and the phase delay added by the wall. They have different values among different materials and even among the formulations of a given type of plastic. Both properties are dependent on frequency and temperature.

7
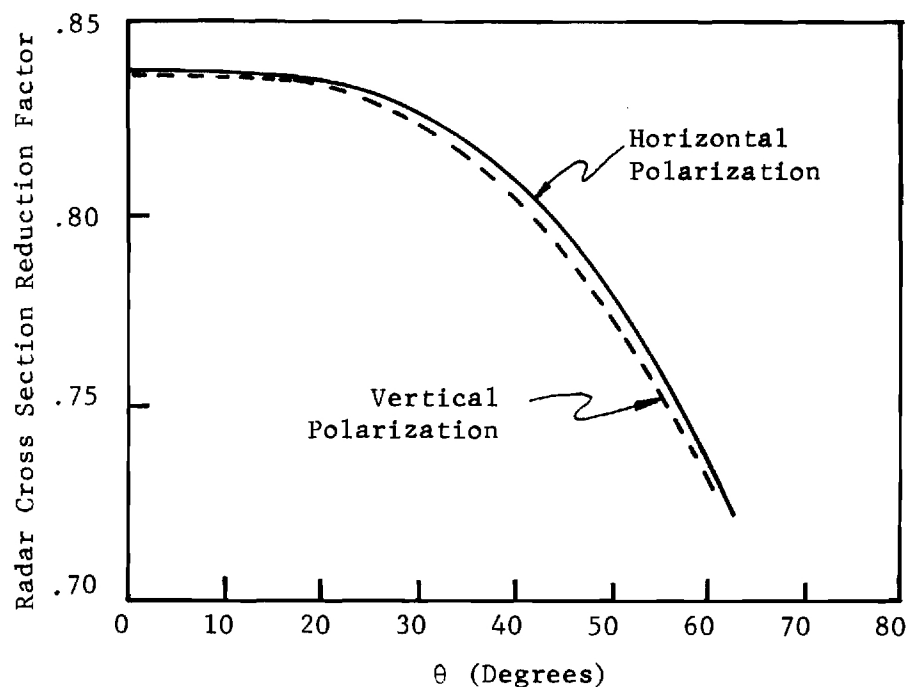
(a) $\epsilon_{rs} = 2.76$, $\tan \delta_s = 0.0045$; $\epsilon_{rc} = 1.07$, $\tan \delta_c = 0.0002$
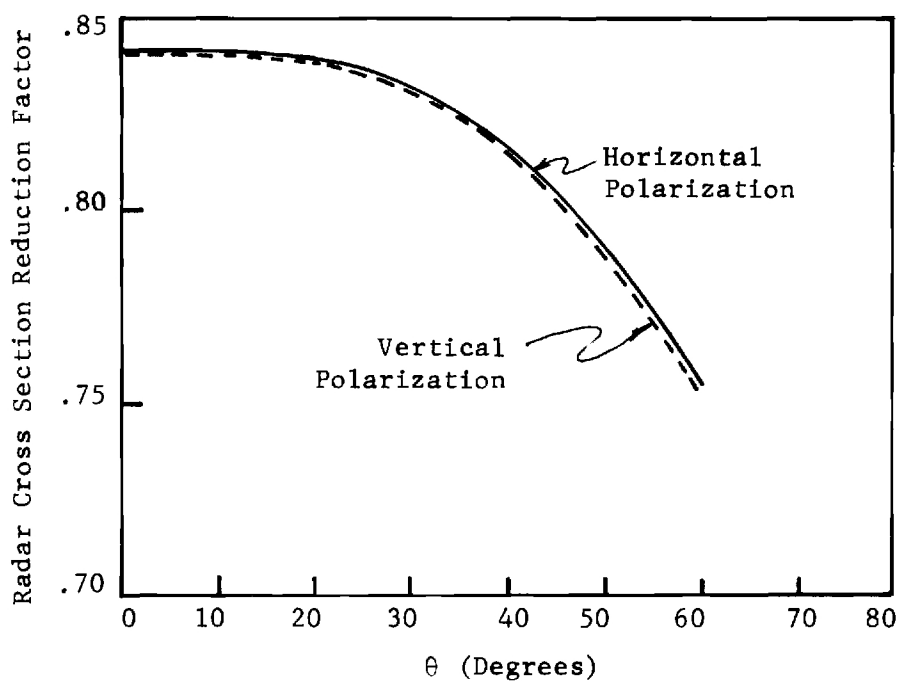
(b) $\epsilon_{rs} = 4.26$, $\tan \delta_s = 0.0040$; $\epsilon_{rc} = 1.07$, $\tan \delta_c = 0.0002$

Figure 3. Radar Cross Section Reduction Factor Versus
θ in Equation (1) For Two Shell Materials
(Half Wavelength Thickness).

8

The most extensive source of data on microwave properties of plastics is that of Reference 3. From that reference, it can be concluded that the variability of ϵ_{rs} and tan δ_s can be considerable within the formulations of a given plastic type. This variability is summarized by the envelopes specified in Table I and Figure 4. These summaries express the domain of ϵ_{rs} and tan δ_s for the six candidate shell materials from X-band data at a nominal temperature of 20°C. The domains shown are not to be interpreted such that no modern formulations will be encountered outside their bounds, for the epoch of the data set from which they were drawn is several years ago. The numbers in the rectangular domains of Figure 4 are used for easy reference to these domains in later discussions.

From the data of Reference 3 and the tolerance considerations of the next section, it can be concluded that the temperature dependence of ϵ_r and tan δ is not serious. Further, no sure way is seen to infer the X-band values from data taken at low frequencies, because the rate of decrease with increasing frequency is widely variable among the various plastic types.

The variability of the data of Reference 3 among the different formulations coupled with the tolerance considerations of the next section imply that data obtained previously on a controlled standard formulation or obtained currently on new plastic forms should be available for use in the wall design process.

The above conclusion is not necessarily as harsh with respect to the foam filler, or core, material. The low ratio of plastic-to-air volumes of foam materials results in only a weak dependence of its dielectric properties on the parent material, provided the key independent property is taken to be the density of the foam. That is, plastic foams with the same density will have approximately the same values of ϵ_{rc} and tan δ_c whether polystyrene, polyurethane or polyethylene. The values for a 4-#/ft^3 foam are expected to be 1.07 and 0.0002 for ϵ_{rc} and tan δ_c, respectively. Substantial departure from these values might result if the parent materials depart appreciably from the characteristics typical of the types mentioned, especially in the case of larger tan δ_c.
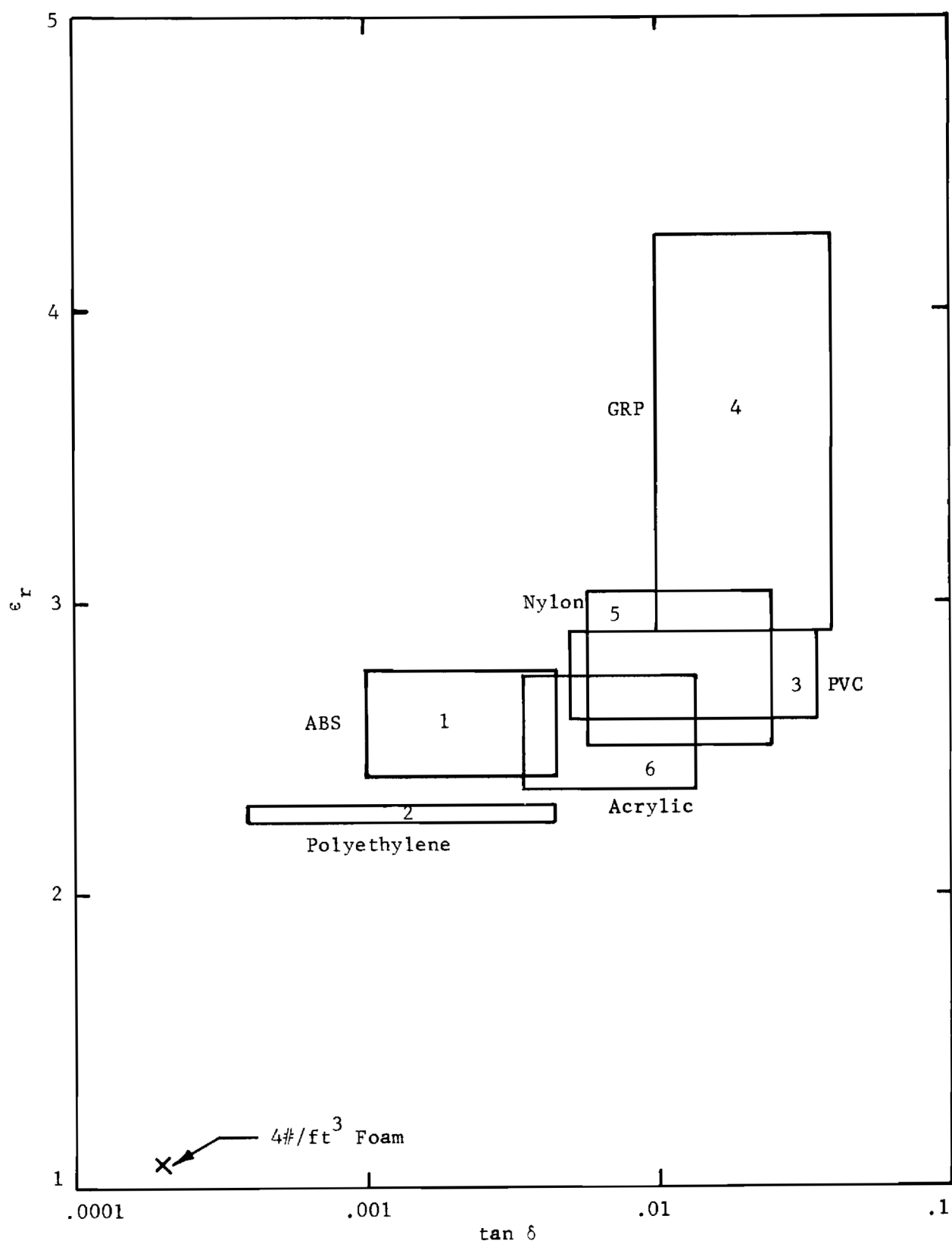
Figure 4. Domain of Dielectric Properties of Candidate Shell Materials.

10

Table I. Dielectric Properties of Candidate Shell Materials[1]

Material	Range of e_r	Range of tan δ	Mean Values[2]
ABS	2.40 - 2.76	0.001 - 0.0045	2.58/0.0028
Acrylic	2.36 - 2.75	0.0034 - 0.0135	2.56/0.0085
Nylon	2.50 - 3.03	0.0057 - 0.025	2.77/0.0154
Polyethylene	2.24 - 2.31	0.0004 - 0.0044	2.28/0.0024
Polyvinyl-chloride	2.60 - 2.90	0.005 - 0.035	2.75/0.020
Glass reinforced Polyester	2.91 - 4.26	0.01 - 0.04	3.59/0.025

Notes: 1. Principal source is Reference 3

2. Format: e_r/tan δ

11

The dielectric constant and loss tangent will scale for other densities of foam as follows:

$$\epsilon_{rc} \simeq 1 + 0.02 \, \rho_c \qquad\qquad (2)$$

$$\tan \delta_c \simeq 10^{-4}(1.7 + 0.07 \, \rho_c), \qquad \rho_c < 40, \qquad (3)$$

where ρ_c is in units of $\#/\text{ft}^3$. The formula for loss tangent is not expected to remain valid below 1 $\#/\text{ft}^3$, where the loss tangent drops more rapidly than equation (3) predicts.

C. Wall Thickness Tolerance

Deviations in nominal thickness of a wall from the optimum value are tolerable, but there is a penalty of increased radar signal loss. The establishment of thickness tolerance requires information about the loss as a function of thickness and a criterion on maximum acceptable loss. In Figure 5 is plotted percent transmitted power as a function of wall thickness for both polarizations and for incidence angles of 0, 15, 30, 45 and 60 degrees. The values of ϵ_r and tan δ assumed are 3.03 and 0.0128, respectively, which are for a panel of a particular formulation of Nylon. Other similar plots are collected in Appendix A.

The ordinate of Figure 5 is $100|T|^2$, where T is the one-way transmission factor. Thus, radar (two-way) signal loss in dB, L', is found from

$$L' = -20 \log \left\{ |T|^2 \right\}, \qquad\qquad (4)$$

where the convention that loss factors be greater than unity (having positive logarithms) is retained by the negative. In the figures the incidence angle labels are not shown explicitly, but the curves can be identified easily by the following rules. There is one curve on each graph that is identical for both parallel and perpendicular polarization; it corresponds to an incidence angle of 0 degrees. For perpendicular polarization and thicknesses between

12

the optimum values, the transmission factor decreases monotonically with increasing incidence angle. Hence, the curve for 60 degrees incidence fluctuates most widely of those plotted for perpendicular polarization. For parallel polarization, the transmission factor increases monotonically from 0 toward the Brewster angle, which is near 60 degrees for the materials considered here. Thus, the ordering of the curves is unambiguous except in the vicinity of the optimum thickness values.

The range of acceptable nominal thicknesses can be found in the following way. Suppose that a radar signal loss of 2 dB is tolerable. This corresponds to a one-way power transmission factor of about 80%. At that level, thicknesses of the material of Figure 5 in the ranges shown in Table II are allowed for the polarizations shown. A maximum incidence angle of 35 degrees is assumed consistent with the given reflector-cylindrical wall geometry. Within the ranges of thickness shown, the radar signal loss should be $\leq$ 2 dB.

Table II. Example of Allowed Thickness Ranges;
Transmission > 80%

| Polarization | Index | | |
	n = 0	n = 1	n = 2
Perpendicular	0-0.085"	0.306-0.457"	0.700-0.813"
Parallel	0-0.114"	0.255-0.468"	0.635-0.803"

In Appendix A, curves of transmission factor vs thickness are presented for values of ϵ_r and tan δ corresponding to the corners of the rectangles in Figure 4. When the values of ϵ_r and tan δ are known for a particular material of interest, the appropriate ranges of thickness acceptable for electrical purposes can be found by interpolation using the method of paragraph 25.2.66 of Reference 4.

There is no unique way of arriving at criteria for maximum acceptable transmission loss, but any valid criterion must reflect the constraints imposed by the engineering process. The principal parameter available to the designer which can compensate for the wall loss is reflector size. The

13

FIGURE 5. SINGLE LAYER TRANSMISSION EFFICIENCY

SHELL: ER=3.03 TAND=0.0129
CORE: ER=1.00 TAND=0.0000

b. PARALLEL POLARIZATION

THICKNESS IN INCHES

0.0 0.2 0.4 0.6 0.8 1.0 1.2

TRANSMITTED POWER (PERCENT)

a. PERPENDICULAR POLARIZATION

THICKNESS IN INCHES

0.0 0.2 0.4 0.6 0.8 1.0 1.2

TRANSMITTED POWER (PERCENT)
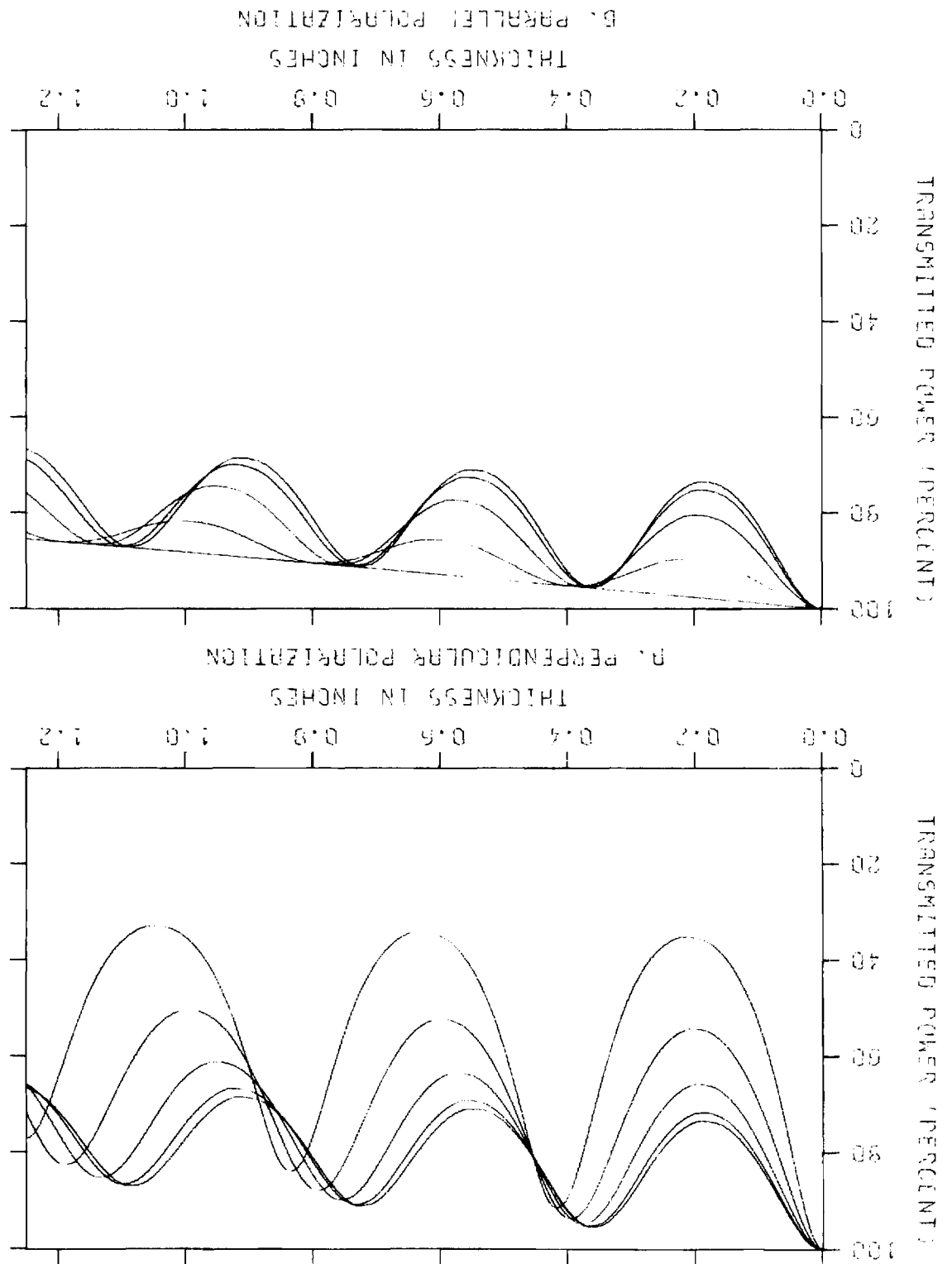
size dimension, L, which is the distance from the origin of the corner coordinate system along one principal axis to an intersection of the four plate edges, is related to the maximum radar cross section, σ_{max}, by [5]

$$\sigma_{max} = \frac{4\pi}{3} \frac{L^4}{\lambda^2} \tag{5}$$

From this equation one concludes that a 2 dB reduction in apparent cross section caused by wall loss can be compensated by an 11% increase in the linear dimensions of the reflector. The impact of a given increase in size on other buoy design considerations cannot be evaluated isolated from the total design problem, so it is not practical to advocate a specific maximum acceptable wall loss here.

In addition to the control required of the nominal thickness, the uniformity of thickness must also be controlled. The radar signal loss caused by a thickness variation over the shell area is given in terms of the r.m.s. thickness variation in Table III.

Table III. Loss Caused by Non-Uniform Shell Thickness

RMS Thickness Variation	Two-Way Loss
$0.1 \cdot \lambda_o / \sqrt{2\epsilon_r}$	0.4 dB
$0.2 \cdot \lambda_o / \sqrt{2\epsilon_r}$	1.6 dB
$0.3 \cdot \lambda_o / \sqrt{2\epsilon_r}$	3.8 dB

It can be seen from the tabulated entries that the loss in dB is proportional approximately to the square of the thickness variation. Greater thickness variation is allowed for low dielectric constant materials than for high. The first entry corresponds to a tolerance of $\pm$ 0.06 in. or $\pm$ 0.045 in. respectively for ϵ_{rs} = 2.3 and 4.0 respectively.

15

III. EFFECTS OF RADOME ON RADAR REFLECTOR CROSS SECTION

Up to this point, the design of the dielectric shell, or radome, to be used to enclose the corner reflector cluster has been based on the theory of plane wave propagation through flat dielectric panels. This is a valid approach, and it is the only practical approach to the electromagnetic design of the radome. However, the flat-panel design approach neglects the effects of the three-dimensional geometry of the radome and reflector and, for this reason, does not yield a precise measure of the performance of the corner reflector cluster when the radome is placed around it. It is highly desirable, therefore, to pursue this aspect of the problem and obtain an analytical measure of the effects of the radome on the radar cross section of the corner reflector cluster, and to verify to what accuracy the flat panel model approximates the exact buoy geometry.

Appendix B contains the details of an analysis of the corner reflector cluster enclosed by a cylindrical radome with the intervening space filled by a low-density dielectric foam material to add structural rigidity. For any given orientation of the cylindrical buoy, the analysis yields a measure of the reduction in radar cross section of the corner reflector cluster due to the relatively thin outer cylindrical shell and the low-density dielectric foam material. Since the efficiency of the radome-enclosed reflector depends on the polarization of the electromagnetic wave radiated by a distant ship antenna, reduction factors are defined for both horizontally and vertically polarized waves as follows:

$$P_H = \frac{\text{Radar Cross Section of Reflector with Radome, Horizontal Polarization}}{\text{Radar Cross Section of Reflector without Radome, Horizontal Polarization}}$$

$$P_V = \frac{\text{Radar Cross Section of Reflector with Radome, Vertical Polarization}}{\text{Radar Cross Section of Reflector without Radome, Vertical Polarization}}$$

The definitions of horizontal and vertical polarizations are made from the alignment of the electric field with the horizontal or vertical directions.

16

Note that p_H and p_V are reduction factors; i.e., the radar cross section of
the reflector with radome is obtained by multiplying the radar cross section
of the reflector without the radome by p_H (or by p_V, depending on the polari-
zation of the incident wave).

The specific cylindrical radome structure considered for the computations
is shown in Figure 6. The outer surface of the cylindrical shell is specified
in the primed coordinate system shown in the figure by

$$x'^2 + y'^2 = \rho_1'^2 \tag{6}$$

where ρ_1' is the radius of the outer surface of the shell. The thickness of
the shell is denoted by d. (The reader is referred to Appendix B for the
definitions of the coordinate systems used in the analysis.) All computations
of p_H, p_V were carried out for $\rho_1' = 22.5$ inches and the microwave frequency
of 9.350 Gigahertz.

Three orientations of the buoy were considered in the computations. The
first orientation (Orientation #1) was such that the plane wave was incident
along the y'-axis of Figure 6. Orientation #1 is referred to as a "static"
orientation inasmuch as the axis of the cylindrical buoy (z'-axis) is vertical
with respect to the sea surface. It is noted that for Orientation #1, the
largest radar cross section of the cluster is presented to the incident wave
that is available under static conditions.

The second orientation used (Orientation #2) was such that the maximum
radar cross section of the reflector (three-bounce reflection) was presented
to the incident wave. In this case, the "active area" (see Appendix B)
of the reflector is a six-sided figure. Orientation #2 was obtained by tilting
the buoy 19.47 degrees with respect to the vertical (z-axis) as shown in
Figure 8. Clearly, Orientation #2 is not a static orientation and would be
encountered only under rough sea conditions, and even then only a small
percentage of the time.

The third orientation considered (Orientation #3) was identical to
Orientation #2 except that the angle of tilt, γ_3, was only 7 degrees. This

17
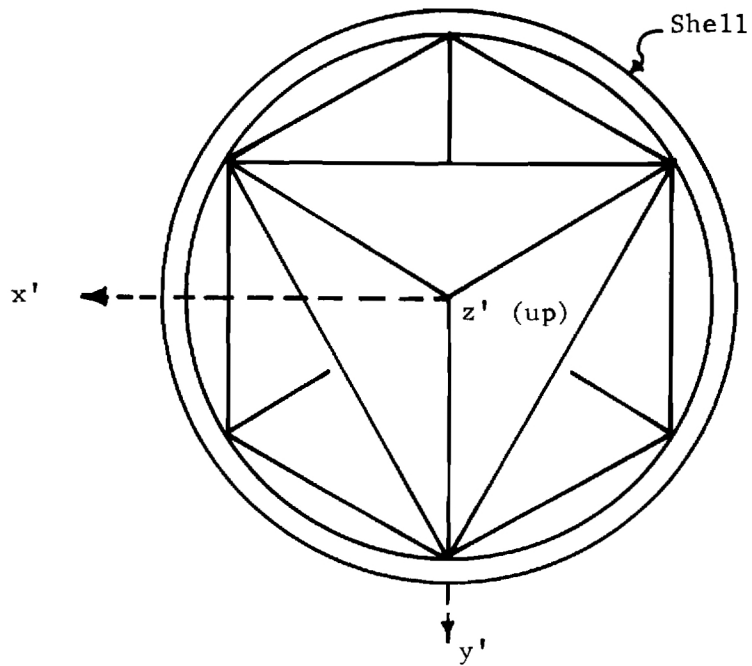
(a) Top View Showing Corner Reflector Cluster Inside.
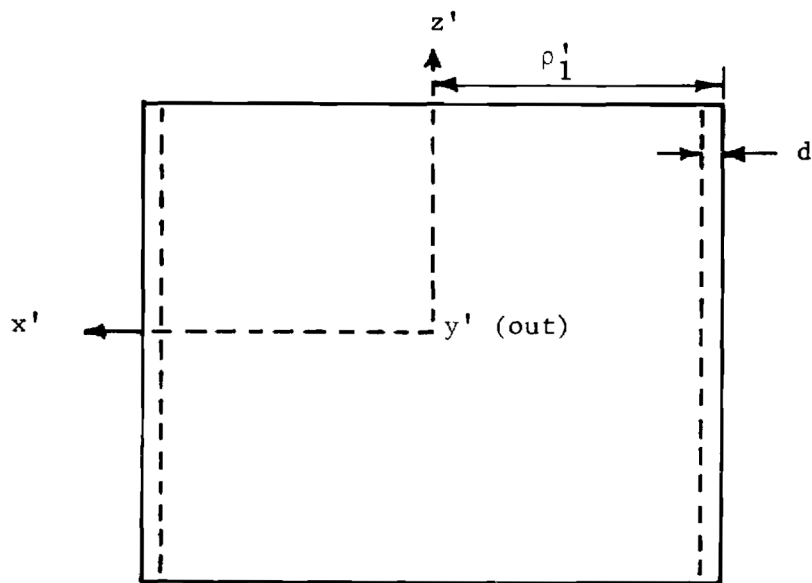
(b) Side View (Reflector Omitted).

Figure 6. Cylindrical Radome Geometry Used for Computations.

18

ORIENTATION #1

$\alpha_1 = 90°$ $\beta_1 = 180°$ $\gamma_1 = 90°$

$\alpha_2 = 0°$ $\beta_2 = 90°$ $\gamma_2 = 90°$

$\alpha_3 = 90°$ $\beta_3 = 90°$ $\gamma_3 = 0°$
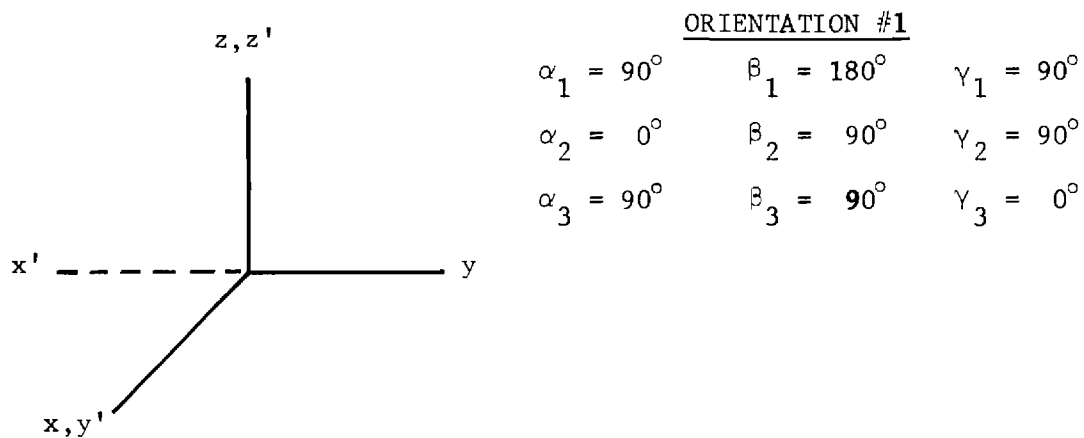
(a) Rotation of Radome Coordinate System.
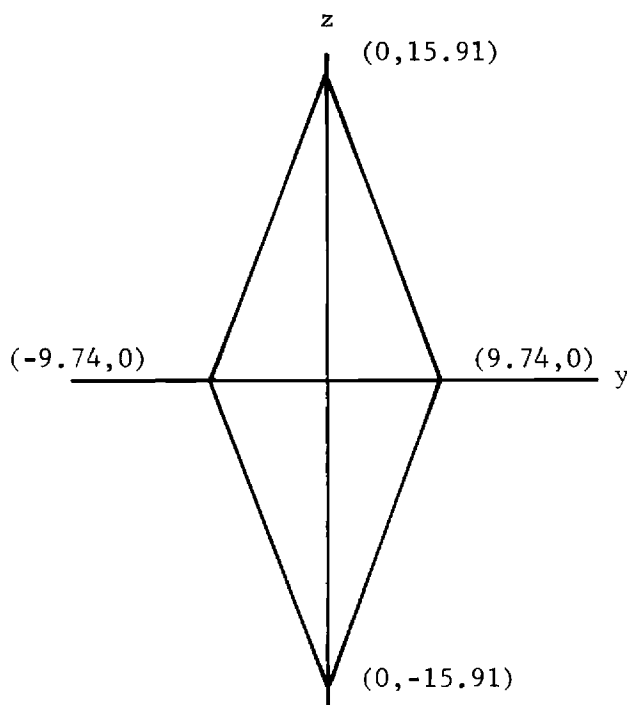
(b) Active Area in yz-Plane.

Figure 7.   Orientation of Cylindrical Buoy to Present
Largest Radar Cross Section of Corner Reflector
Cluster for Static Conditions.

19

ORIENTATION #2

$$\alpha_1 = 90° \qquad \beta_1 = 180° \qquad \gamma_1 = 90°$$

$$\alpha_2 = 19.47° \qquad \beta_2 = 90° \qquad \gamma_2 = 70.53°$$

$$\alpha_3 = 109.47° \qquad \beta_3 = 90° \qquad \gamma_3 = 19.47°$$

(y'z'-plane coincides with xz-plane)

(a) Rotation of Radome Coordinate System.

(b) Active Area in yz-Plane.
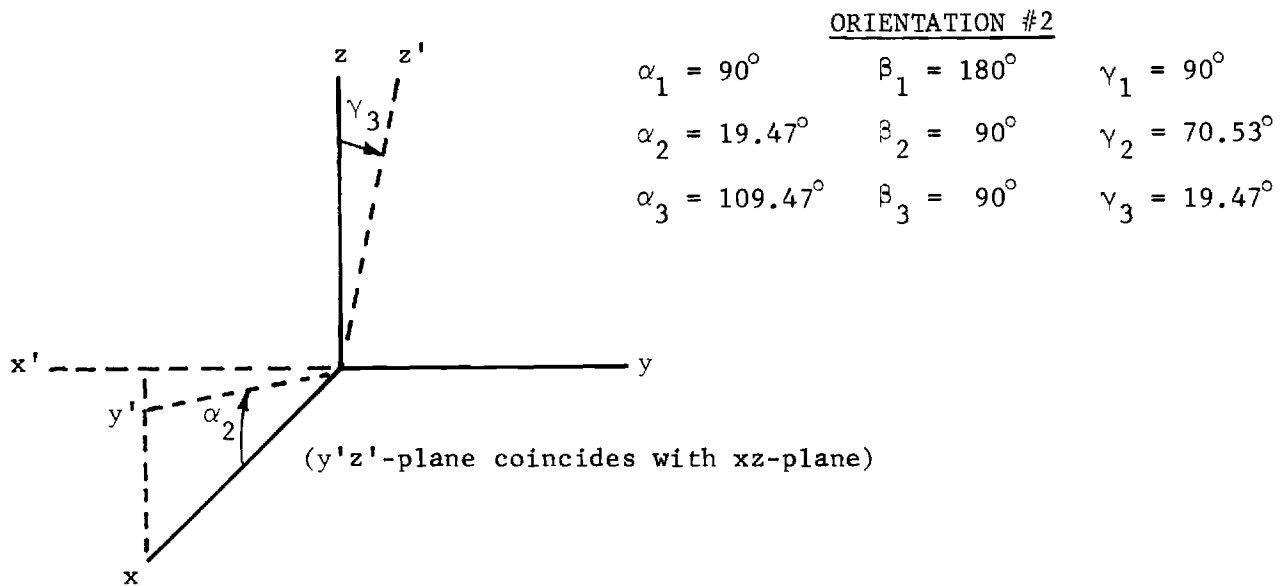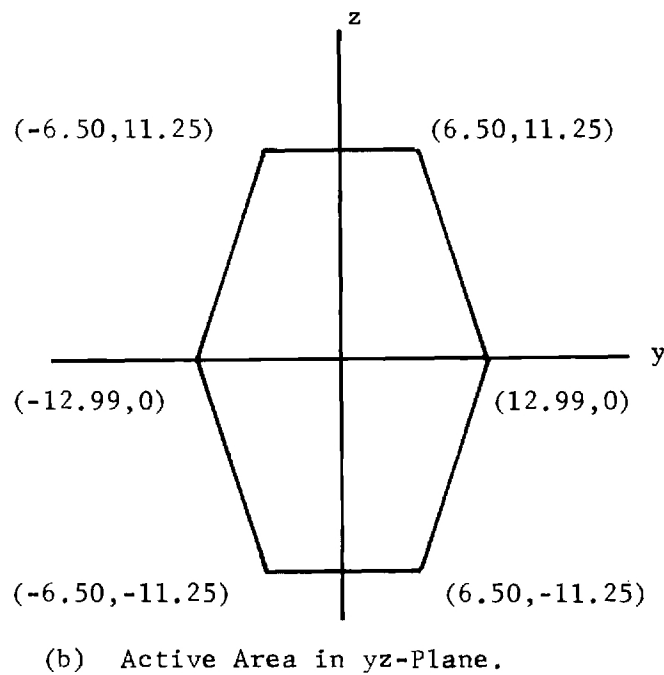
Figure 8. Orientation of Cylindrical Buoy to Present Maximum Radar Cross Section of Corner Reflector Cluster.

20

value of $\gamma_3 = 7$ degrees corresponds nominally to one standard deviation for an assumed Gaussian probability density function describing the frequency of occurrence of tilt angles. This third orientation could be expected to occur frequently under rough sea conditions; e.g., sea state 5.

It is noted that Orientations #2 and #3 are obtained from Orientation #1 by simply varying the direction angle γ_3 (or, equivalently, α_2). It is further noted that the maximum widths of the active area of the reflector are obtained for these orientations; hence, the maximum values of incidence angles of the plane wave on the cylindrical shell are also obtained. Consequently, the transmission losses associated with the cylindrical shell will have their greatest effects on reducing the radar cross section of the reflector and "worse case" conditions will prevail in the values of p_H and p_V obtained.

For Orientations #1 and #2, the quantities p_H, p_V were computed for thirty combinations of values of relative dielectric constant and loss tangent of the shell materials. These values correspond to the coordinates of the corners of the rectangles shown in Figure 4 and to the coordinates of the first moments of the rectangles. The thickness, d, of the shell was that given by Equation (1) for n = 1 and $\theta = 0$ (half-wavelength thickness at normal incidence). The computations were also carried out for n = 2 ($\theta = 0$) in Equation (1) (full wavelength thickness at normal incidence). The computations of p_H, p_V were first carried out using the following values of dielectric constant and loss tangent for the core dielectric:

$$\epsilon_{rc} = 1.07 \qquad\qquad \tan \delta_c = 0.0002$$

The computations were then repeated for a core dielectric of free space; i.e.,

$$\epsilon_{rc} = 1.00 \qquad\qquad \tan \delta_c = 0.0000$$

The purpose of using free space as the core material was to separate the effects of the core material from those of the shell.

The results of the computations are given in Tables IV-IX for Orientation #1; the results for Orientation #2 are omitted for brevity.

Figures 7 and 8 help clarify the orientations of the buoy. Referring to these tables, it is seen that there is one table for each rectangular block shown in Figure 4. The block is identified at the top of each table. Referring to Table IV, it is seen that Table IV actually consists of two parts with the upper part (Table IV(a)) applying to a half-wavelength thickness of the dielectric shell material and the lower part applying to a full wavelength thickness. Table IV (a) consists of nine rectangles with each rectangle containing four numbers. The values of relative dielectric constant and loss tangent corresponding to each rectangle in Table IV (a) are given symbolically by ERMIN, TDMIN, etc., along the left and bottom; e.g., the rectangle in the lower left corner of Table IV (a) corresponds to ϵ_r = 2.40, tan δ = 0.0010 of the shell material. The four numbers in each rectangle are the computed values of p_H and p_V. The following key is used:

(1) Upper left number: p_H for ϵ_{rc} = 1.07, tan δ_c = 0.0002
(4 #/ft^3-density foam core).

(2) Upper right number: p_V for ϵ_{rc} = 1.07, tan δ_c = 0.0002
(4 #/ft^3-density foam core).

(3) Lower left number: p_H for ϵ_{rc} = 1.00, tan δ_c = 0.0000
(free space core).

(4) Lower right number: p_V for ϵ_{rc} = 1.00, tan δ_c = 0.0000
(free space core).

The above explanation of the organization of Table IV applies to Tables V-IX as well.

Examination of the data shown in Tables IV-IX reveal some interesting results. First note that for any given value of ϵ_{rs} and tan δ_s, the radar cross section reduction factor is nearly the same for either polarization. Next, note that p_H and p_V are much stronger functions of tan δ_s than of ϵ_{rs}; the larger tan δ_s, the smaller p_H or p_V regardless of the value of ϵ_{rs}. Most importantly, note the effects of using a core dielectric of ϵ_{rc} = 1.07, tan δ_c = 0.0002 by comparing the two upper numbers in any rectangle to the two lower numbers in that same rectangle. It is seen that, in general, the effects

22

BLOCK 1 MATERIAL

(a) Half Wavelength Thickness

ϵ_{rs} / $\tan \delta_s$

	P_H / P_V (TDMIN)		P_H / P_V (TDAVG)		P_H / P_V (TDMAX)	
ERMAX	.858	.857			.837	.836
	.990	.990			.966	.965
ERAVG			.846	.845		
			.978	.977		
ERMIN	.856	.855			.836	.835
	.990	.990			.966	.966

(b) Full Wavelength Thickness

ϵ_{rs} / $\tan \delta_s$

	P_H / P_V (TDMIN)		P_H / P_V (TDAVG)		P_H / P_V (TDMAX)	
ERMAX	.834	.832			.794	.792
	.976	.974			.929	.927
ERAVG			.811	.810		
			.951	.949		
ERMIN	.830	.828			.791	.789
	.974	.973			.928	.927

Table IV. Computed Reduction in Radar Cross Section of Corner Reflector Cluster Due to Radome for Orientation #1 (See Figure 7).

23

BLOCK 2 MATERIAL

ϵ_{rs}

	P_H / P_V		P_H / P_V		P_H / P_V	
ERMAX	.859	.858			.836	.835
	.994	.994			.967	.967
ERAVG.			.847	.846		
			.980	.980		
ERMIN	.858	.858			.835	.835
	.994	.993			.967	.967
	TDMIN		TDAVG		TDMAX	

$\tan \delta_s$

(a) Half Wavelength Thickness

ϵ_{rs}

	P_H / P_V		P_H / P_V		P_H / P_V	
ERMAX	.835	.833			.791	.789
	.981	.980			.929	.928
ERAVG			.812	.811		
			.955	.953		
ERMIN	.834	.832			.790	.788
	.981	.980			.929	.927
	TDMIN		TDAVG		TDMAX	

$\tan \delta_s$

(b) Full Wavelength Thickness

Table V. Computed Reduction in Radar Cross Section of Corner Reflector Cluster Due to Radome for Orientation #1 (See Figure 7).

BLOCK 3 MATERIAL

ϵ_{rs}		P_H / P_V		P_H / P_V		P_H / P_V	
	ERMAX	.834	.833			.675	.673
		.962	.962			.777	.775
	ERAVG			.751	.749		
				.866	.865		
	ERMIN	.833	.833			.677	.676
		.963	.962			.781	.780
		TDMIN		TDAVG		TDMAX	

$$\tan \delta_s$$

(a)   Half Wavelength Thickness

ϵ_{rs}		P_H / P_V		P_H / P_V		P_H / P_V	
	ERMAX	.789	.787			.518	.515
		.922	.920			.603	.600
	ERAVG			.640	.637		
				.747	.744		
	ERMIN	.787	.785			.521	.519
		.922	.920			.609	.606
		TDMIN		TDAVG		TDMAX	

$$\tan \delta_s$$

(b)   Full Wavelength Thickness

Table VI.   Computed Reduction in Radar Cross Section of Corner Reflector Cluster Due to Radome for Orientation #1 (See Figure 7).

ϵ_{rs}

	P_H / P_V		P_H / P_V		P_H / P_V	
ERMAX	.803	.801			.636	.633
	.922	.921			.730	.726
ERAVG			.719	.717		
			.827	.825		
ERMIN	.805	.804			.651	.649
	.929	.928			.750	.748
	TDMIN		TDAVG		TDMAX	

$\tan \delta_s$

(a) Half Wavelength Thickness

ϵ_{rs}

	P_H / P_V		P_H / P_V		P_H / P_V	
ERMAX	.732	.729			.464	.460
	.849	.846			.535	.530
ERAVG			.589	.586		
			.683	.680		
ERMIN	.735	.733			.483	.480
	.858	.856			.563	.559
	TDMIN		TDAVG		TDMAX	

$\tan \delta_s$

(b) Full Wavelength Thickness

Table VII. Computed Reduction in Radar Cross Section of Corner Reflector Cluster due to Radome for Orientation #1 (See Figure 7).

26

BLOCK 5 MATERIAL

ϵ_{rs}

	P_H / P_V		P_H / P_V		P_H / P_V	
ERMAX	.830	.829			.723	.721
	.957	.957			.833	.831
ERAVG			.775	.774		
			.894	.893		
ERMIN	.829	.828			.726	.725
	.958	.958			.839	.837
	TDMIN		TDAVG		TDMAX	

tan δ_s

(a)   Half Wavelength Thickness

ϵ_{rs}

	P_H / P_V		P_H / P_V		P_H / P_V	
ERMAX	.782	.780			.595	.592
	.913	.912			.692	.689
ERAVG			.682	.679		
			.796	.794		
ERMIN	.779	.777			.598	.596
	.913	.911			.700	.697
	TDMIN		TDAVG		TDMAX	

tan δ_s

(b)   Full Wavelength Thickness

Table VIII.   Computed Reduction in Radar Cross Section of Corner Reflector Cluster due to Radome for Orientation #1 (See Figure 7).

27

ϵ_{rs}

	P$_H$ / P$_V$ (TDMIN)		P$_H$ / P$_V$ (TDAVG)		P$_H$ / P$_V$ (TDMAX)	
ERMAX	.843	.842			.786	.784
	.974	.973			.907	.905
ERAVG			.813	.812		
			.940	.939		
ERMIN	.843	.841			.786	.785
	.974	.973			.909	.908

$\tan \delta_s$

(a) Half Wavelength Thickness

ϵ_{rs}

	P$_H$ / P$_V$ (TDMIN)		P$_H$ / P$_V$ (TDAVG)		P$_H$ / P$_V$ (TDMAX)	
ERMAX	.806	.804			.700	.698
	.943	.942			.818	.816
ERAVG			.750	.748		
			.878	.876		
ERMIN	.802	.801			.699	.698
	.942	.941			.821	.819

$\tan \delta_s$

(b) Full Wavelength Thickness

Table IX. Computed Reduction in Radar Cross Section of Corner Reflector Cluster due to Radome for Orientation #1 (See Figure 7).

28

of the low-density foam core are such as to reduce the radar cross section quite drastically from the value obtained using a core dielectric of free space.

Similar computations of p_H and p_V were carried out for Orientation #2. The results of these computations show the same general trends as were observed for Orientation #1. However, the values of p_H and p_V were lower for Orientation #2 than for Orientation #1, indicating a dependency of these factors on the tilt angle γ_3. This is not an unexpected result since the incidence angles of the plane wave on the outer surface of the cylindrical shell are much larger than those for Orientation #1; hence, the transmission coefficients of the shell are lower in this case. (Additional computations for Orientation #2 in which θ in Equation (1) was varied from 0 to 60 degrees showed that the optimum shell thickness is still given by Equation (1) with $\theta = 0$ degrees.)

Using the computed values of p_H and p_V for Orientations #1 and #2 and averaging over the thirty combinations of $(\epsilon_{rs}, \tan \delta_s)$, it was found that the values of p_H and p_V for Orientation #2 can be obtained almost exactly from the corresponding values for Orientation #1 by multiplying by the "tilt factor" $p_\gamma = 0.88$.

A tilt factor of $p_\gamma = 0.98$ was found for the case of Orientation #3 ($\gamma_3 = 7$ degrees) in a manner similar to that described above. The tilt factor at $\gamma_3 = 0$ degrees is, of course, unity. Using these three values of tilt factor, an empirical relationship between tilt factor and tilt angle was surmised. This relationship is shown graphically in Figure 9. Using the curve in Figure 9, the radar cross section reduction factors may be found with good accuracy for any tilt angle between zero and 19.47 degrees by multiplying the numbers in Tables IV-IX by the tilt factor corresponding to the given tilt angle. It is believed that the simple relationship between tilt factor and tilt angle is a consequence of the cylindrical radome geometry and that similar, if not identical, relationships would hold for cylinders of radii other than the $\rho_1' = 22.5$ inches used here.
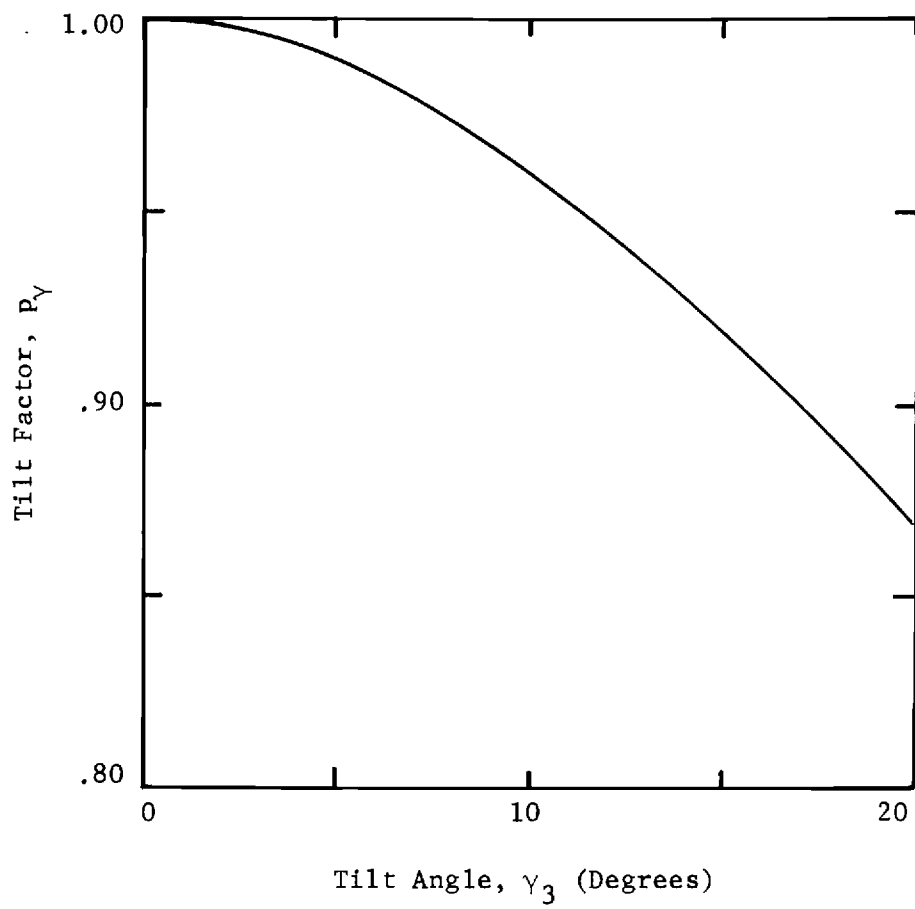
Figure 9. Empirical Relationship Between Tilt Factor
and Tilt Angle.

The introduction of the tilt factor greatly simplifies the computation of the radome/reflector performance. However, the computations of p_H and p_V for arbitrary values of shell and core parameters are quite involved. It is desirable, therefore, to derive a simple model of the radome/reflector system which yields reasonably accurate values of p_H and p_V without having to go through the lengthy computations indicated by the analysis in Appendix B. Such a model is the flat-panel model presented below.

Flat Panel Model for Performance Prediction

The flat panel model is shown in Figure 10. The incident plane wave is assumed to be normally incident on the flat dielectric panel which represents the shell. The electric field associated with each ray traversing the panel is weighted by the transmission coefficient, $T_{\perp fp}$, of the panel which is computed on the basis of an infinitely deep core dielectric backing the panel. While traveling in the core dielectric a distance $2\rho_1'$, the wave is attenuated by the factor $e^{-2\alpha_c \rho_1}$, where

$$\alpha_c = \frac{\sqrt{2} \ \pi \sqrt{\epsilon_{rc}}}{\lambda_o} \sqrt{\sqrt{1 + (\tan \delta_c)^2} - 1} \tag{7}$$

Each retro-reflected ray is weighted by the transmission coefficient of the panel upon traversing the panel from the core dielectric back into free space. Because of reciprocity, the transmission coefficient for the retro-reflected ray is the same as that of the incident ray. Noting that all retro-reflected rays are in phase on any plane parallel to the surface of the panel, the reduction in radar cross section of the reflector due to the flat panel and core material is given by

$$P_{oc} = \frac{\left| \iint_S T_{\perp fp}^2 e^{-2\alpha_c \rho_1'} \, dydz \right|^2}{\left| \iint_S dydz \right|^2} \tag{8}$$

31
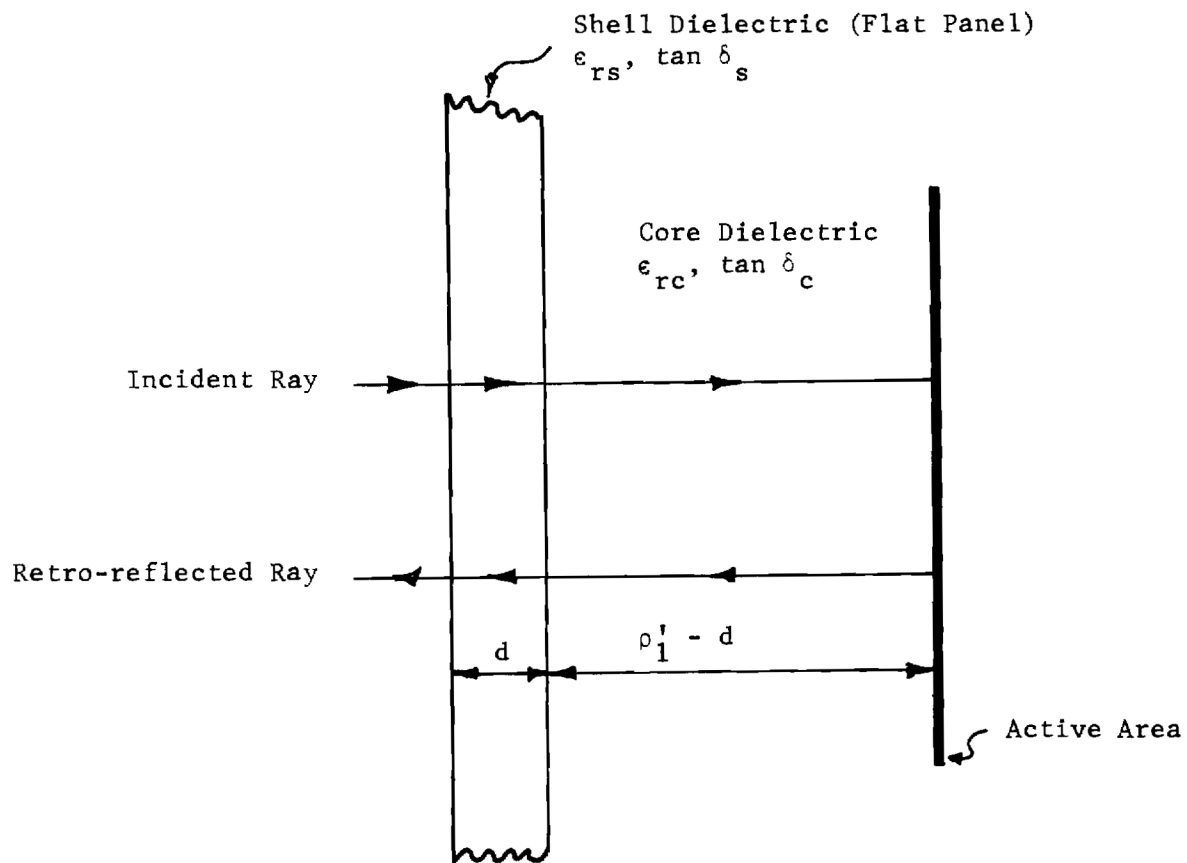
Figure 10. Flat Panel Model of Radome/Reflector System.

or, since the integrand of the numerator is independent of position (y,z) in the active area,

$$P_{oc} = \frac{\left| T_{\perp fp}{}^2 e^{-2\alpha_c \rho_1'} \right|^2 \left| \int\int_S dydz \right|^2}{\left| \int\int_S dydz \right|^2} \tag{9}$$

Cancelling common terms yields the final form of the result:

$$P_{oc} = \left| T_{\perp fp} \right|^4 e^{-4\alpha_c \rho_1'} \tag{10}$$

where α_c is given by equation (7) and ρ_1' is the radius of buoy in the same units of measure as the free space wavelength, λ_o, in equation (7).

The quantity $\left| T_{\perp fp} \right|$ can be found from the graphs of Appendix A for the combinations of $(\epsilon_{rs}, \tan \delta_s)$ and $\epsilon_{rc} = 1.07$, $\tan \delta_c = 0.0002$ for which the graphs apply. An example will illustrate the procedure. Refer to Figure A-2(a) and select the curve for normal incidence (uppermost curve). The optimum half-wavelength shell thickness is given by Equation (1) as

$$d_{opt} = \frac{.5\lambda_o}{\sqrt{\epsilon_{rs}}} = 0.407 \text{ inch} \tag{11}$$

where the value of $\epsilon_{rs} = 2.40$ is given in the figure title. The free space wavelength for the frequency $f = 9.350$ GHz is given by

$$\lambda_o = \frac{29.97925}{f(2.54)} = 1.262 \text{ inches} \tag{12}$$

Locate the point 0.407 on the horizontal scale of Figure A-2(a) and obtain the ordinate on the uppermost curve. This yields a value of approximately 99.9% for the transmitted power. Denoting the percent of transmitted power by P, the relationship between $\left| T_{\perp fp} \right|$ and P is given by

33

$$\frac{P}{100} = \left| T_{\perp fp} \right|^2 \ Re\left\{ \sqrt{\varepsilon_{rc}(1 - j \tan \delta_c)} \right\} \tag{13}$$

Using the values of ε_{rc} = 1.07, $\tan \delta_c$ = 0.0002 given in the figure title, and the value of P = 99.9, there results

$$\left| T_{\perp fp} \right|^2 = \frac{99.9}{100} \ \frac{1}{\sqrt{1.07}} = 0.962 \tag{14}$$

Squaring this result yields $\left| T_{\_fp} \right|^4$; viz.,

$$\left| T_{\perp fp} \right|^4 = 0.925 \tag{15}$$

The quantity, p_{oc}, given by equation (10) above can now be computed by multiplying $\left| T_{\perp fp} \right|^4$ by the factor $e^{-4\alpha_c \rho_1^{'}}$ = 0.95, where α_c has been computed from equation (7) using the values ε_{rc} = 1.07, $\tan \delta_c$ = 0.0002 and $\rho_1^{'}$ = 22.5 inches. There results

$$p_{oc} = (0.925)(0.955) = 0.885 \tag{16}$$

which compares favorably with the values of p_H = 0.856, p_V = 0.856 given in Table IV(a) for the cylindrical buoy case. This comparison serves as a valid check on the accuracy of the flat panel model. The small loss in accuracy introduced by using the flat panel model is more than offset by the reduction in complexity of the computations. In addition, the tilt factor can be applied to values of p_{oc} obtained using the flat panel model to find reduction factors at other tilt angles.

Transmission Factors for Other Materials

For values of ε_{rs}, $\tan \delta_s$, ε_{rc}, $\tan \delta_c$ other than those represented in the graphs of Appendix A, the quantity $\left| T_{\perp fp} \right|$ may be computed directly in the following way:

$$\begin{bmatrix} T_{fp} \\ 0 \end{bmatrix} = \begin{bmatrix} A & B \\ C & D \end{bmatrix} \begin{bmatrix} 1 \\ R_{\perp fp} \end{bmatrix} \tag{17}$$

where

$$\begin{bmatrix} A & B \\ C & D \end{bmatrix} = \frac{1}{(1 - r_{10})(1 - r_{21})} \begin{bmatrix} e^{-\gamma_s d} & -r_{10} e^{\gamma_s d} \\ -r_{10} e^{-\gamma_s d} & e^{\gamma_s d} \end{bmatrix} \tag{18}$$

$$\gamma_s = \alpha_s + j\beta_s \tag{19}$$

$$\left\{ \begin{matrix} \alpha_s \\ \beta_s \end{matrix} \right\} = \frac{\sqrt{2}\ \pi\ \sqrt{\epsilon_{rs}}}{\lambda_o} \sqrt{\sqrt{1 + (\tan \delta_s)^2} \mp 1} \tag{20}$$

$$\gamma_o = j\frac{2\pi}{\lambda_o} \tag{21}$$

$$\gamma_c = \alpha_c + j\beta_c \tag{22}$$

$$\left\{ \begin{matrix} \alpha_c \\ \beta_c \end{matrix} \right\} = \frac{\sqrt{2}\ \pi\ \sqrt{\epsilon_{rc}}}{\lambda_o} \sqrt{\sqrt{1 + (\tan \delta_c)^2} \mp 1} \tag{23}$$

$$r_{10} = \frac{\gamma_s - \gamma_c}{\gamma_s + \gamma_c} \tag{24}$$

$$r_{21} = \frac{\gamma_o - \gamma_s}{\gamma_o + \gamma_s} \tag{25}$$

$$R_{\perp fp} = -\ C/D \tag{26}$$

$$|T_{\perp fp}| = |A + BR_{\perp fp}| \tag{27}$$

This computation, to say the least, leaves much to be desired in the way of simplicity.

A computational method for obtaining an approximation to $|T_{\perp fp}|$ for the case of $d = d_{opt}$ is outlined below. The method is based on an analysis of a low-loss transmission line and yields best results for small values of $\tan \delta_s$. The order of computations is as follows:

$$\Gamma_1 = \frac{\sqrt{\epsilon_{rs}} - \sqrt{\epsilon_{rc}}}{\sqrt{\epsilon_{rs}} + \sqrt{\epsilon_{rc}}} \tag{28}$$

$$n\alpha_s \lambda_s = n\sqrt{2}\ \pi\ \sqrt{\sqrt{1 + (\tan \delta_s)^2} - 1} \tag{29}$$

(n = 1 for half-wavelength thickness; n = 2 for full wavelength thickness of the shell)

$$A = \Gamma_1\ e^{-n\alpha_s \lambda_s} \tag{30}$$

$$\Gamma_2 = \frac{\dfrac{1 + A}{1 - A} - \sqrt{\epsilon_{rs}}}{\dfrac{1 + A}{1 - A} + \sqrt{\epsilon_{rs}}} \tag{31}$$

$$|T_{\perp fp}| \approx \frac{(1 + \Gamma_1)(1 + \Gamma_2)}{1 + A} \triangleq |T_V| \tag{32}$$

(VALID FOR OPTIMUM THICKNESSES ONLY)

36

For the parameter values of the preceding example, a value of $|T_V| = 0.983$ is obtained. The true value of $|T_{\perp fp}|$ was found above to be 0.981, which is slightly less than the approximate value. Using the value of $|T_V|$ in Equation (10) and the value of $e^{-4\alpha_c\rho_1'}$ found earlier, there results

$$P_{oc} = 0.89125 \tag{33}$$

which is greater than the "exact" value given in Table IV(a), 0.856. The value of P_{oc} given by Equation (33) compares favorably with the exact value. It is emphasized that $|T_V|$ given by Equation (32) is valid **only** for optimum thicknesses of the shell and is a good approximation to $|T_{\perp fp}|$ for small values of $\tan \delta_s$; the smaller $\tan \delta_s$, the better the approximation.

In summary, it is concluded that the flat panel model of the radome/reflector system can be used to obtain a reasonably accurate estimate of the reduction in radar cross section of the reflector due to the cylindrical radome shell and low-density foam core for both horizontal and vertical polarization of the incident plane wave and for orientations of the buoy such that the return signal is due to rays undergoing a three-bounce reflection. The reduction in radar cross section, to be redundant, is given by Equation (10)

$$P_{oc} = |T_{\perp fp}|^4 e^{-4\alpha_c\rho_1'} \tag{10}$$

where $T_{\perp fp}$ is the flat panel transmission coefficient of the shell of thickness d for normal incidence and backed by an infinitely deep core dielectric medium, and ρ_1' is the radius of the cylindrical shell. The core attenuation constant, α_c, is given by Equation (7) as

$$\alpha_c = \frac{\sqrt{2}\,\pi\,\sqrt{\epsilon_{rc}}}{\lambda_o} \sqrt{\sqrt{1 + (\tan \delta_c)^2} - 1} \tag{7}$$

where ϵ_{rc} is the relative dielectric constant of the low-density foam core and $\tan \delta_c$ is the loss tangent.

It is understood that the value of p_{oc} yielded by equation (10) closely approximates the value of p_H (or p_V) that would be obtained for Orientation #1 through the computations indicated by the analysis in Appendix B. The tilt factor plotted in Figure 9 may be applied to the value of p_{oc} given by equation (10) to obtain a close approximation to p_H (or p_V) for other buoy tilt angles, γ_3.

IV. REFERENCES

1. T. E. Tice, "Techniques for Airborne Radome Design," Technical Report AFAL-TR-66-391, Air Force Avionics Laboratory, December 1966.

2. J. A. Stratton, <u>Electromagnetic Theory</u>, McGraw-Hill, 1941; Chapter 9.

3. A. R. vonHippel, <u>Dielectric Materials and Applications</u>, the MIT Press, 1954.

4. M. Abramowitz and I. A. Stegun, <u>Handbook of Mathematical Functions</u>, National Bureau of Standards, Applied Mathematics Series, 55, U. S. Government Printing Office, June 1964.

5. L. N. Ridenour, <u>Radar System Engineering</u>, McGraw-Hill, 1947, Chapter 3.

6. J. H. Richmond, "Calculation of Transmission and Surface Wave Data for Plane Multilayers and Inhomogeneous Plane Layers," Report 1751-2, 31 October 1963, Antenna Laboratory, The Ohio State University Research Foundation; prepared under Contract Number AF 33(615)-1081, Research and Technology Division, Wright-Patterson AFB, Ohio.

APPENDIX A

ONE-WAY TRANSMISSION EFFICIENCY OF PLANE DIELECTRIC PANEL

This appendix contains graphs of the transmission efficiencies of single layer, plane dielectric panels as functions of thickness, incidence angle, polarization, relative dielectric constant, and loss tangent. In each case, a plane wave is incident on the panel from free space (ε_r = 1.00, tan δ = 0.0); the exit medium consists of a low dielectric constant material (ε_{rc}= 1.07, tan δ_c= 0.0002) whose electrical properties are typical for the $\approx$ 4 lbs./cu.ft. density polyurethane foam to be used in the buoy design.

Before discussing the data shown in the graphs, it is informative to consider the manner in which the data was obtained. Consider the situation depicted in Figure A-1(a) of a perpendicularly polarized plane wave incident on the panel from free space. The plane of incidence is defined by the unit normal to the panel, $\hat{n}$, and the unit propagation vector, $\hat{k}_i$, of the incident plane wave. The electric field intensity vector, $\underline{E}_i$, is perpendicular to the plane of incidence (hence, the nomenclature "perpendicular polarization"); the angle of incidence, θ_i, is defined by

$$\theta_i = \cos^{-1}(- \hat{n} \cdot \hat{k}_i) \tag{A-1}$$

The symbols $\underline{E}_i$ and $\underline{E}_r$ represent the electric field intensities of the incident and reflected waves in the incident medium, and $\underline{E}_t$ represents the electric field intensity of the transmitted wave in the exit medium. The reflection coefficient, $R_\perp$, and the "normal" transmission coefficient, $T_\perp$, of the panel are defined by

$$R_\perp = \frac{E_r(P)}{E_i(P)} \tag{A-2}$$

$$T_\perp = \frac{E_t(Q)}{E_i(P)} \tag{A-3}$$
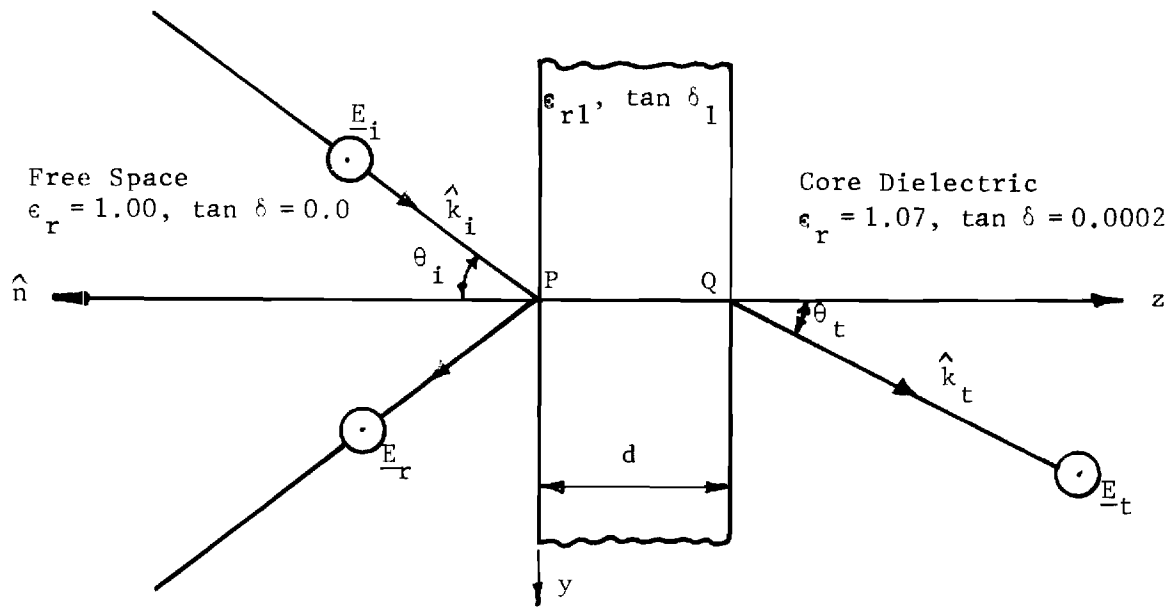
(a)   Perpendicular Polarization
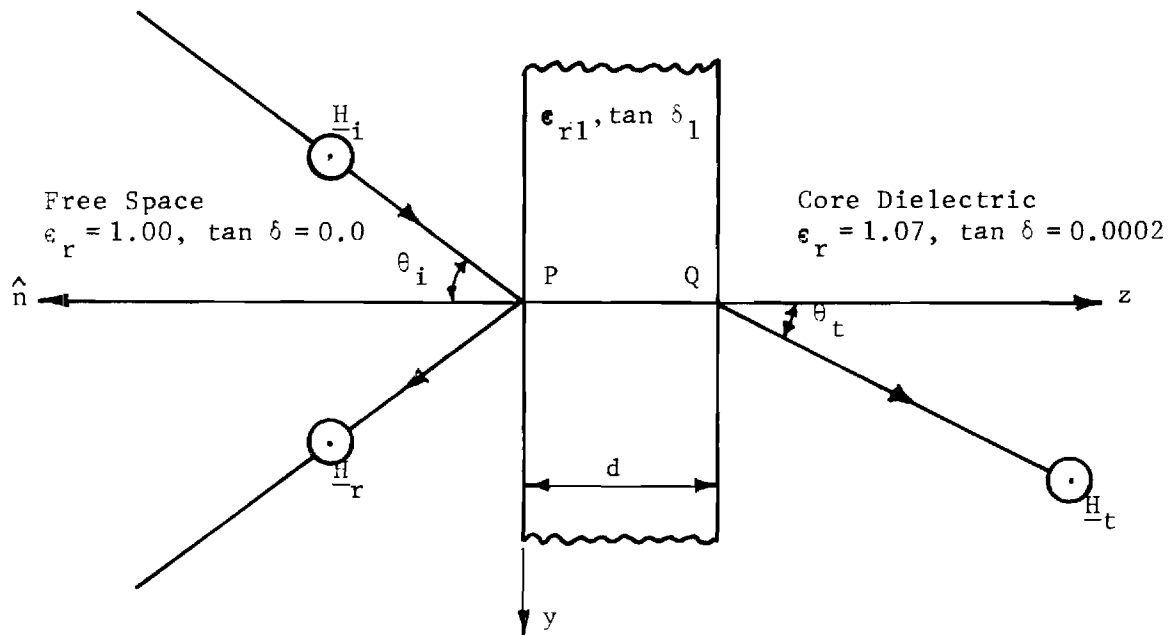
(b)   Parallel Polarization

Figure A-1.   Plane Electromagnetic Wave Incident From Free
Space on Single Layer Dielectric Panel Backed
by Low-Density Foam Core Dielectric.

41

where P represents the incident point and Q the "normal" exit point as shown in the figure.

For the case of parallel polarization ($\underline{E}_i$ lies in the plane of incidence, $\underline{H}_i$ is perpendicular to the plane of incidence) as shown in Figure A-1(b), the reflection and transmission coefficients are defined by

$$R_{\parallel} = \frac{H_r(P)}{H_i(P)} \qquad\qquad\qquad\text{(A-4)}$$

$$T_{\parallel} = \frac{H_t(Q)}{H_i(P)} \qquad\qquad\qquad\text{(A-5)}$$

Equations (A-2) and (A-3) may be interpreted as "voltage" coefficients while Equations (A-4) and (A-5) represent "current" coefficients. The relationship between $\underline{E}$ and $\underline{H}$ for plane waves enables one to rewrite Equations (A-4) and (A-5) in terms of the electric field intensities $E_r(P)$, $E_i(P)$, $E_t(P)$ to obtain the following "voltage" coefficients for the case of parallel polarization:

$$R_{\parallel V} = R_{\parallel} \qquad\qquad\qquad\text{(A-6)}$$

$$T_{\parallel V} = \frac{T_{\parallel}}{\sqrt{\dot{\epsilon}_{rt}}} \qquad\qquad\qquad\text{(A-7)}$$

where $\dot{\epsilon}_{rt} = \epsilon_{rt}(1 - j \tan \delta_t)$, and ϵ_{rt} is the relative dielectric constant of the exit medium and $\tan \delta_t$ is the loss tangent.

The calculations of $R_\perp$, $T_\perp$, $R_\parallel$, $T_\parallel$ are well documented [6]. The power transmission coefficients are defined here as the ratio $(\hat{n} \cdot \underline{S}_t / \hat{n} \cdot \underline{S}_i)$, where $\underline{S}_t$ is the real part of the Poynting vector of the transmitted plane wave and S_i is the real part of the Poynting vector of the incident plane wave. (The Poynting vector is defined as $\underline{S} = \frac{1}{2} \underline{E} \times \underline{H}$.) The power transmission coefficients of the dielectric panel are thus given by

$$\text{PTCPAR} = |T_{\parallel V}|^2 \; \text{Re}\left\{\sqrt{\dot{\epsilon}_{rt}}\right\} \frac{\cos \theta_t}{\cos \theta_i} \qquad\qquad\text{(A-8)}$$

$$\text{PTCPER} = |T_\perp|^2 \; \text{Re}\left\{\sqrt{\dot{\epsilon}_{rt}}\right\} \frac{\cos \theta_t}{\cos \theta_i} \qquad\qquad\text{(A-9)}$$

where $\theta_t = \sin^{-1} \dfrac{\sin \theta_i}{\sqrt{\epsilon_{rt}}}$ while "$| \; |$" denotes magnitude of a complex number and

42

Re $\left\{ \begin{array}{c} \\ \end{array} \right\}$ denotes the real part of a complex number. It is noted that if the exit medium is free space, the power transmission coefficients are given simply by the squared magnitudes of the voltage transmission coefficients. In any case, the transmission efficiency in percent is obtained by multi- plying (A-8) and (A-9) by 100%.

The following thirty figures are graphs of the transmission efficiencies of single layer dielectric panels, one figure for each of the combinations of relative dielectric constant and loss tangent of the panel considered. Each figure consists of two graphs: the upper graph refers to the case of perpen- dicular polarization, whereas the lower graph refers to parallel polarization. Referring to Figure A-2, it is seen that each graph consists of a family of curves. Each curve in the family is for a given angle of incidence: 0, 15, 30, 45, and 60 degrees. The ordinate of a given graph is one-way transmission efficiency in percent; the abscissa is panel thickness in inches at 9.350 GHz. Thus, each curve of a family is a plot of one-way transmission efficiency versus thickness at a prescribed angle of incidence. The ordering of the curves with respect to incidence angle is explained in Section II-C of the main body of the report. The relative dielectric constant (ER) and loss tangent (TAND) of the panel is given in the figure title under the heading "SHELL"; the term "CORE" refers to the exit medium.
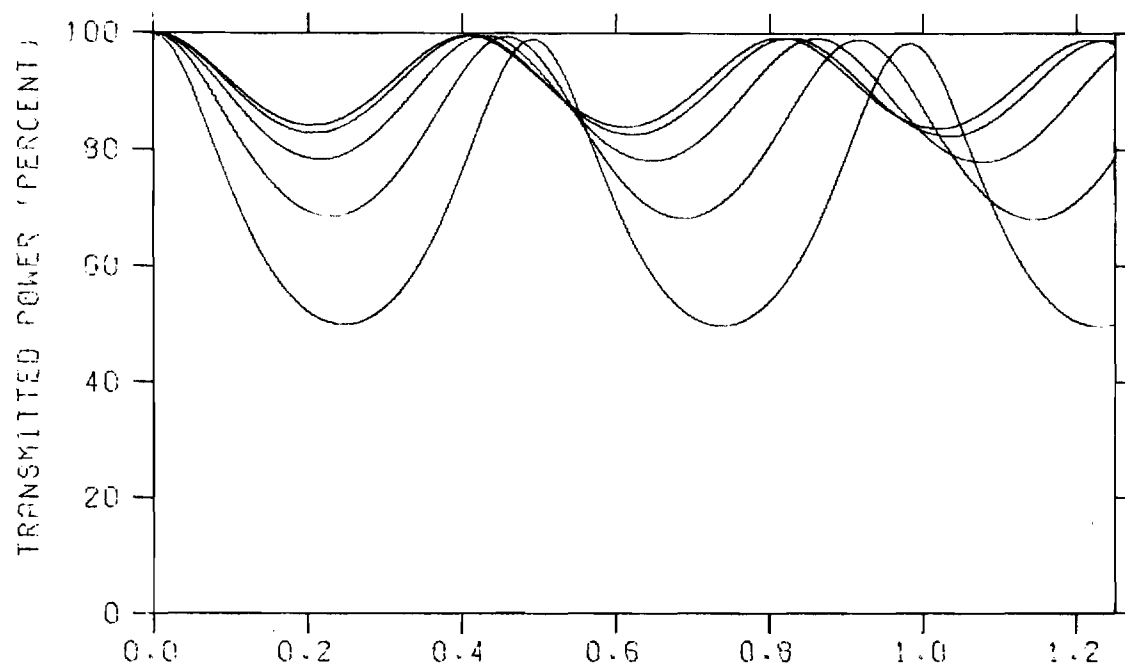
A. PERPENDICULAR POLARIZATION
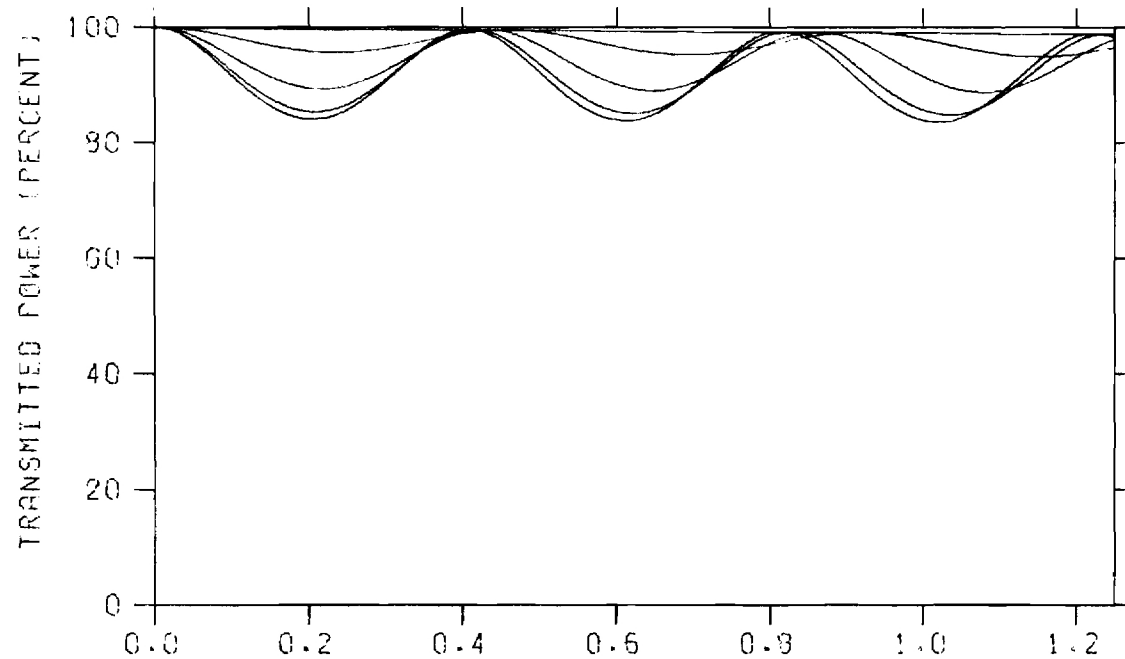
B. PARALLEL POLARIZATION

FIGURE A-2. SINGLE LAYER TRANSMISSION EFFICIENCY

SHELL: ER=2.40   TAND=0.0010

CORE: ER=1.07   TAND=0.0002

44
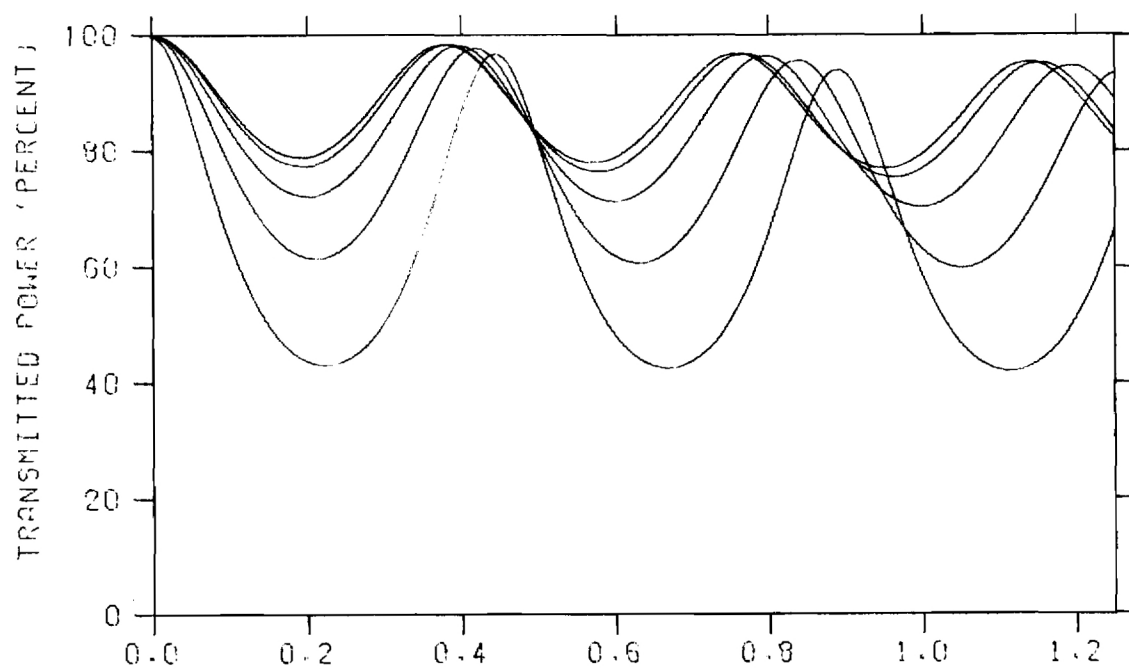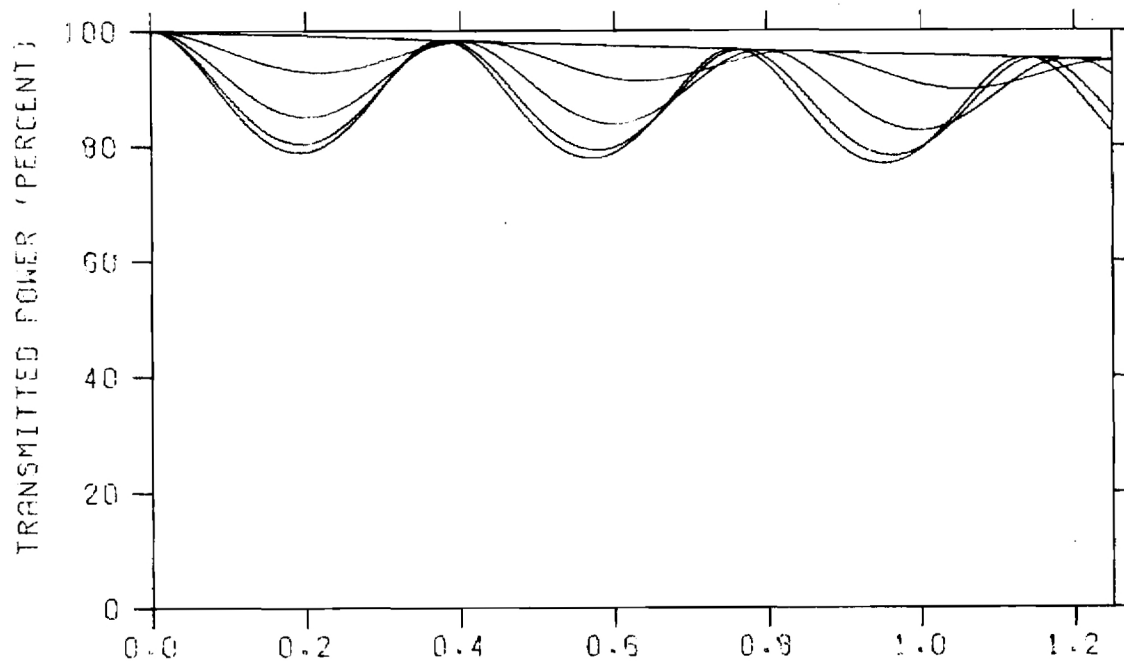
FIGURE A-3. SINGLE LAYER TRANSMISSION EFFICIENCY

SHELL: ER=2.76   TAND=0.0045
CORE: ER=1.07   TAND=0.0002
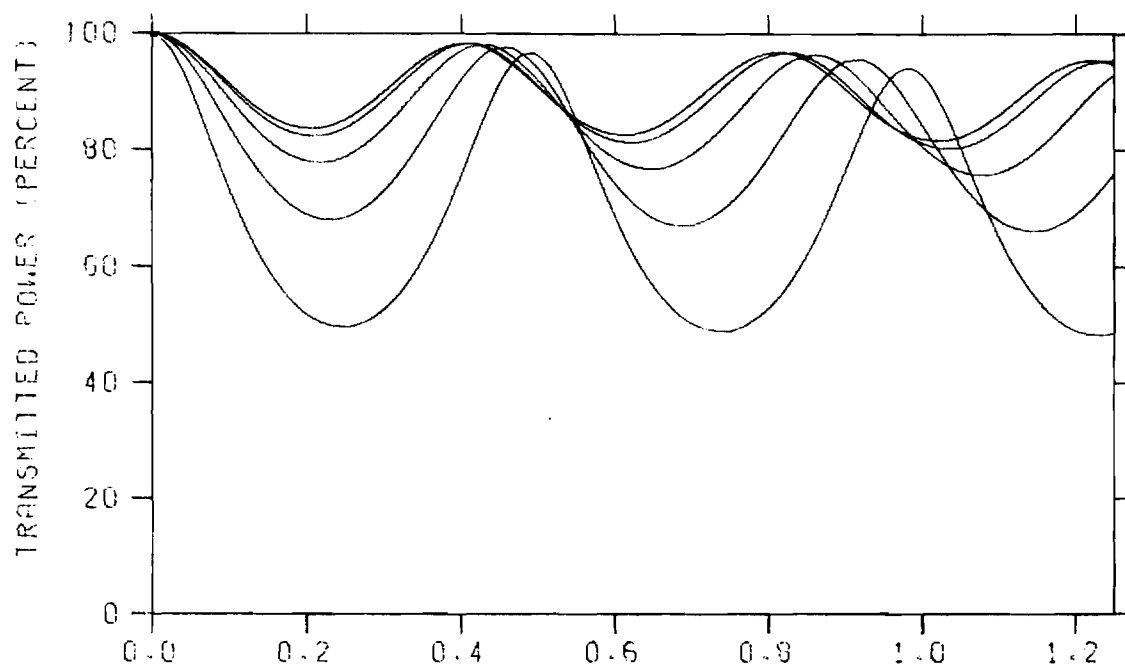
A. PERPENDICULAR POLARIZATION
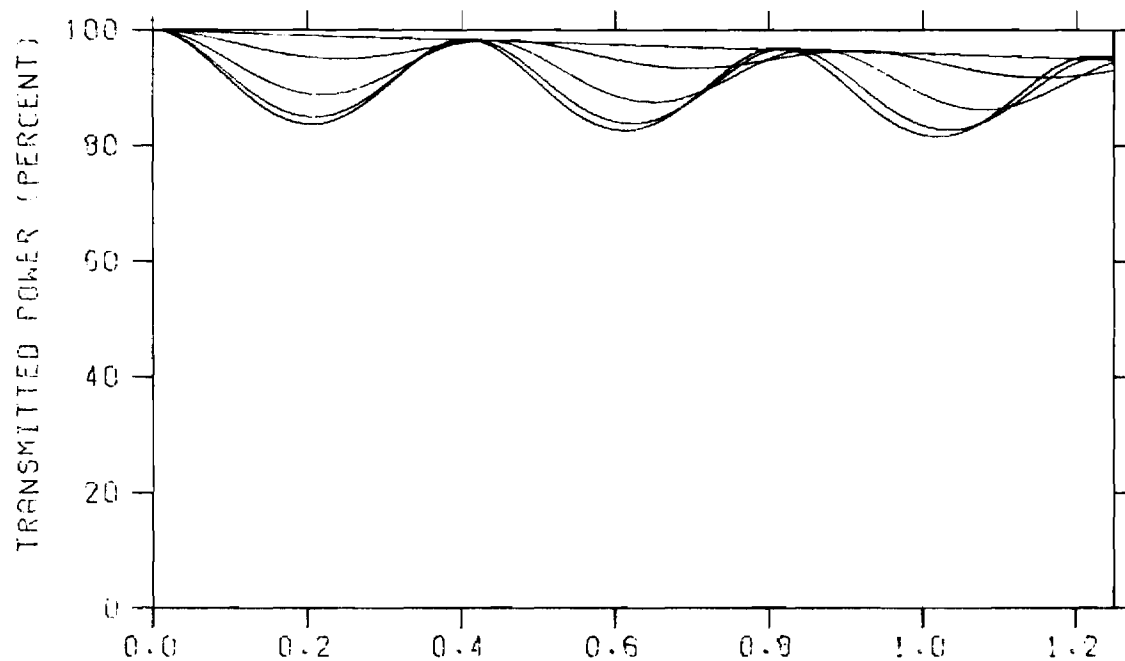
B. PARALLEL POLARIZATION

FIGURE A-4. SINGLE LAYER TRANSMISSION EFFICIENCY

SHELL: ER=2.40 TAND=0.0045

CORE: ER=1.07 TAND=0.0002

46
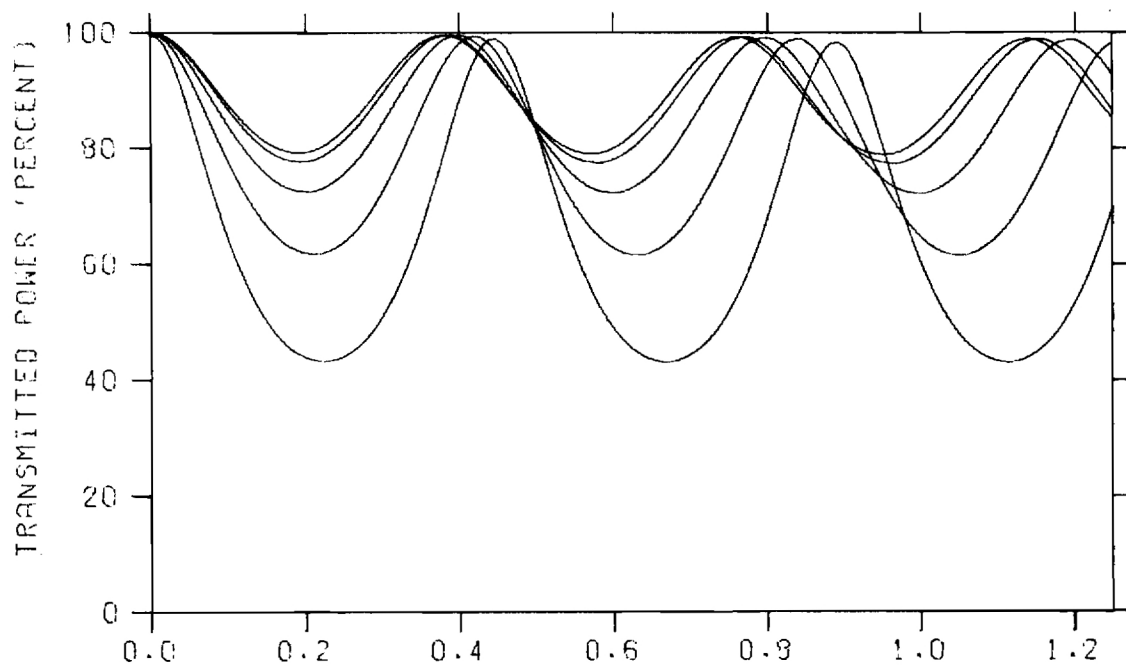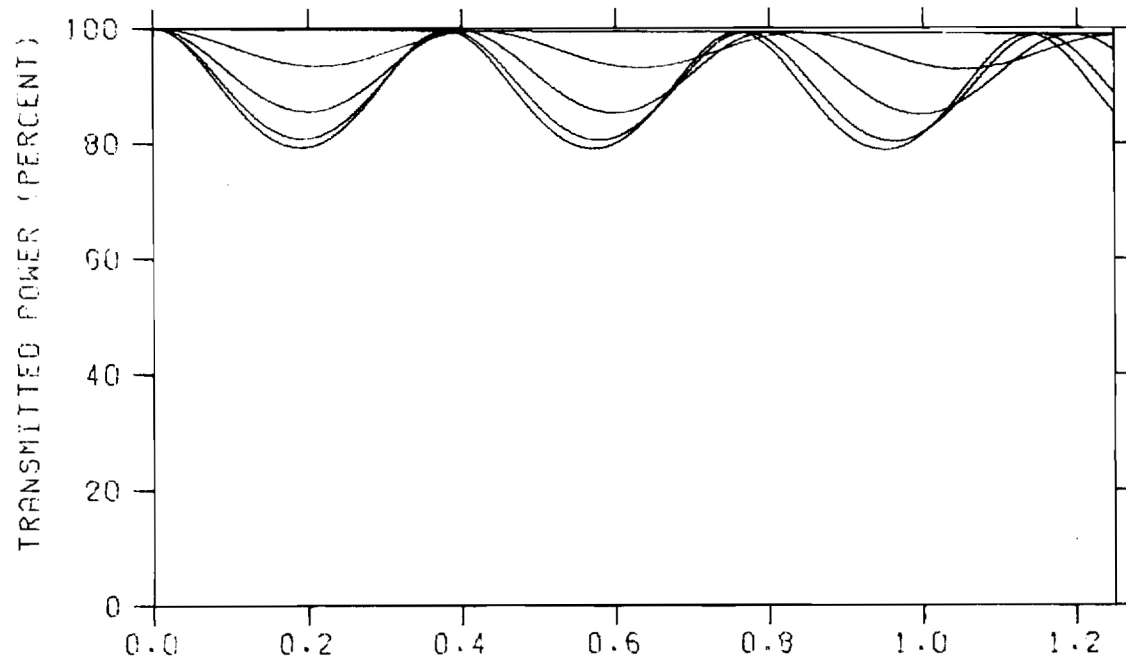
FIGURE A-5 . SINGLE LAYER TRANSMISSION EFFICIENCY

SHELL: ER=2.76 TAND=0.0010

CORE: ER=1.07 TAND=0.0002
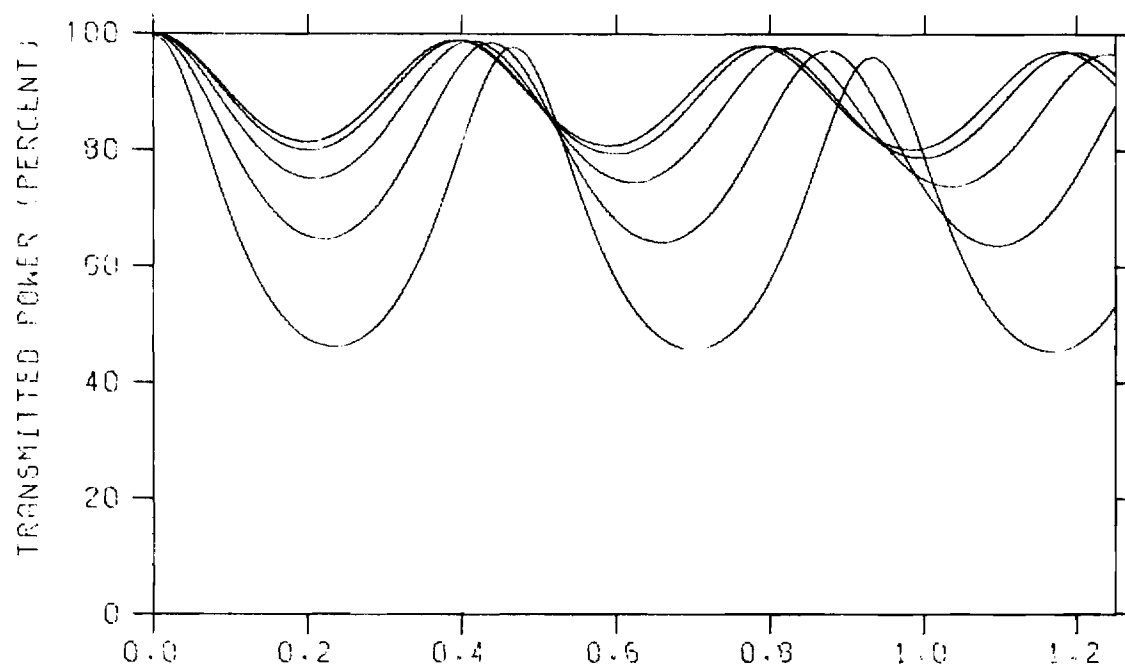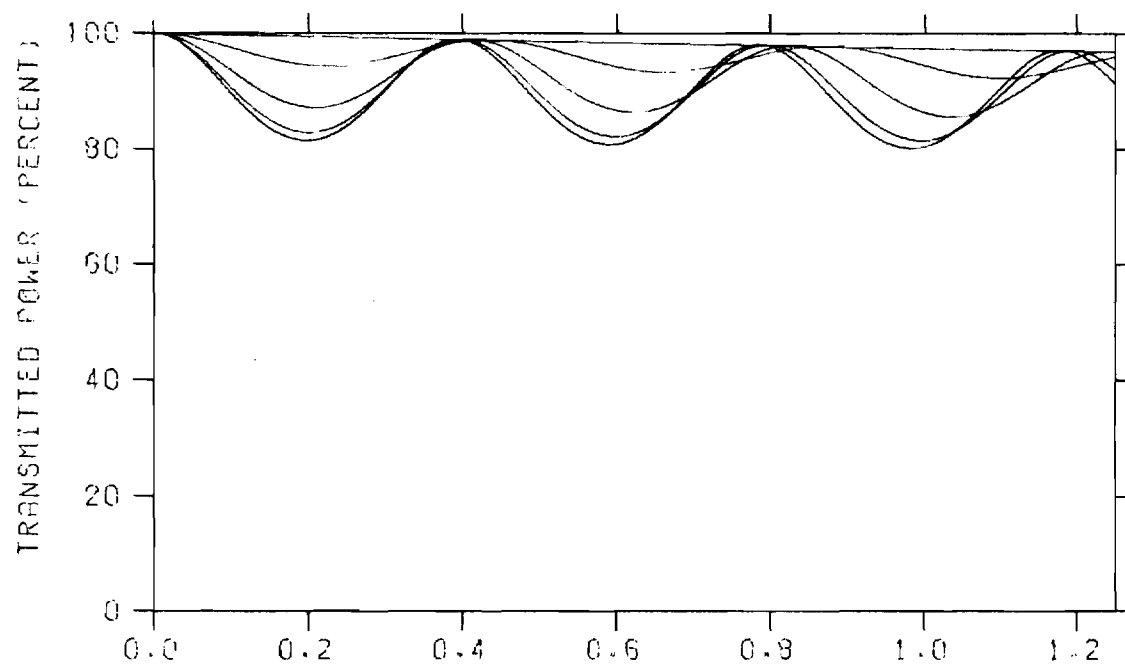
FIGURE A-6. SINGLE LAYER TRANSMISSION EFFICIENCY
SHELL: ER=2.58   TAND=0.0029
CORE: ER=1.07   TAND=0.0002
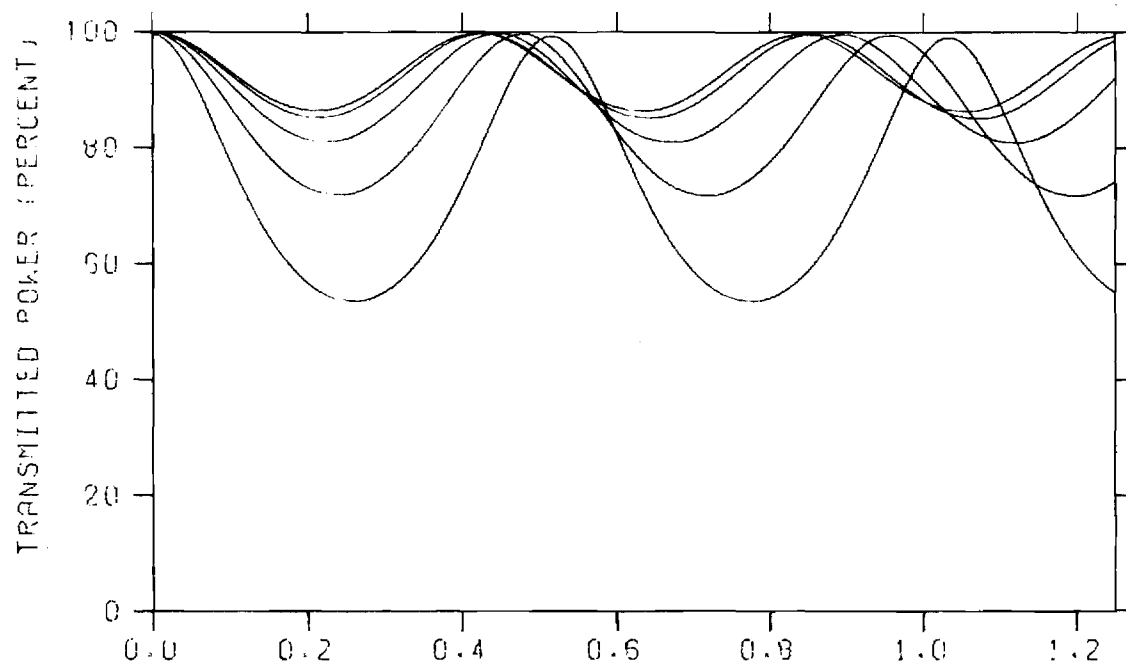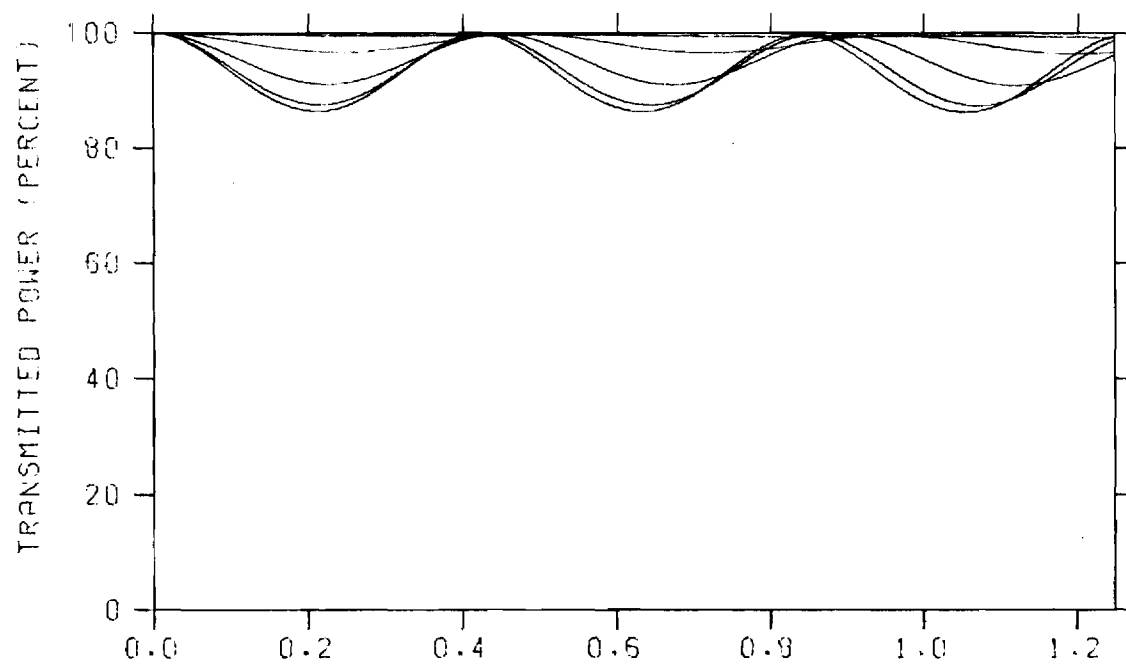
FIGURE A-7. SINGLE LAYER TRANSMISSION EFFICIENCY

SHELL: ER=2.24 TAND=0.0004

CORE: ER=1.07 TAND=0.0002
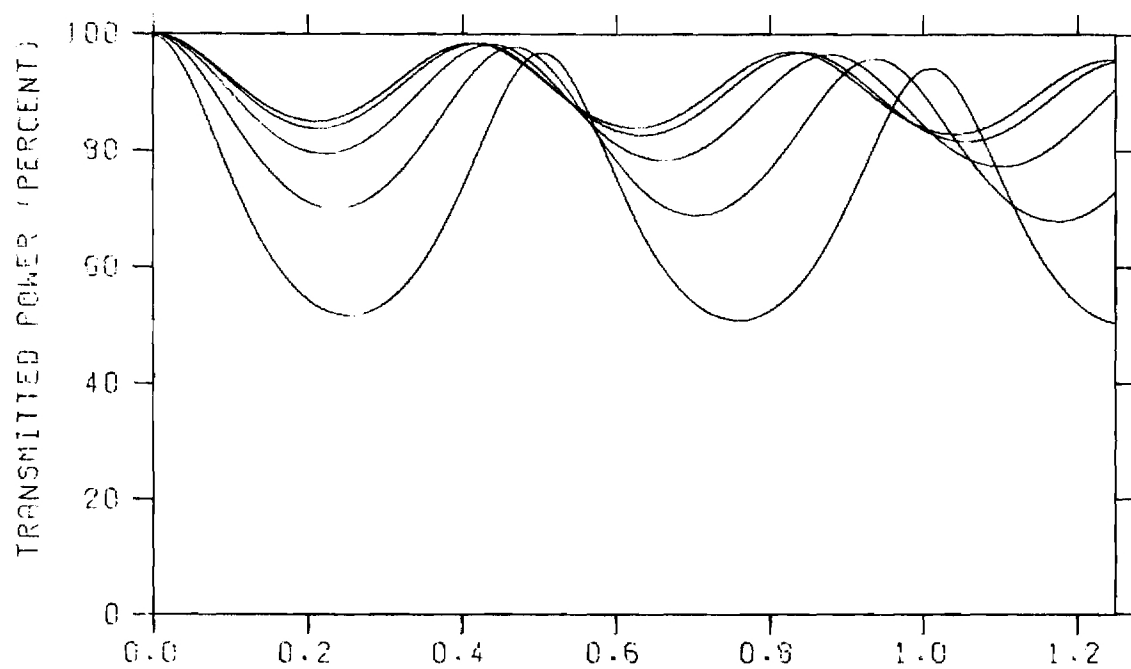
A. PERPENDICULAR POLARIZATION
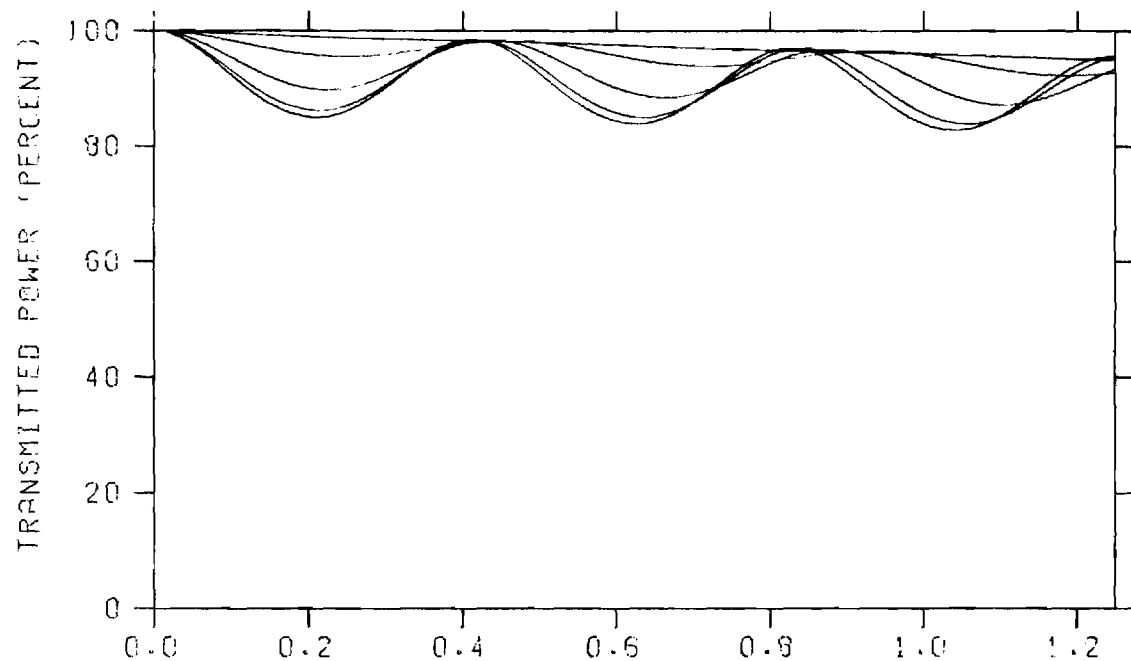
B. PARALLEL POLARIZATION

FIGURE A-8. SINGLE LAYER TRANSMISSION EFFICIENCY

SHELL: ER=2.31   TAND=0.0044

CORE: ER=1.07   TAND=0.0002

50
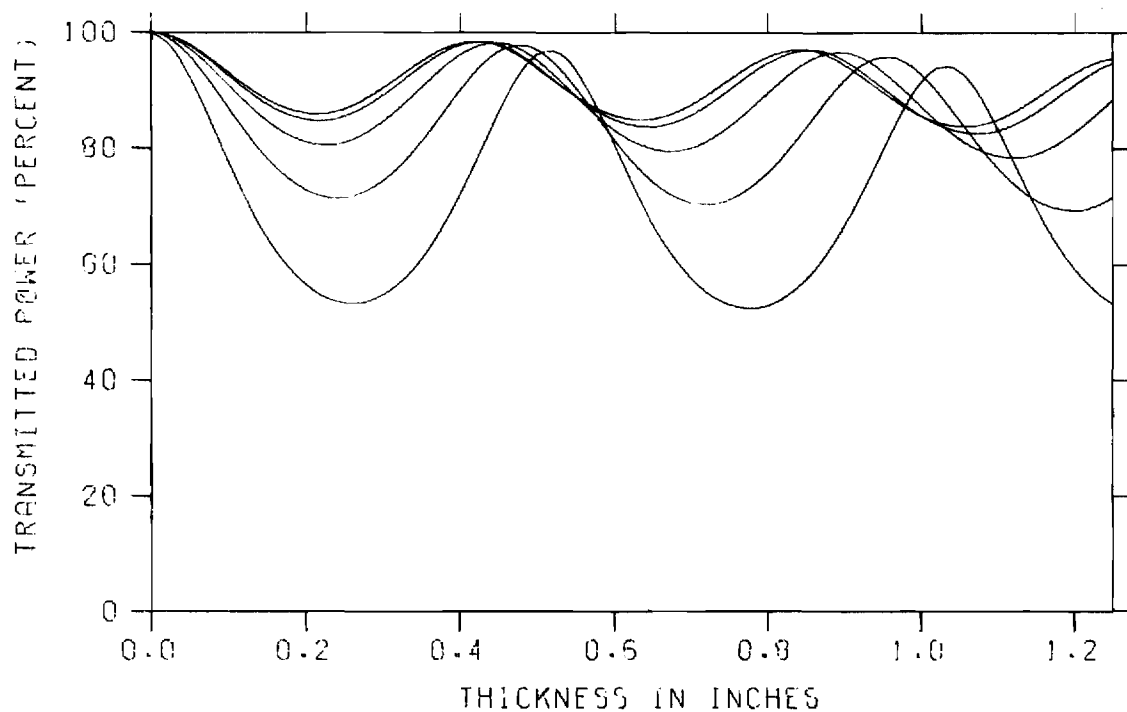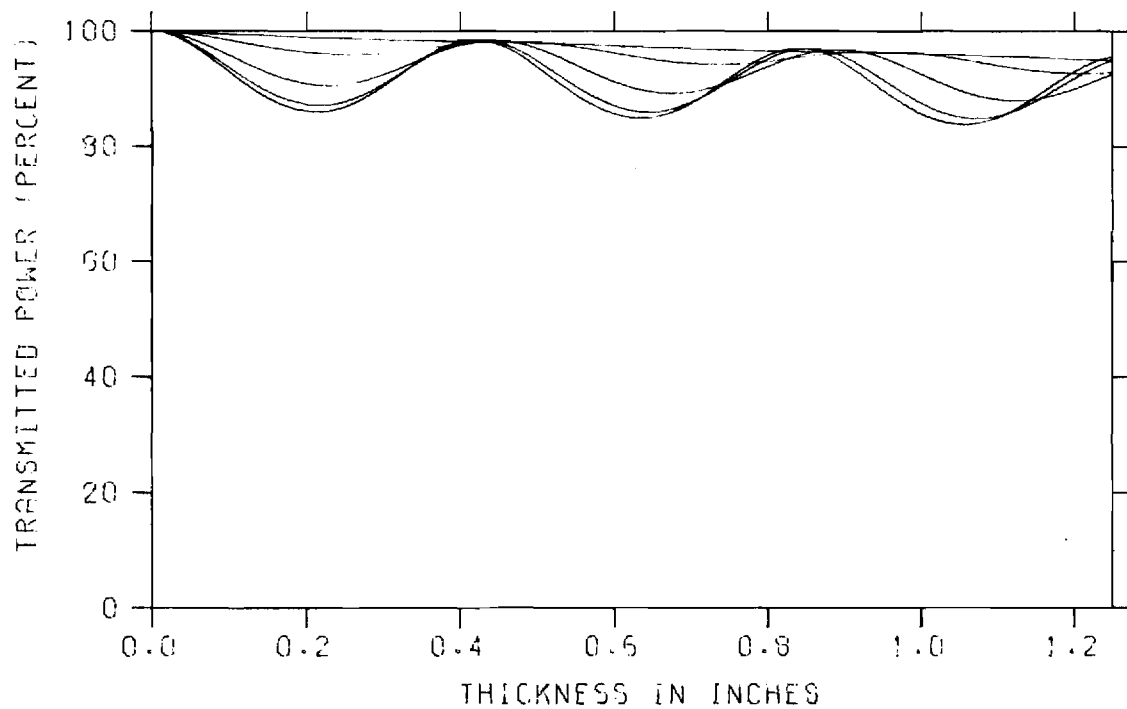
FIGURE A-9. SINGLE LAYER TRANSMISSION EFFICIENCY
SHELL: ER=2.24   TAND=0.0044
CORE: ER=1.07   TAND=0.0002
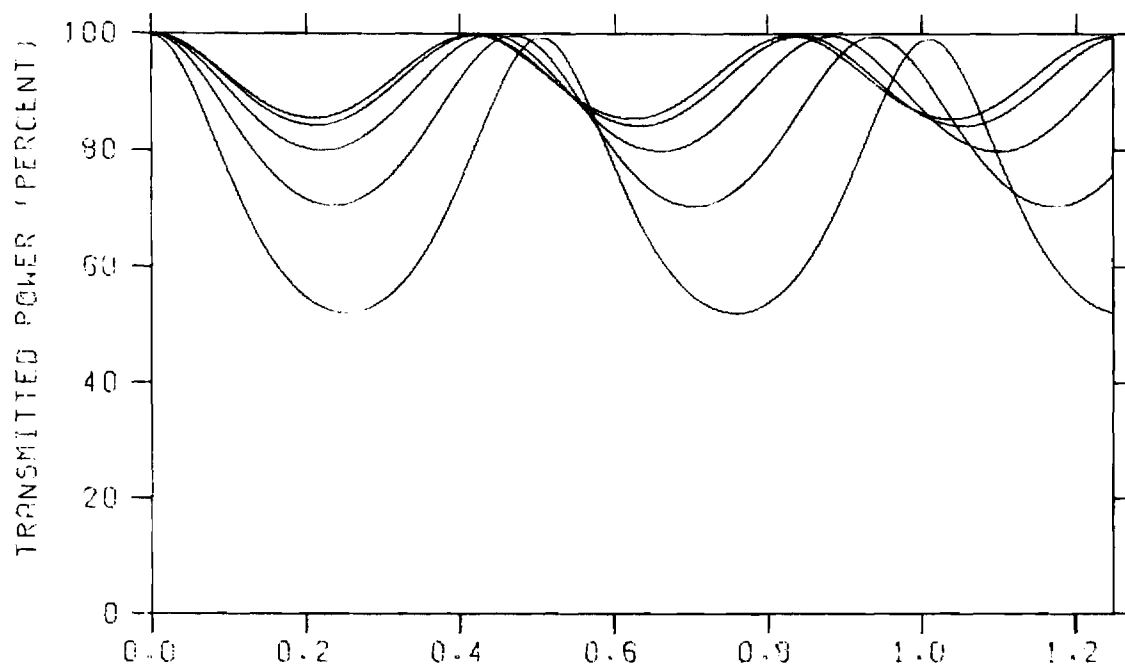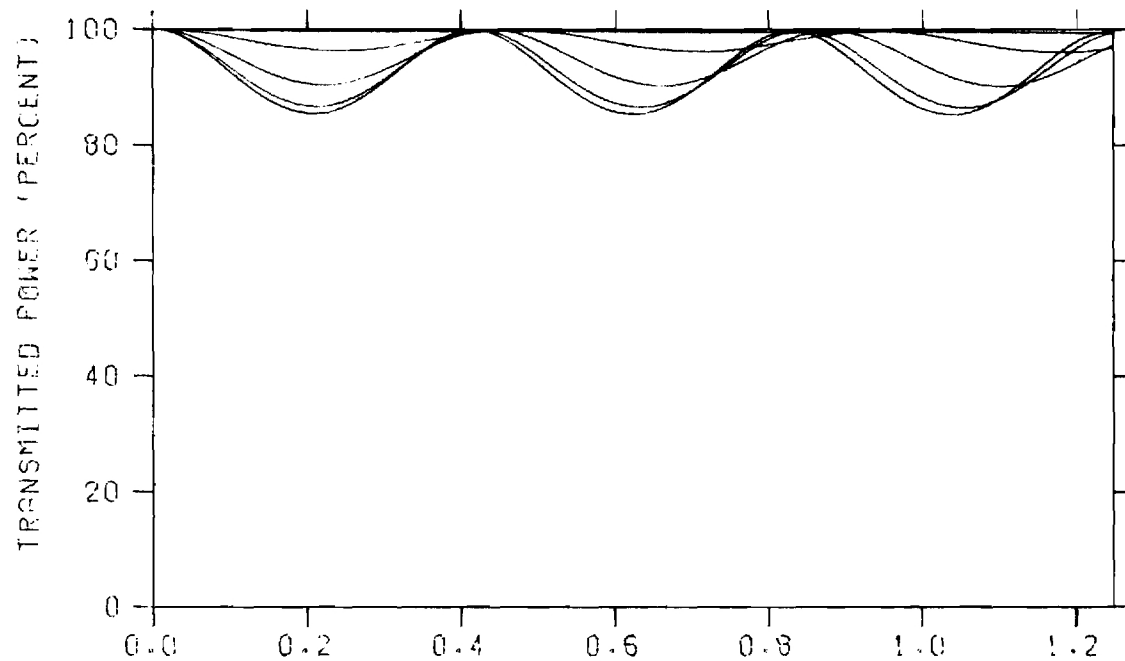
FIGURE A-10. SINGLE LAYER TRANSMISSION EFFICIENCY

SHELL: ER=2.31   TAND=0.0004

CORE: ER=1.07   TAND=0.0002
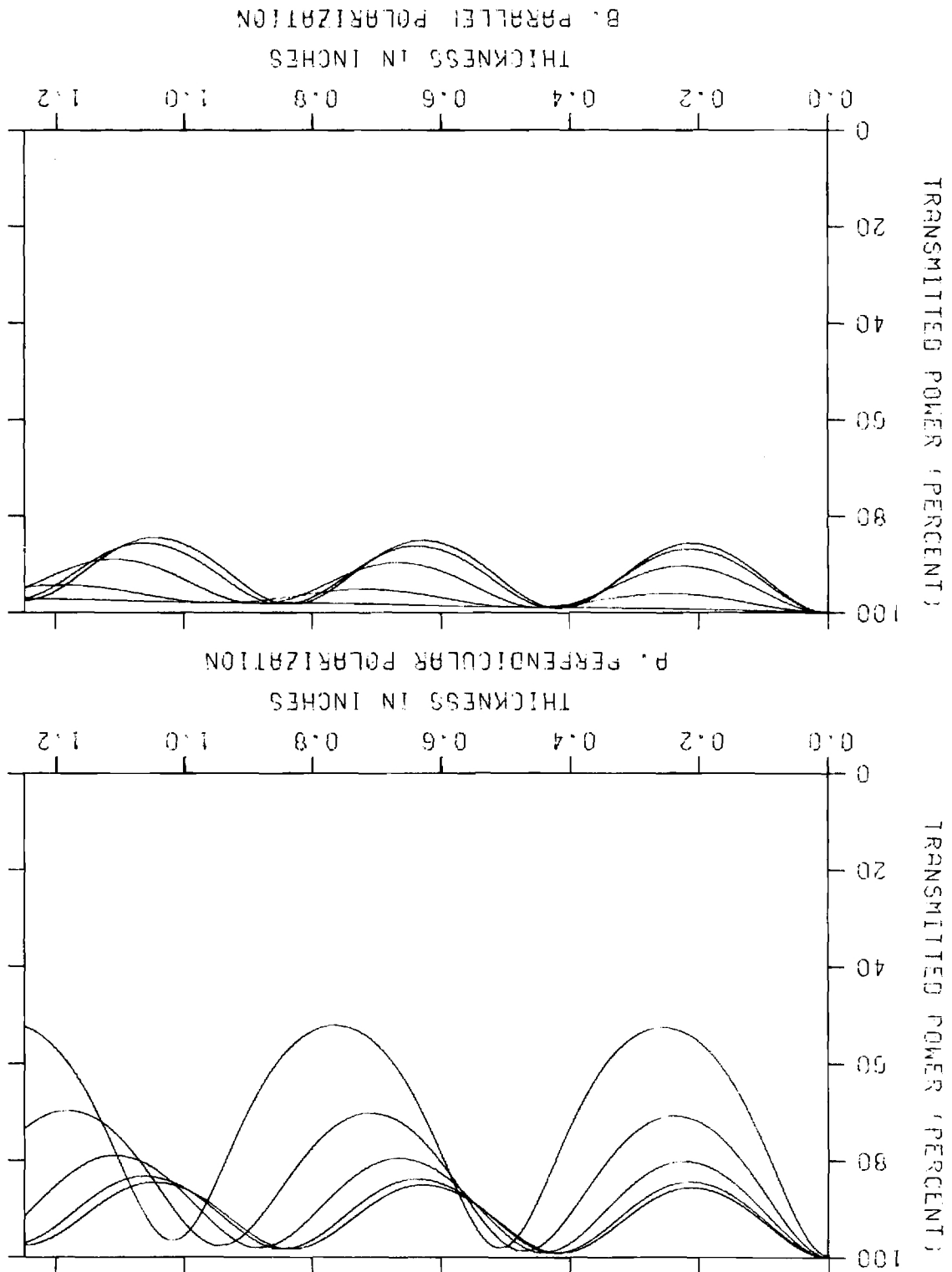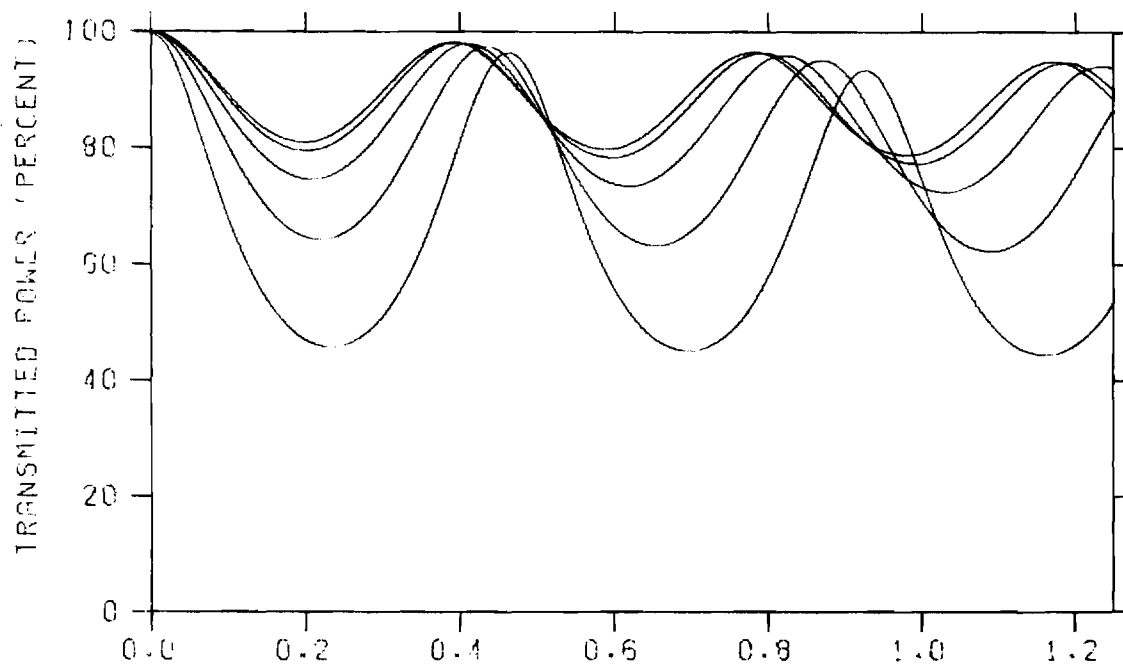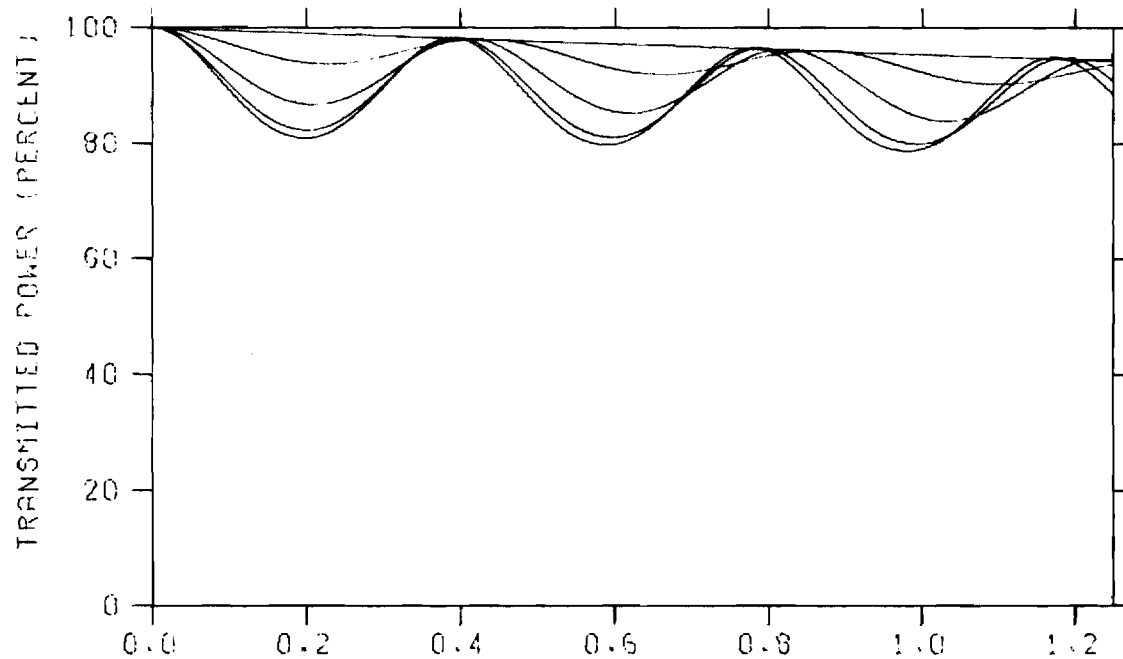
FIGURE A-12   SINGLE LAYER TRANSMISSION EFFICIENCY
SHELL: ER=2.60   TAND=0.0050
CORE: ER=1.07   TAND=0.0002
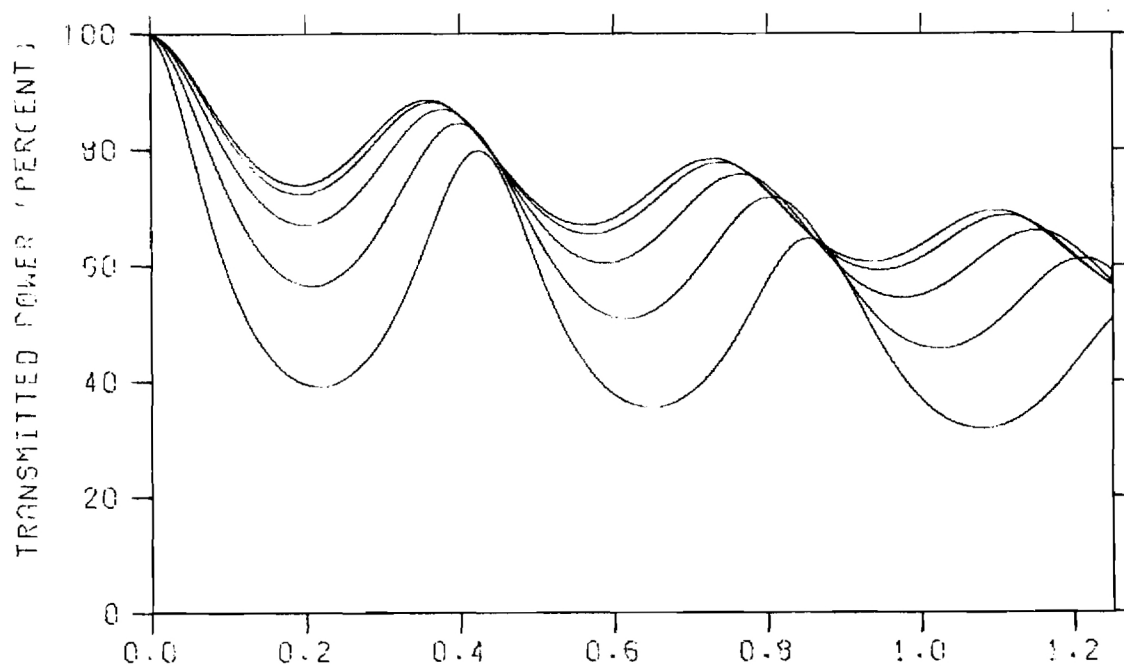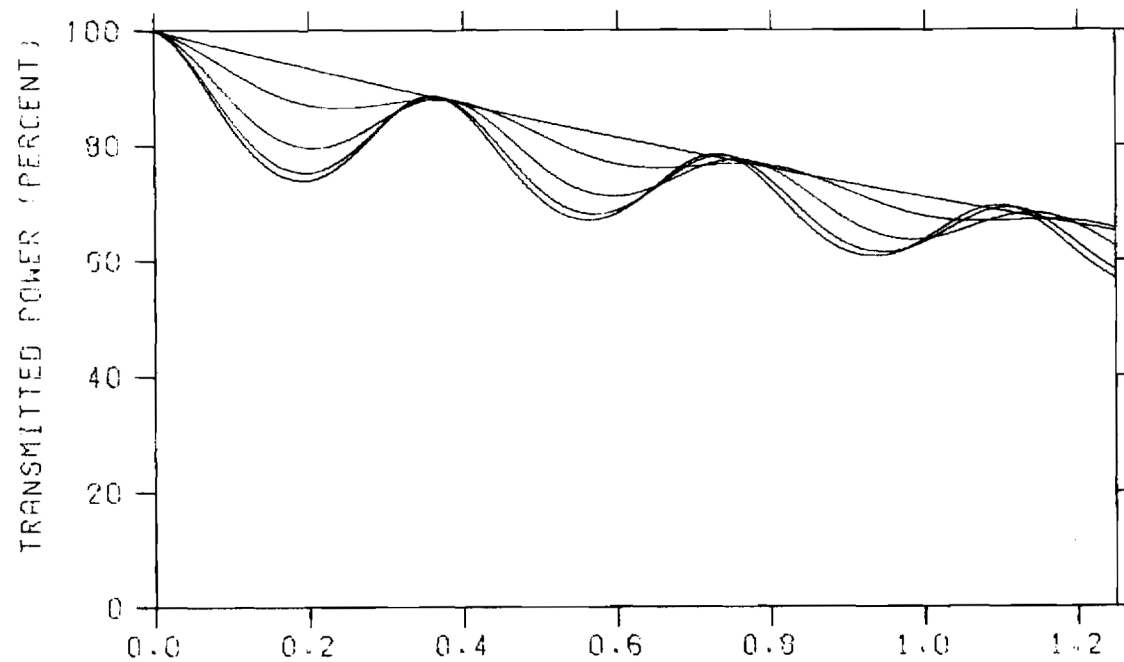
FIGURE A-13. SINGLE LAYER TRANSMISSION EFFICIENCY

SHELL: ER=2.90   TAND=0.0350
CORE: ER=1.07   TAND=0.0002

55 .
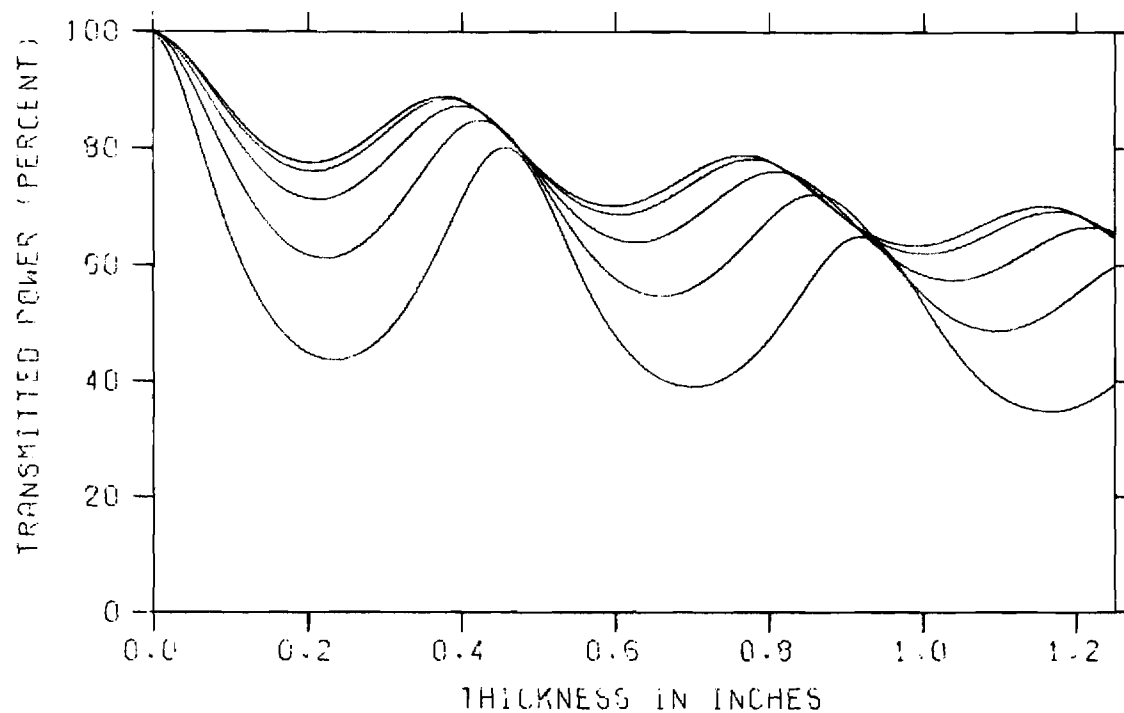
A. PERPENDICULAR POLARIZATION
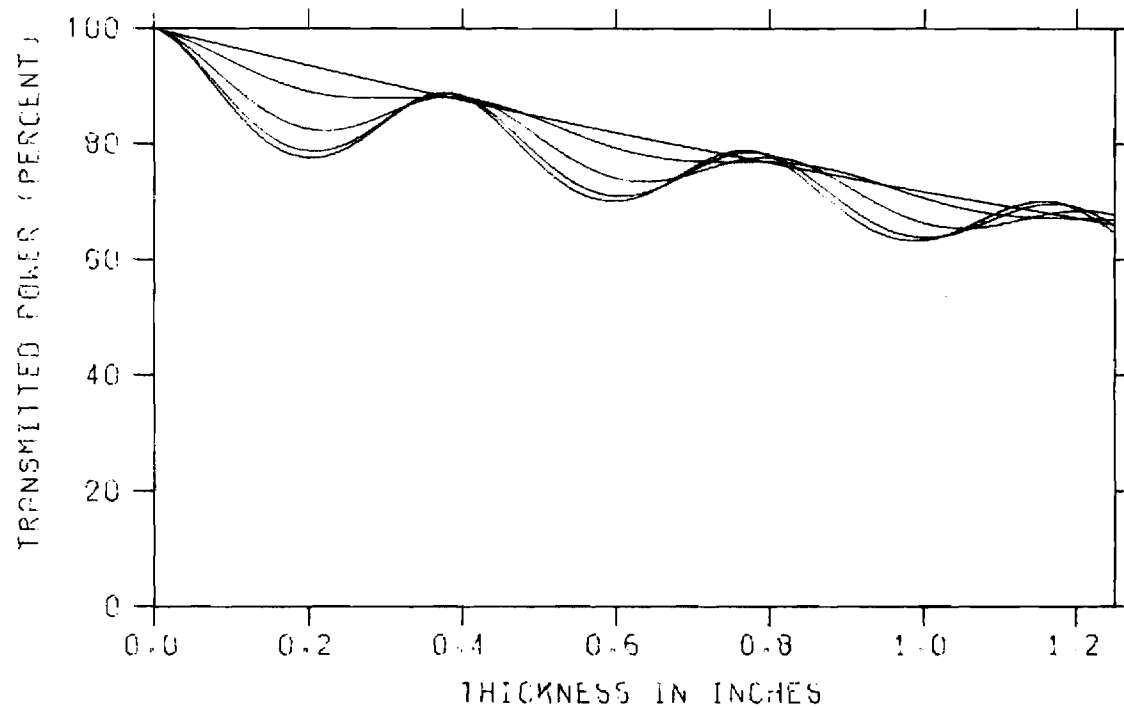
B. PARALLEL POLARIZATION

FIGURE A-14. SINGLE LAYER TRANSMISSION EFFICIENCY
SHELL: ER=2.60   TAND=0.0350
CORE: ER=1.07   TAND=0.0002
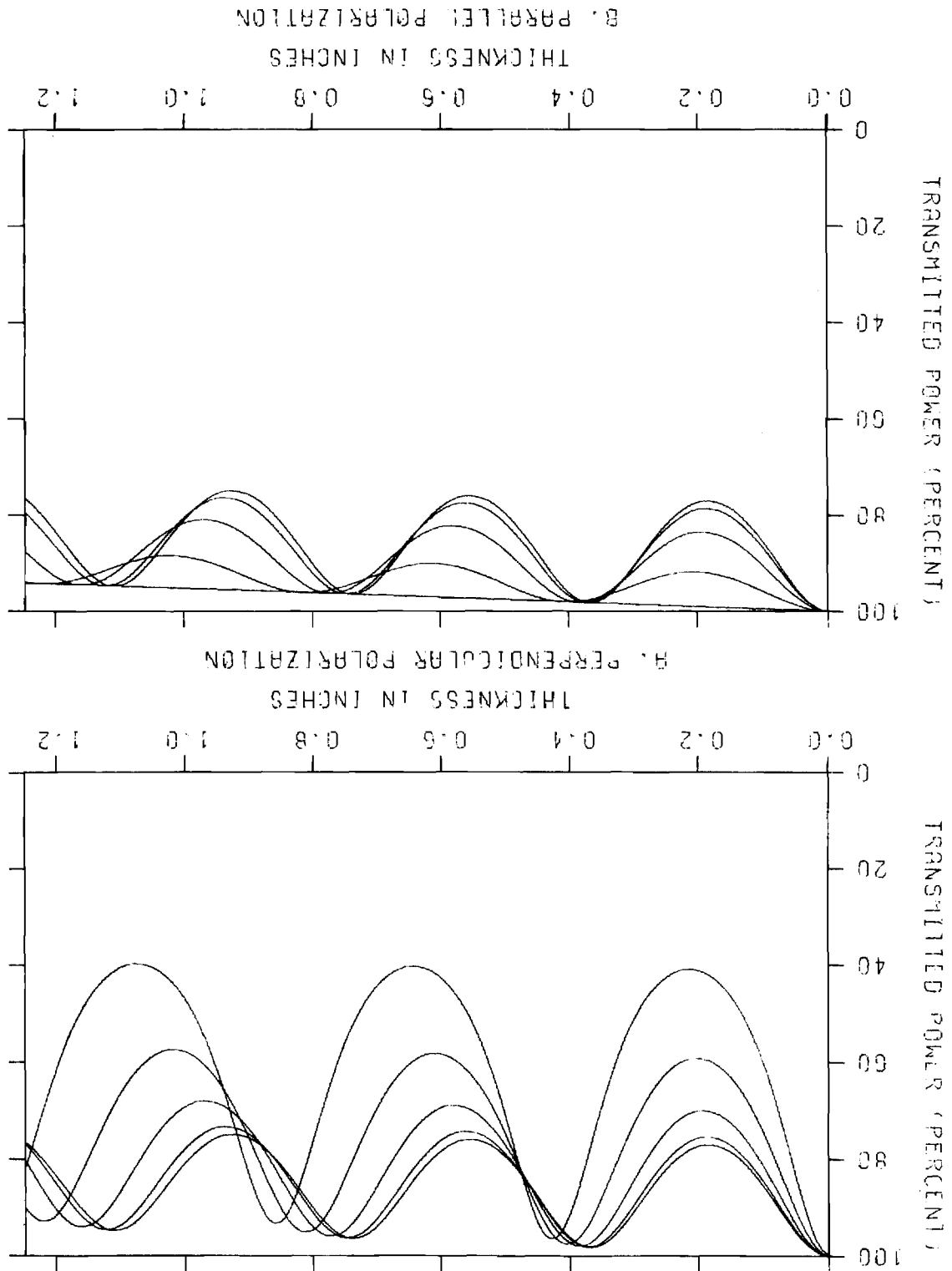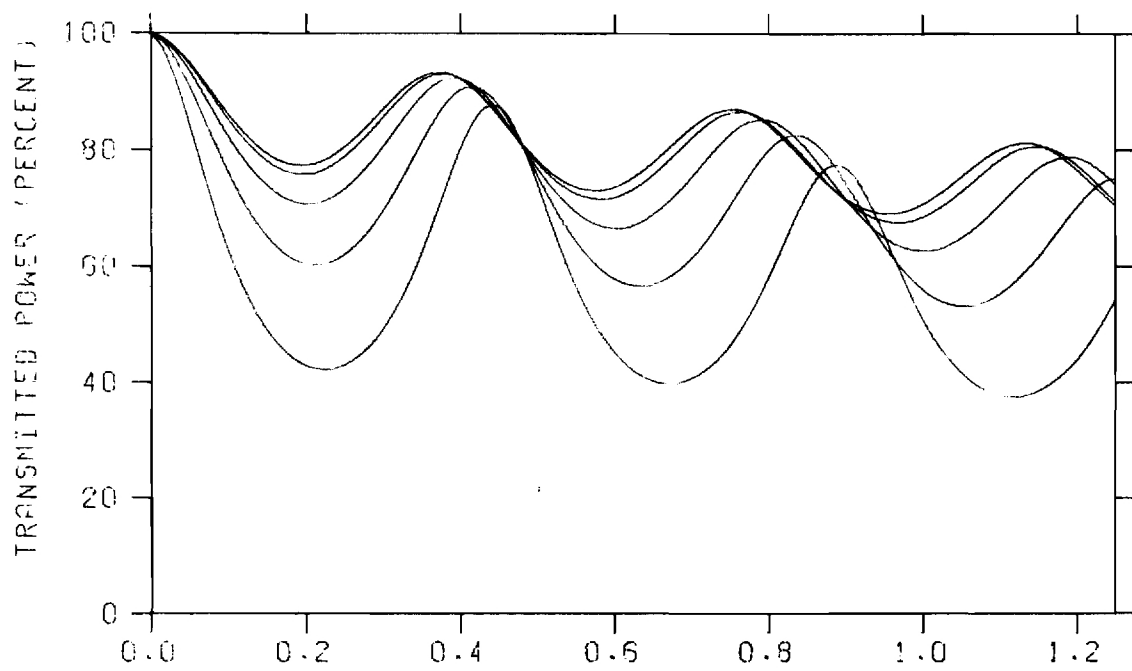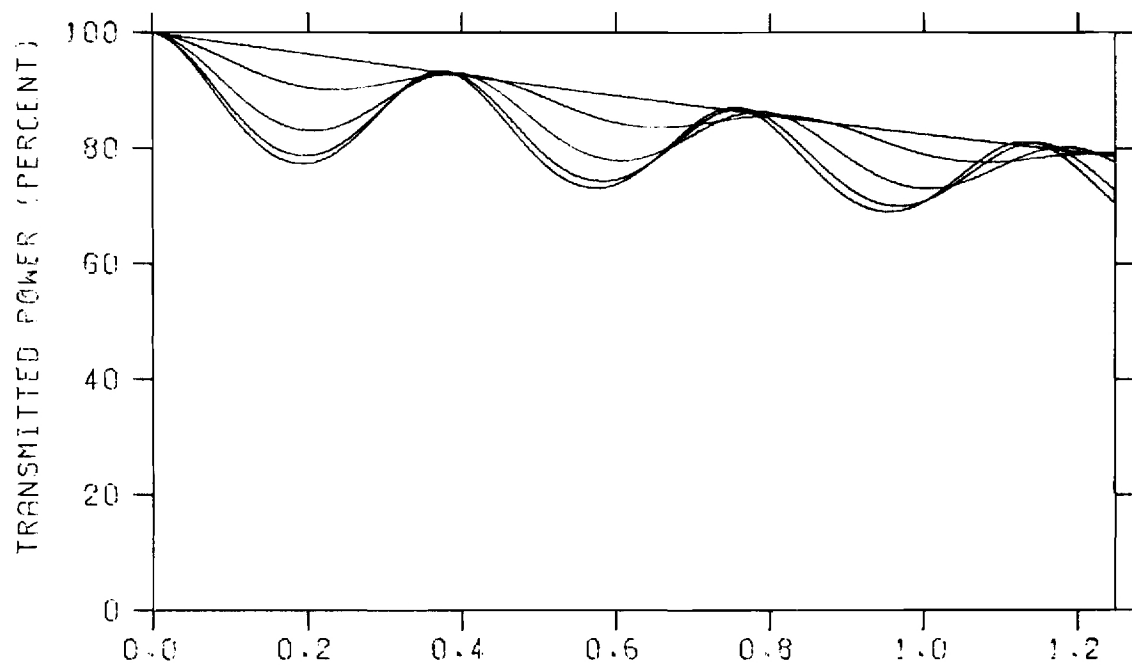
FIGURE A-16. SINGLE LAYER TRANSMISSION EFFICIENCY

SHELL: ER=2.75   TAND=0.0200
CORE: ER=1.07   TAND=0.0002
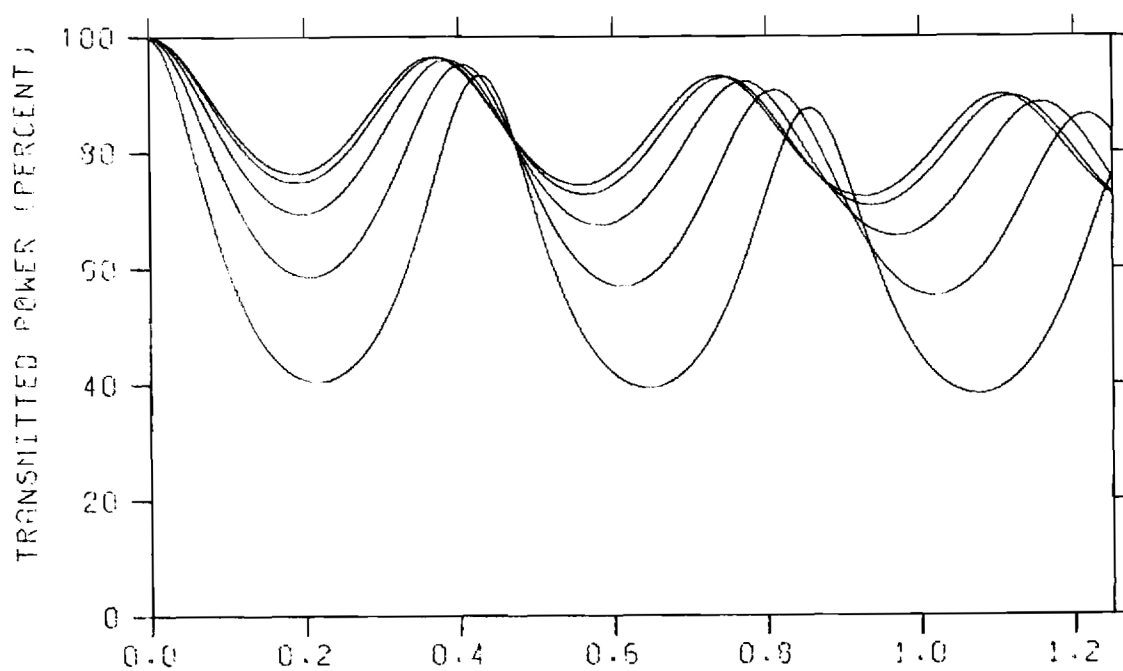
A. PERPENDICULAR POLARIZATION
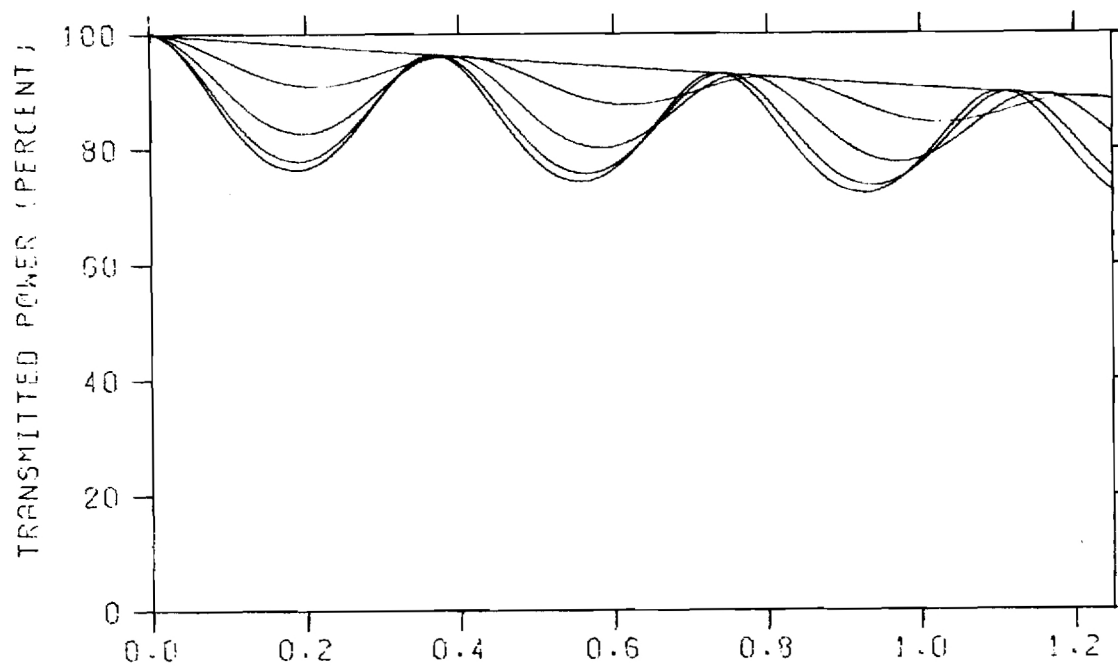
B. PARALLEL POLARIZATION

FIGURE A-17. SINGLE LAYER TRANSMISSION EFFICIENCY

SHELL: ER=2.91   TAND=0.0100
CORE: ER=1.07   TAND=0.0002
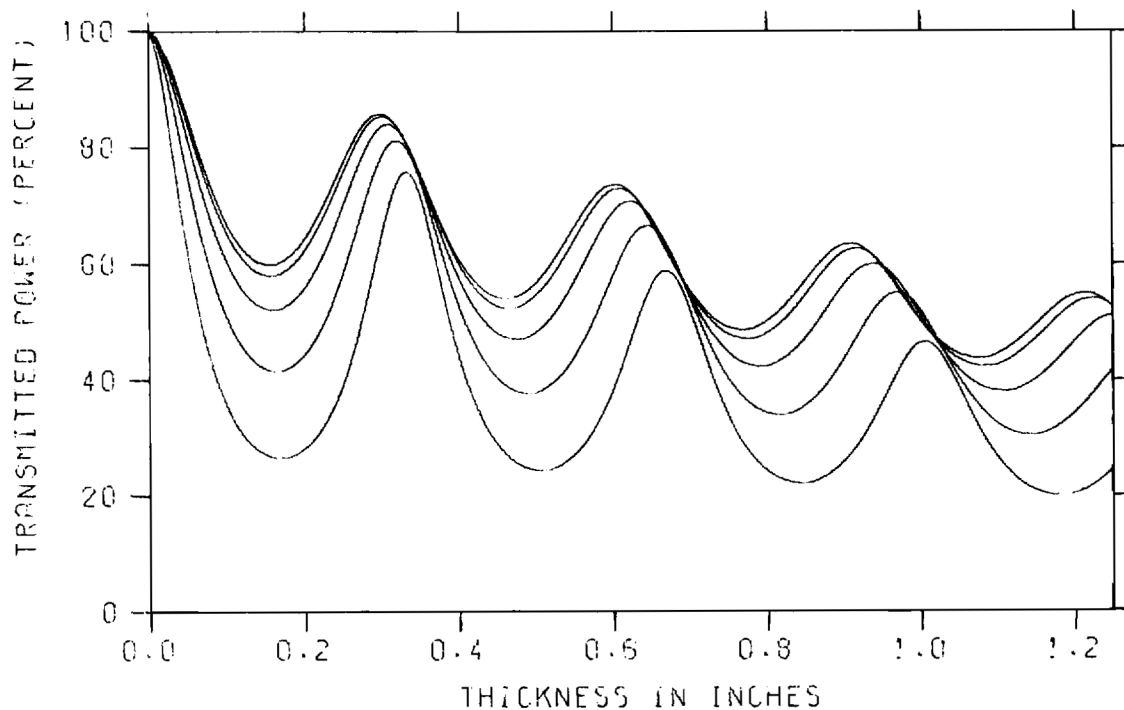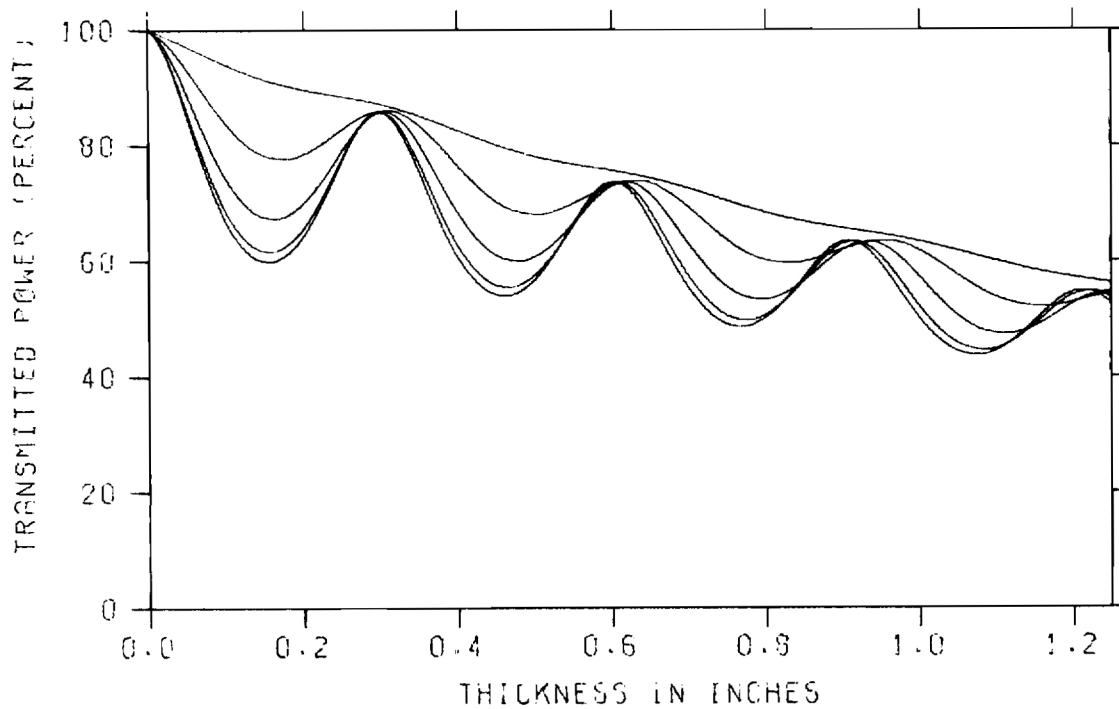
FIGURE A-18. SINGLE LAYER TRANSMISSION EFFICIENCY
SHELL: ER=4.26 TAND=0.0400
CORE: ER=1.07 TAND=0.0002
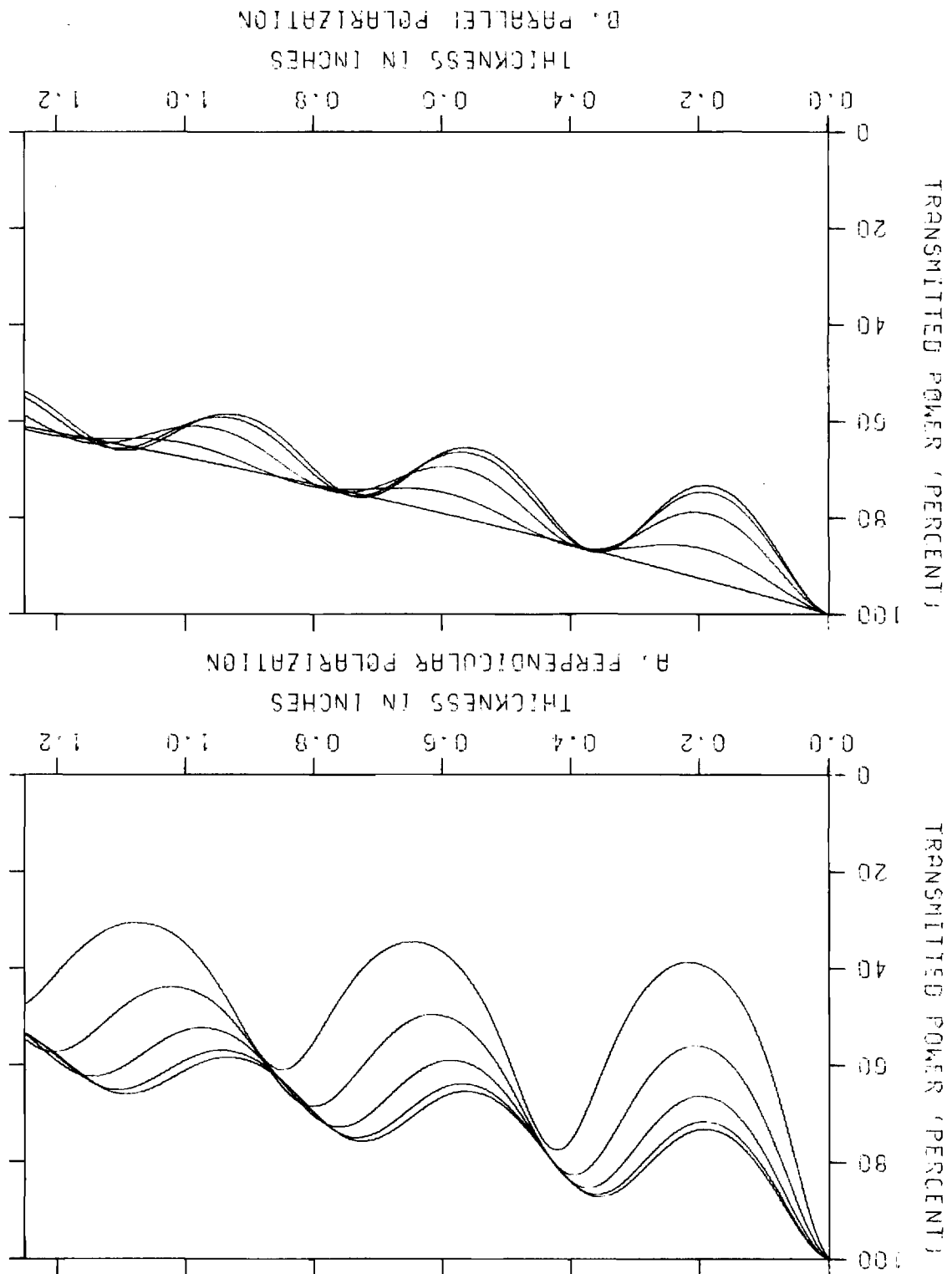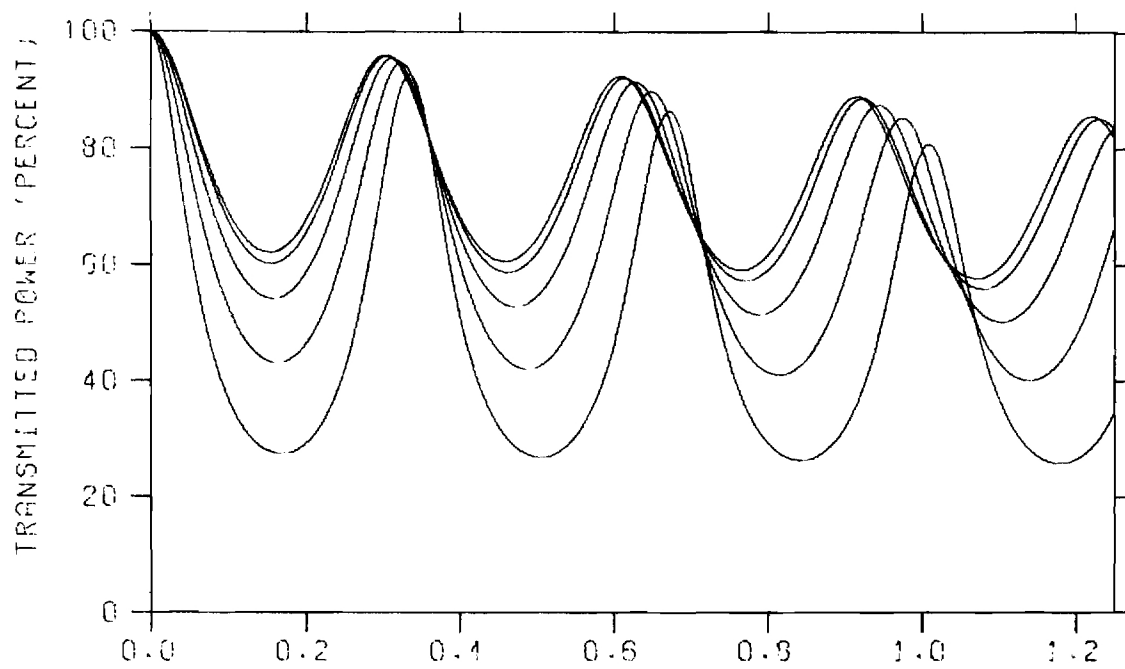
A. PERPENDICULAR POLARIZATION
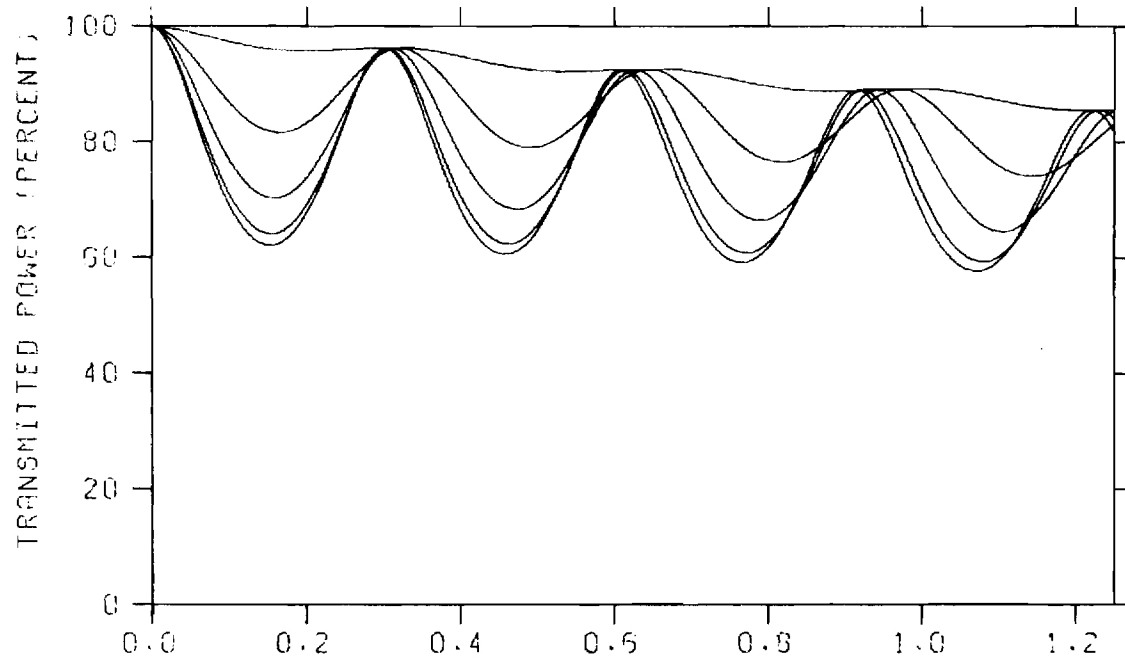
B. PARALLEL POLARIZATION

FIGURE A-20. SINGLE LAYER TRANSMISSION EFFICIENCY

SHELL: ER=4.26   TAND=0.0100

CORE: ER=1.07   TAND=0.0002

62
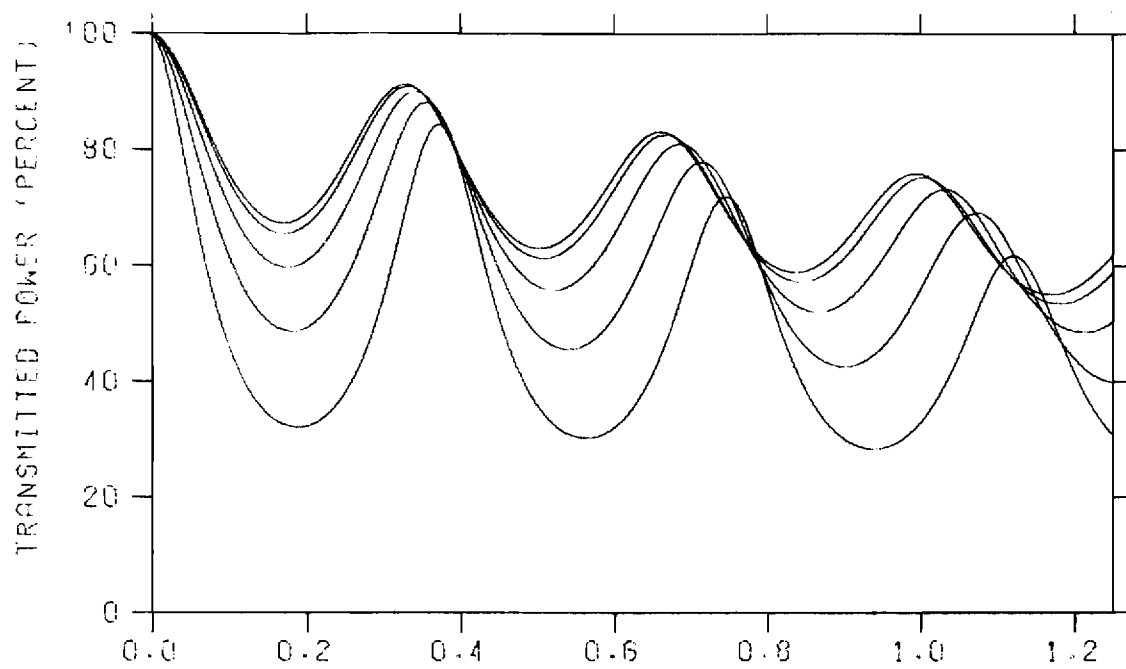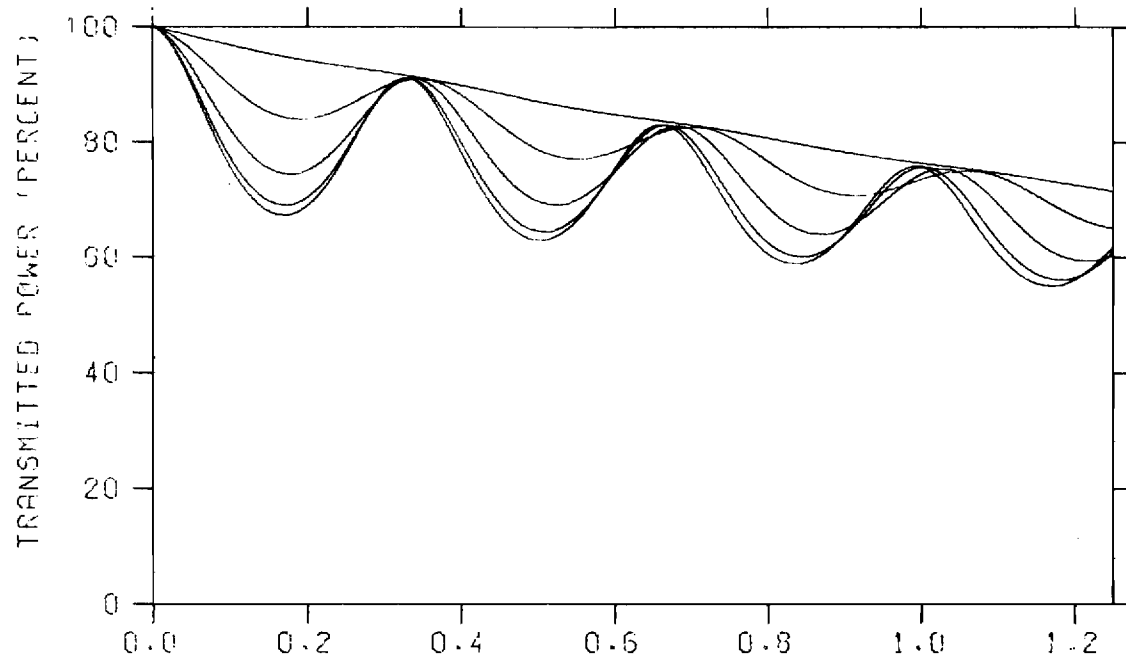
FIGURE A-21. SINGLE LAYER TRANSMISSION EFFICIENCY

SHELL: ER=3.59   TAND.0.0250
CORE: ER=1.07   TAND.0.0002
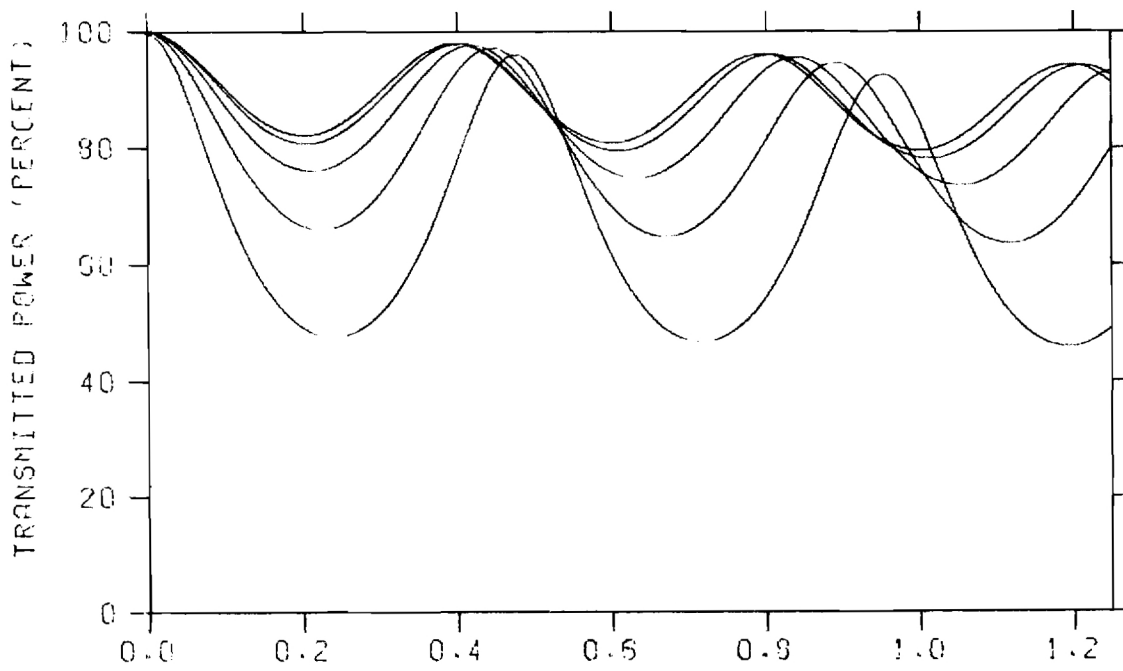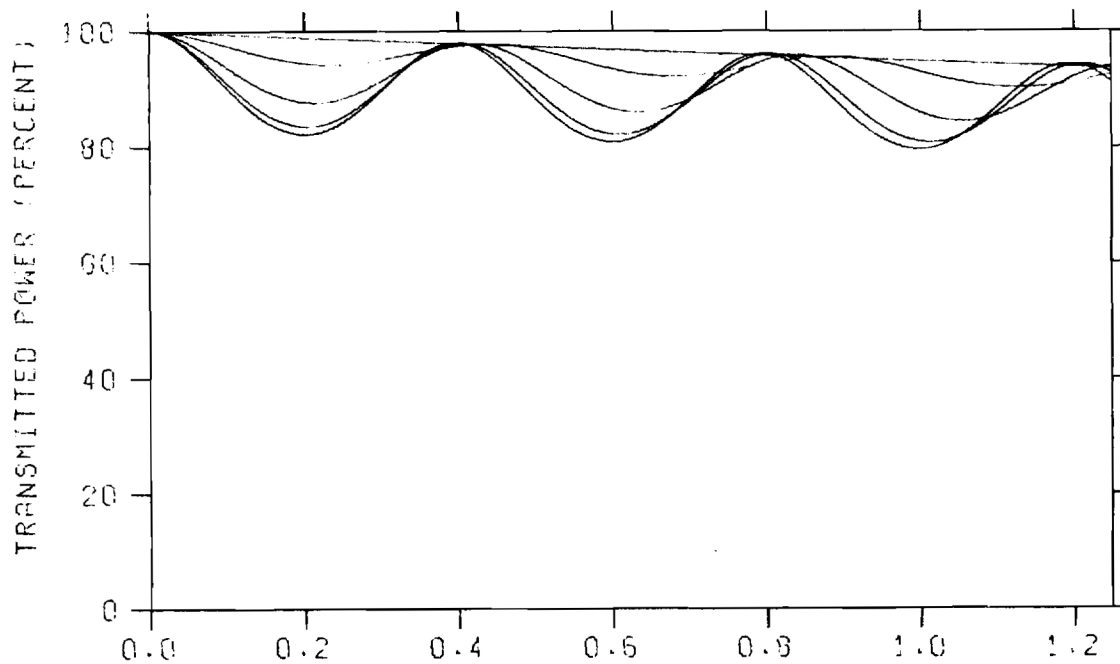
FIGURE A-22. SINGLE LAYER TRANSMISSION EFFICIENCY

SHELL: ER=2.50 TAND=0.0057

CORE: ER=1.07 TAND=0.0002
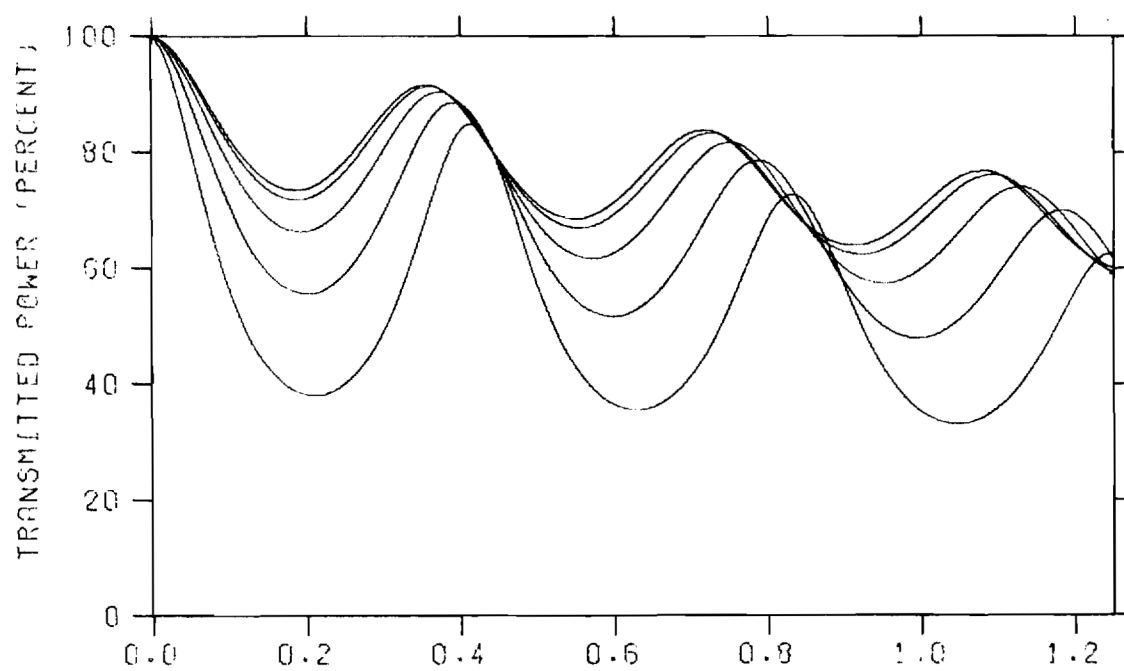
A. PERPENDICULAR POLARIZATION
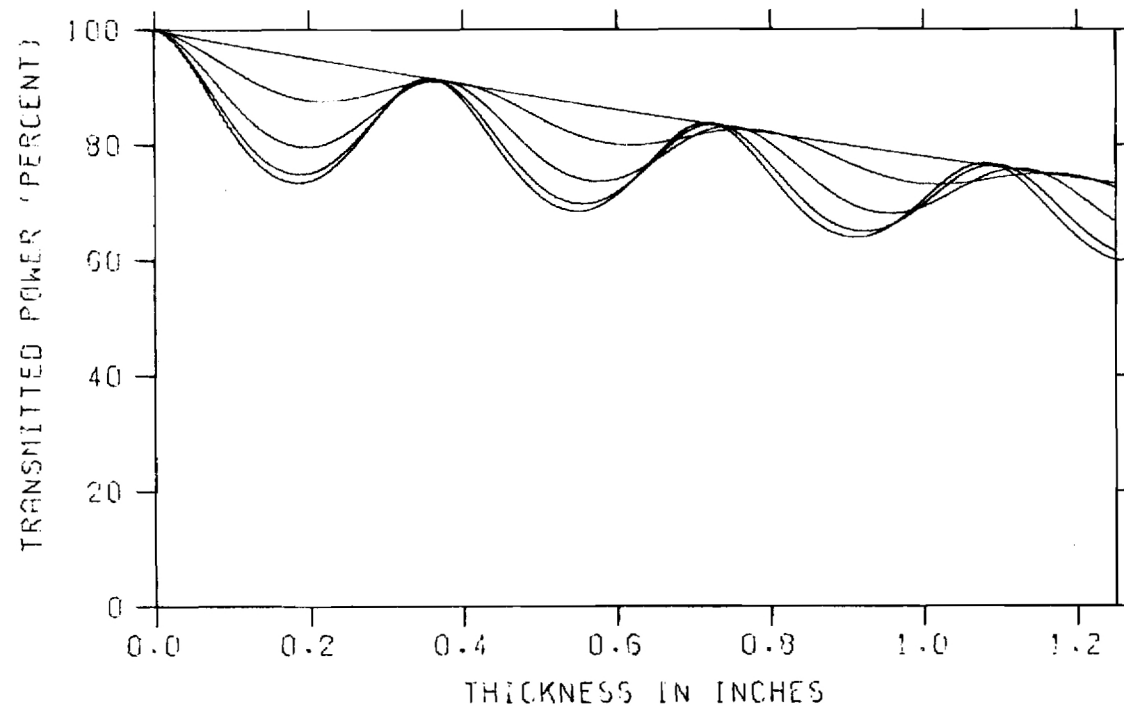
B. PARALLEL POLARIZATION

FIGURE A-23.   SINGLE LAYER TRANSMISSION EFFICIENCY

SHELL: ER=3.03   TAND=0.0250
CORE: ER=1.07   TAND=0.0002
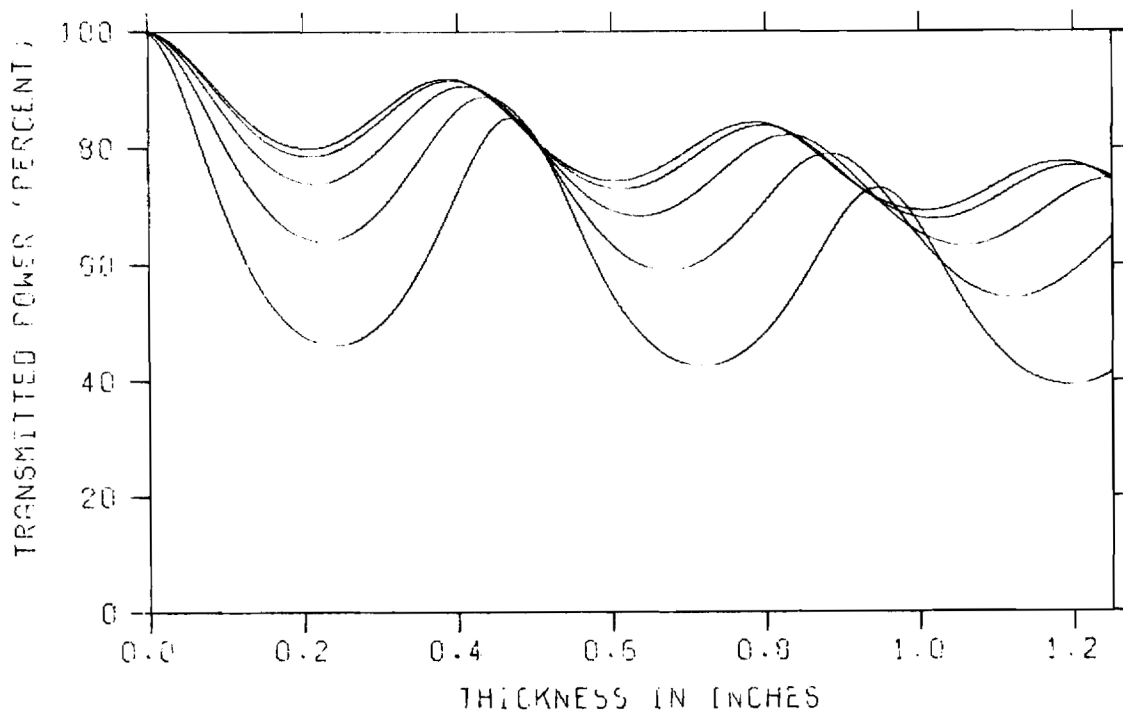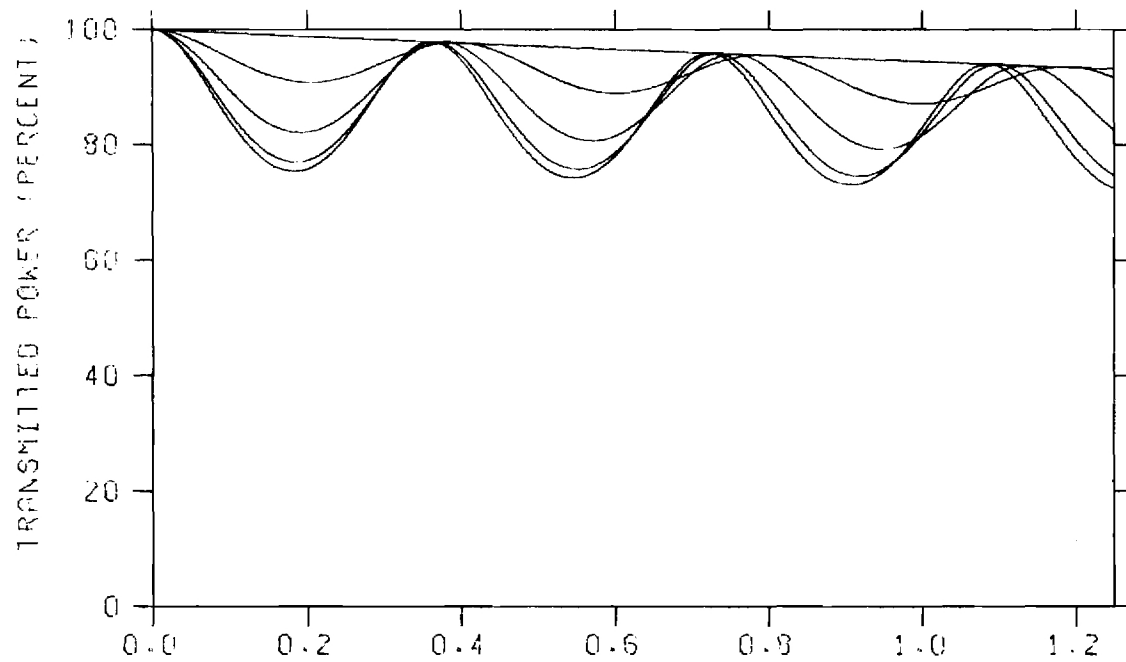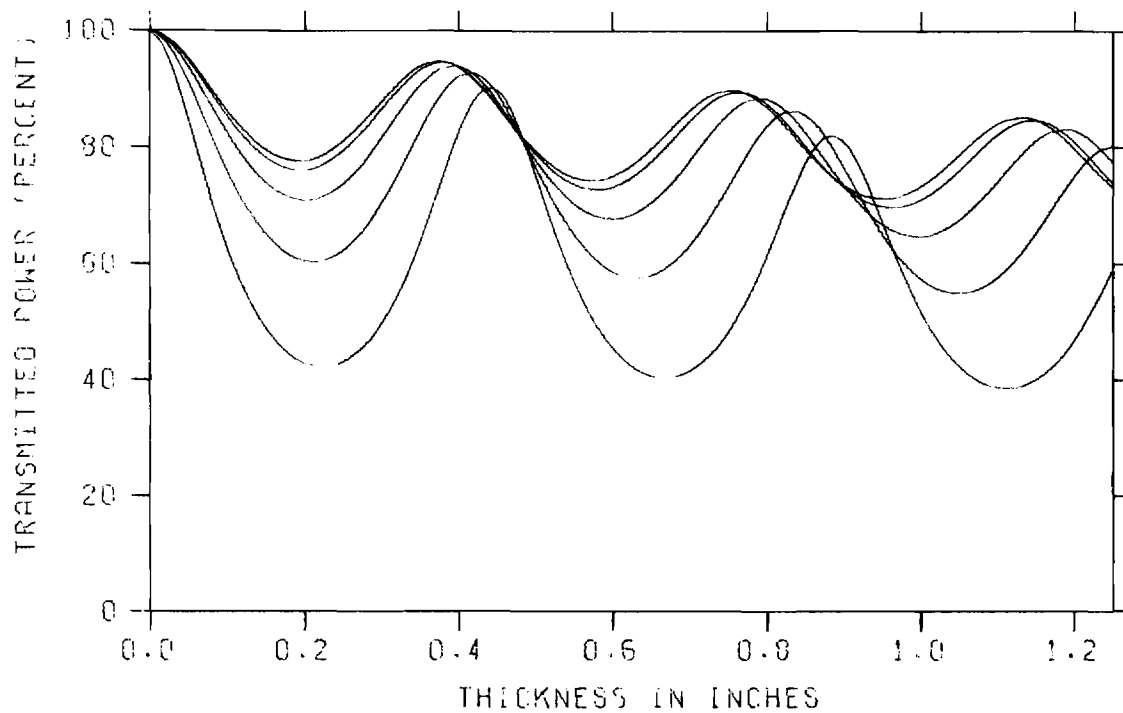
A. PERPENDICULAR POLARIZATION
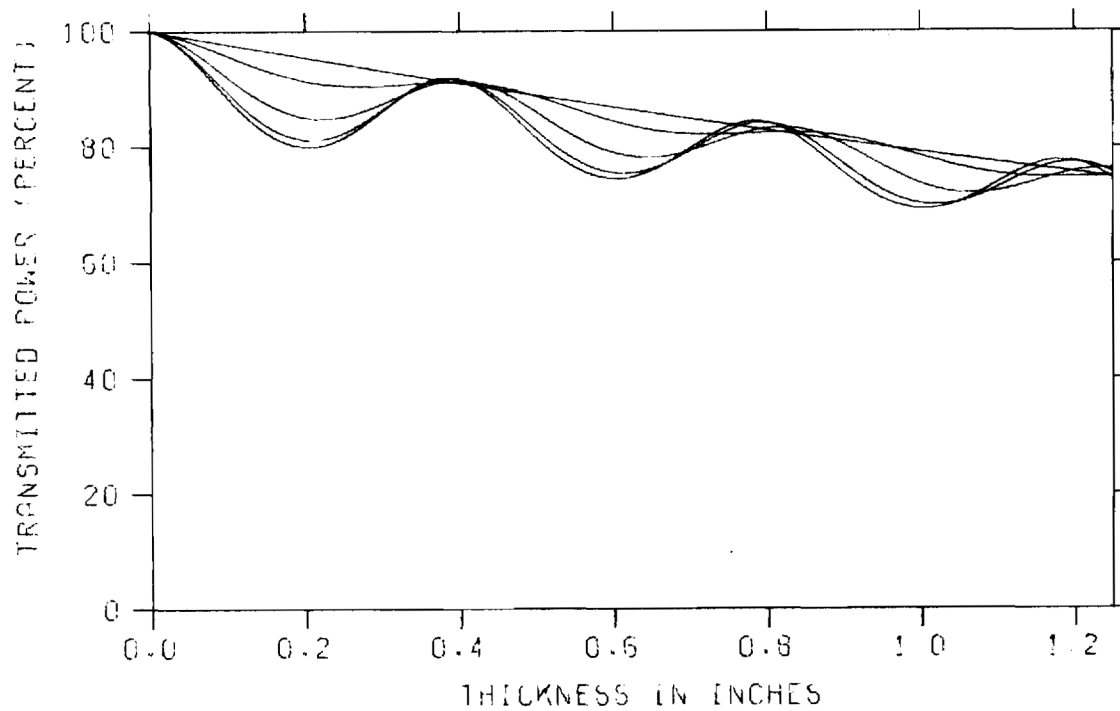
B. PARALLEL POLARIZATION

FIGURE A-24. SINGLE LAYER TRANSMISSION EFFICIENCY

SHELL: ER=2.50   TAND=0.0250
CORE: ER=1.07   TAND=0.0002
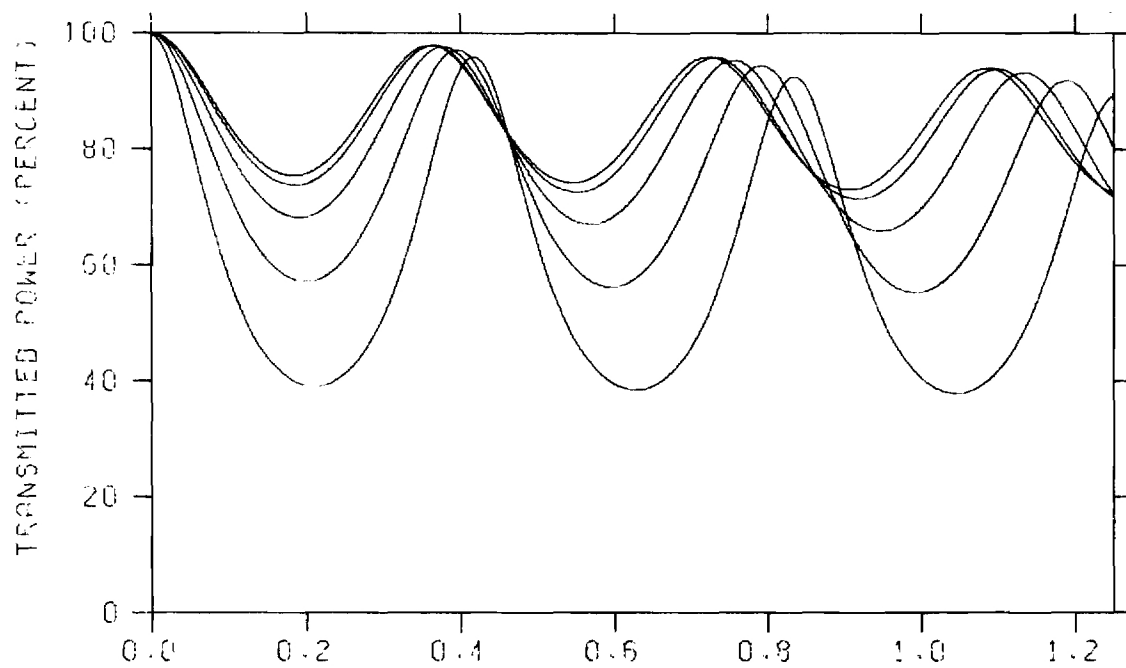
FIGURE A-25. SINGLE LAYER TRANSMISSION EFFICIENCY

SHELL: ER=3.03 TAND=0.0057

CORE: ER=1.07 TAND=0.0002

67
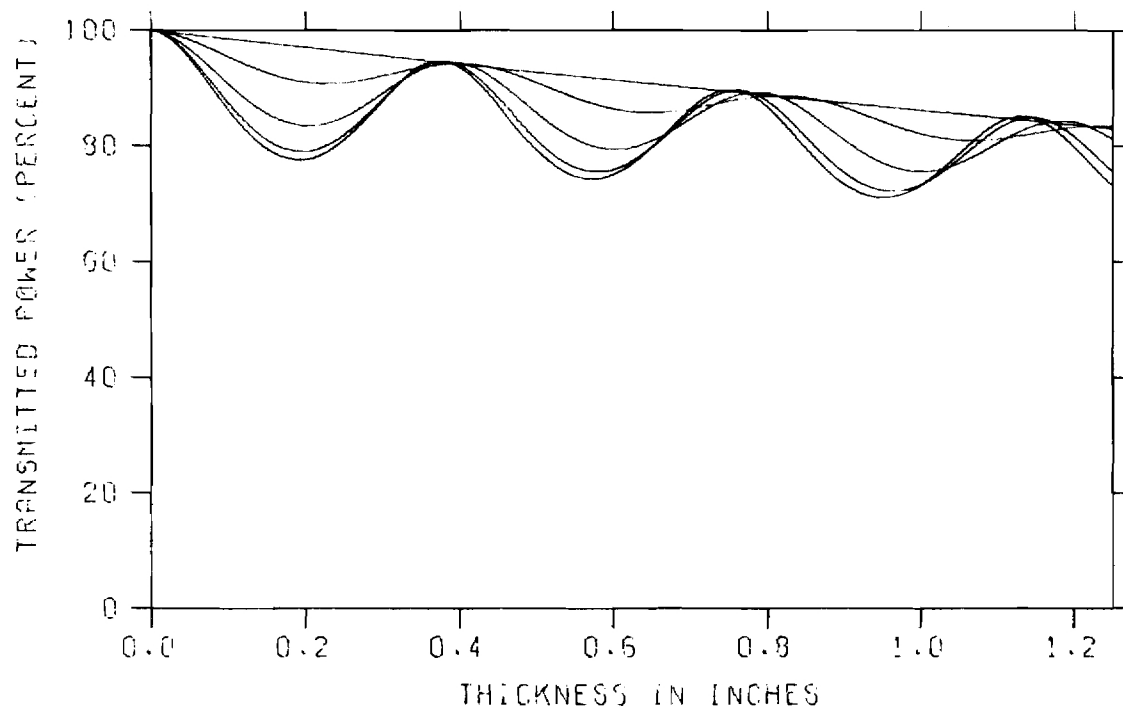
FIGURE A-26. SINGLE LAYER TRANSMISSION EFFICIENCY

SHELL: ER=2.77   TAND=0.0154
CORE: ER=1.07   TAND=0.0002
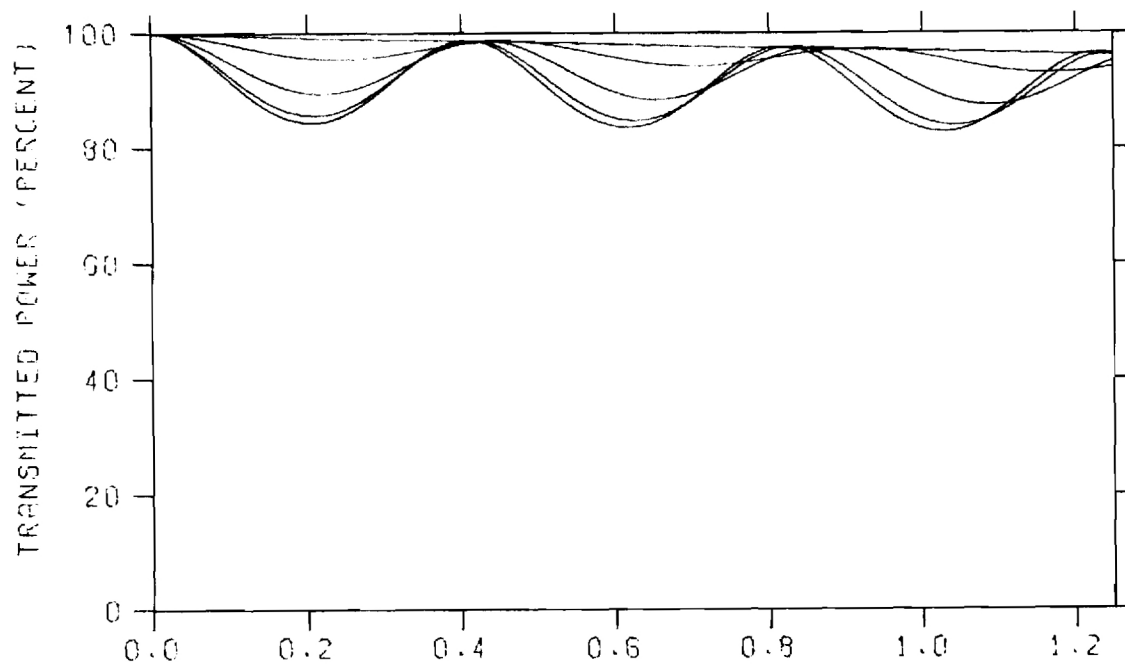
FIGURE A-27. SINGLE LAYER TRANSMISSION EFFICIENCY
SHELL: ER=2.36 TAND=0.0034
CORE: ER=1.07 TAND=0.0002
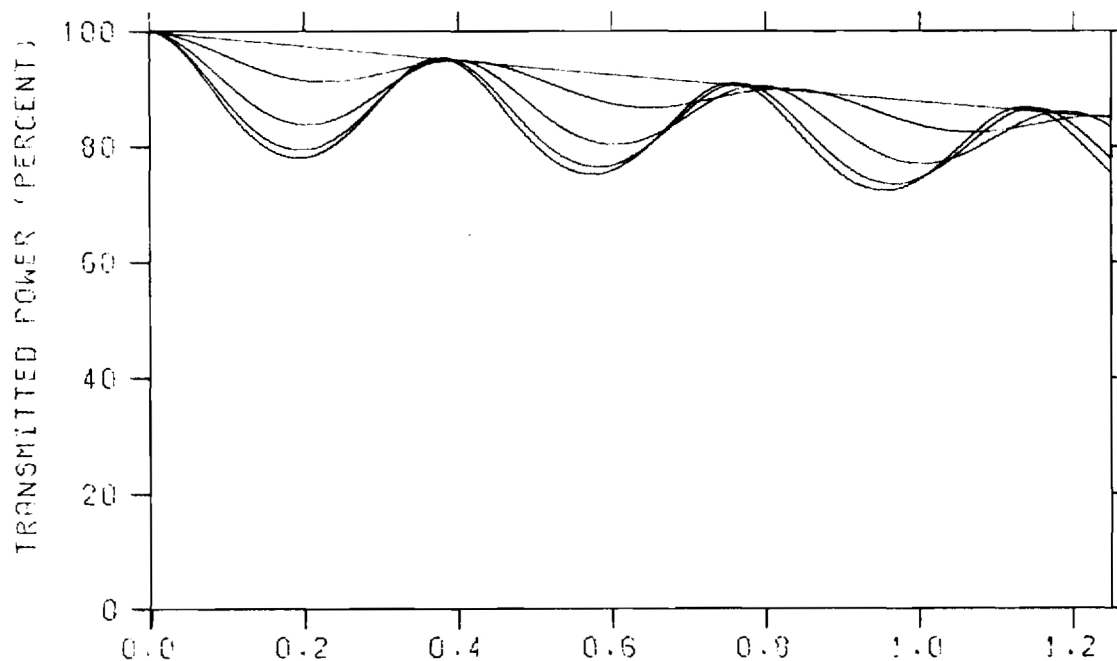
FIGURE A-28. SINGLE LAYER TRANSMISSION EFFICIENCY
SHELL: ER=2.75 TAND=0.0135
CORE: ER=1.07 TAND=0.0002

70

A. PERPENDICULAR POLARIZATION
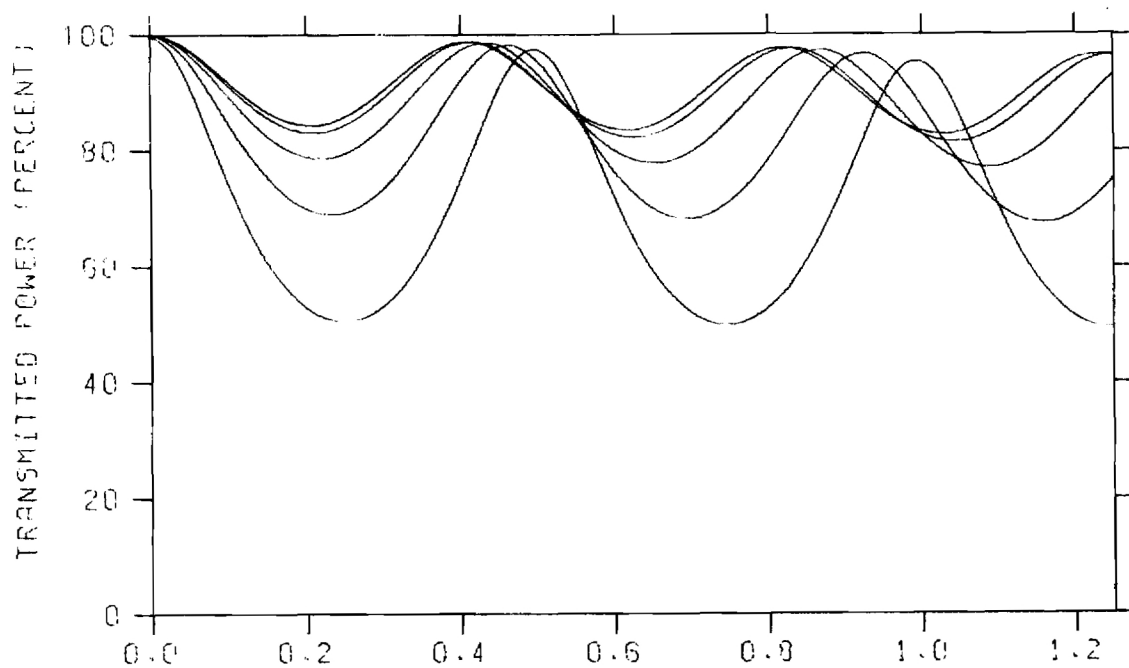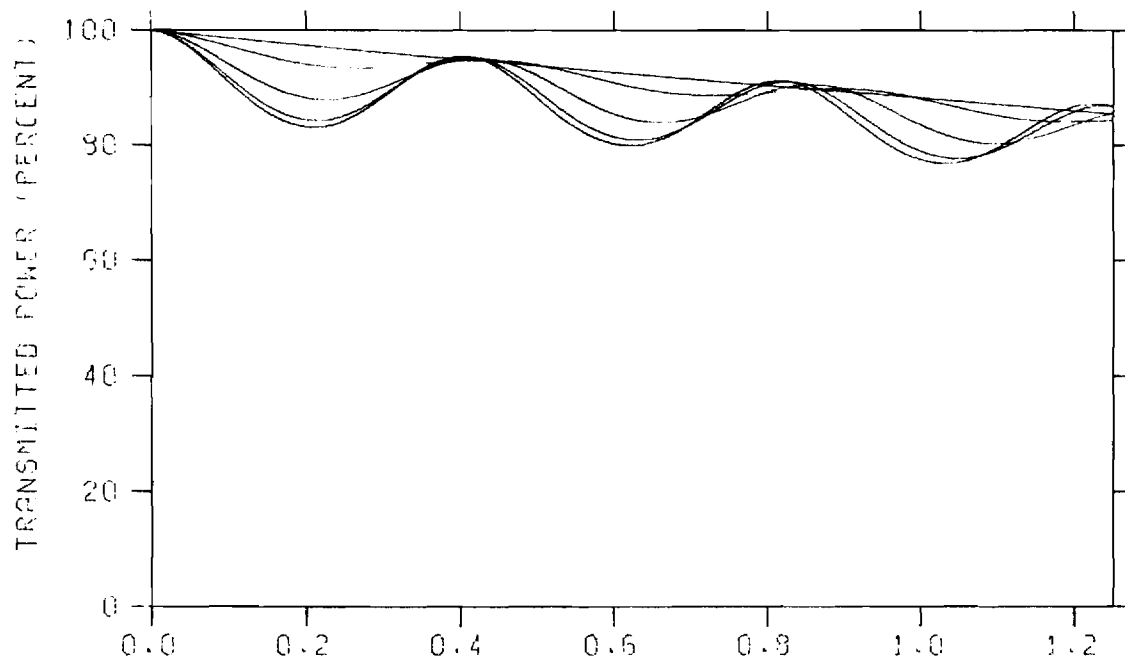

B. PARALLEL POLARIZATION

FIGURE A-29.   SINGLE LAYER TRANSMISSION EFFICIENCY
SHELL: ER=2.36   TAND=0.0135
CORE: ER=1.07   TAND=0.0002
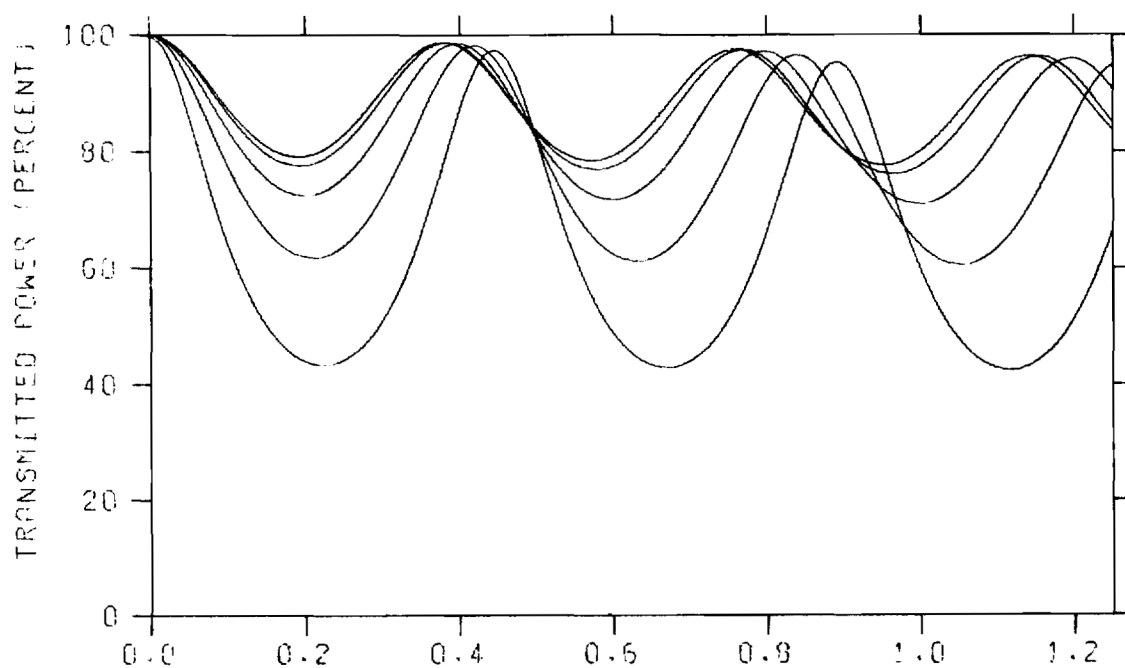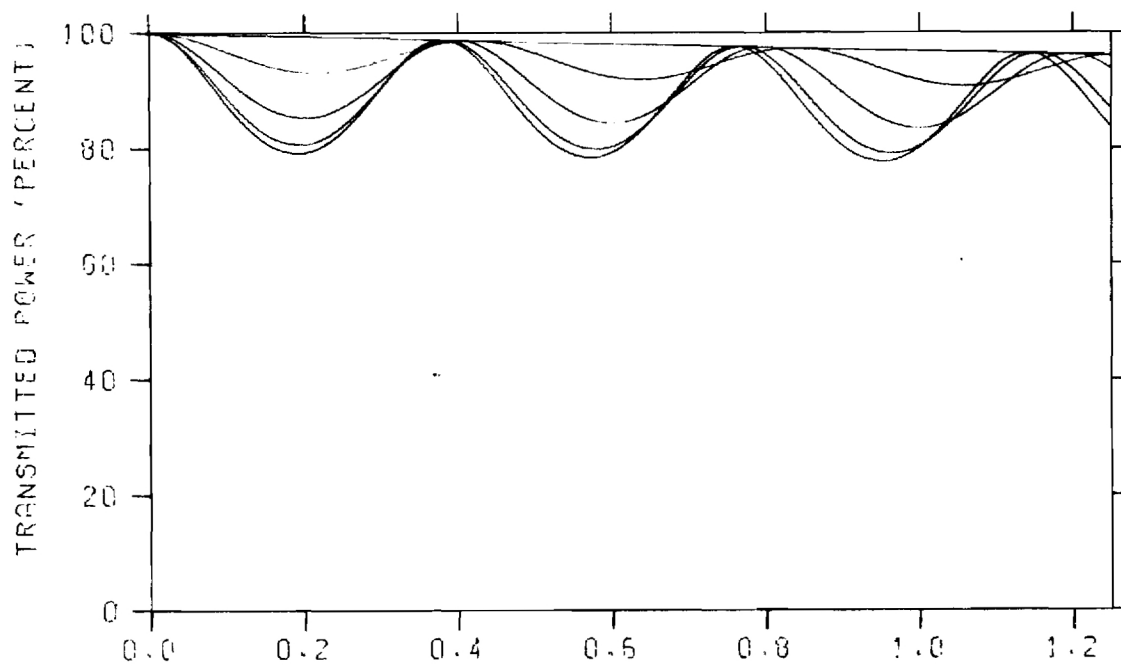
FIGURE A-30. SINGLE LAYER TRANSMISSION EFFICIENCY
SHELL: ER=2.75   TAND=0.0034
CORE: ER=1.07   TAND=0.0002
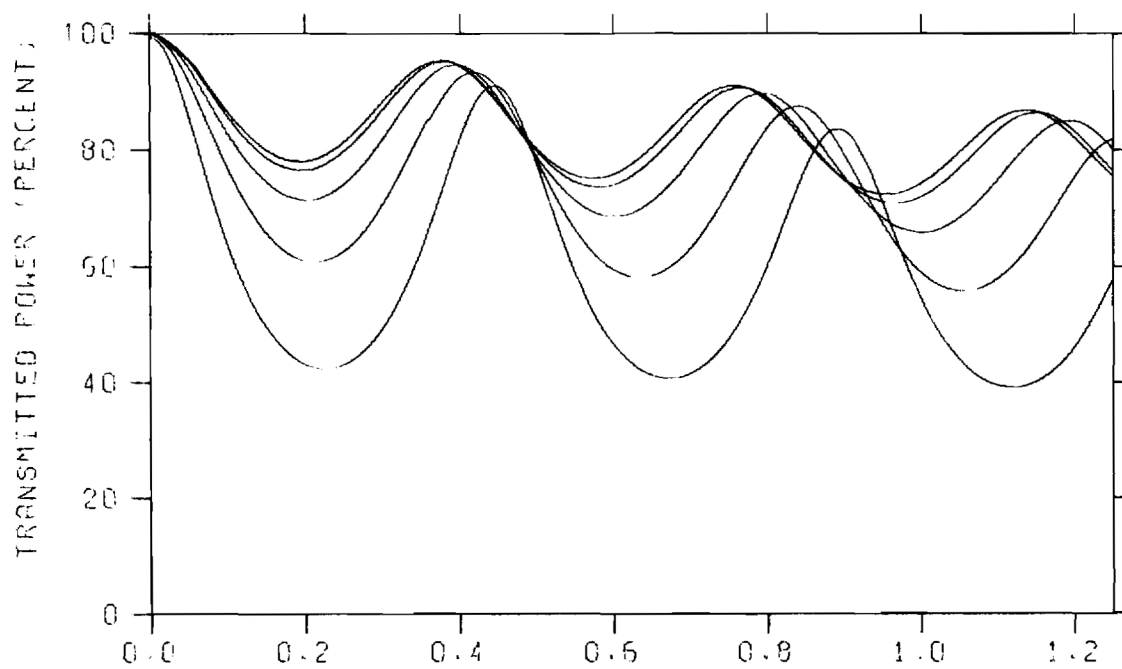
A. PERPENDICULAR POLARIZATION

B. PARALLEL POLARIZATION

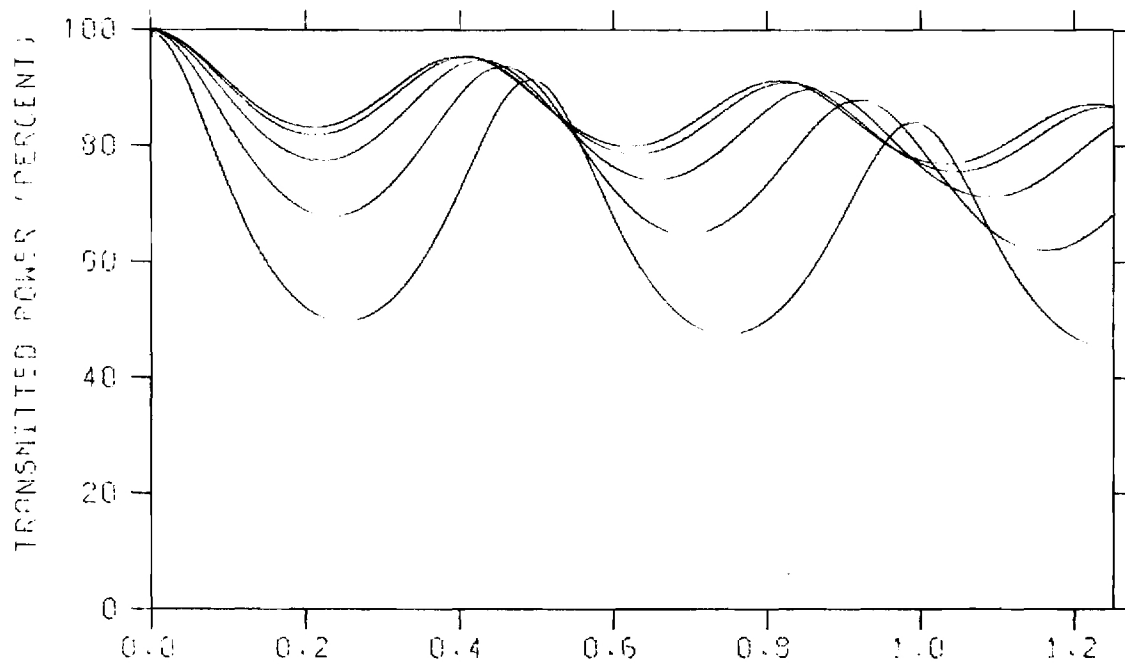FIGURE A-31.   SINGLE LAYER TRANSMISSION EFFICIENCY
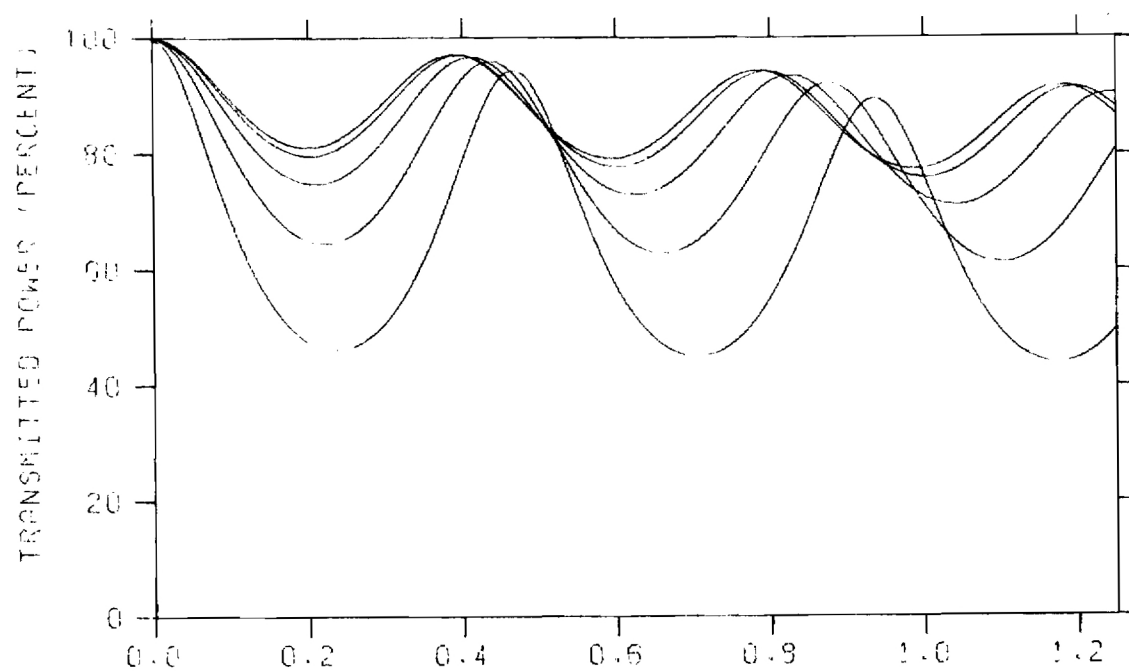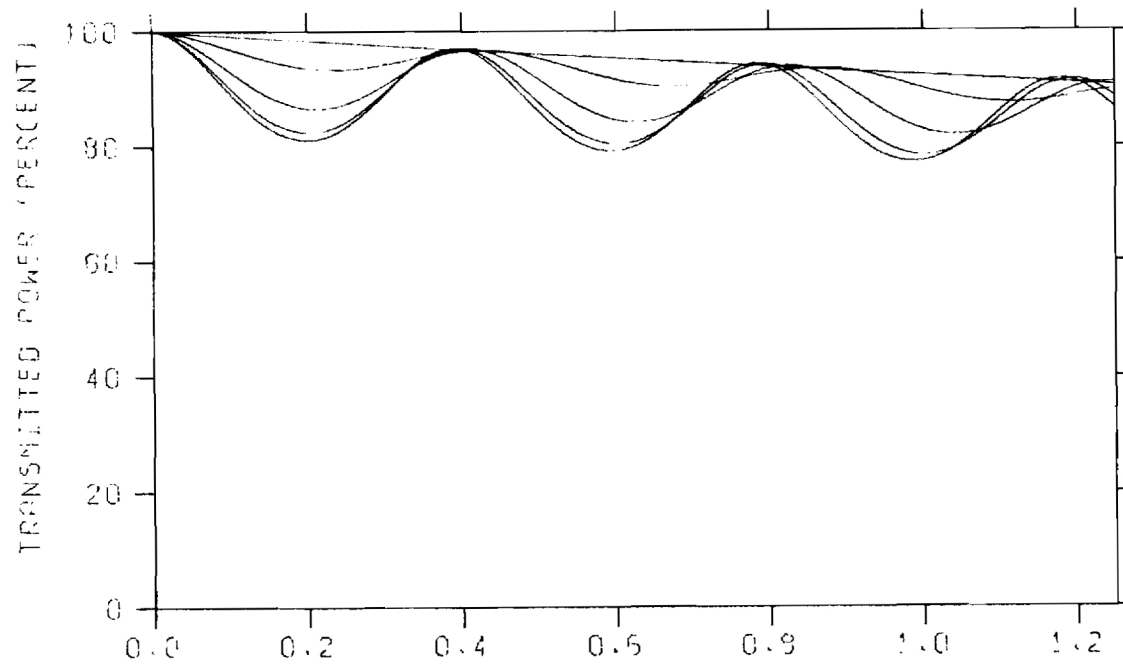SHELL: ER=2.56   TAND=0.0085
CORE: ER=1.07   TAND=0.0002

73

APPENDIX B

ANALYSIS OF CORNER REFLECTOR CLUSTER IN CYLINDRICAL RADOME

This appendix comprises an analysis of the aforementioned corner reflector cluster enclosed by a cylindrical radome to determine the reduction in radar cross section due to the radome. The analysis combines elements of geometrical optics, propagation of plane waves through plane dielectric panels, aperture antenna theory, and polarization properties of antennas to obtain the desired result. The analysis is straightforward, but the geometry of the system introduces considerable tedium into the derivation.

The coordinate systems of interest are shown in Figure B-1. The Cartesian coordinates of a point in the corner reflector system is denoted by (x'', y'', z''). The same point is denoted by (x', y', z') in the buoy coordinate system, and by (x, y, z) in the reference coordinate system where the xy-plane is parallel to the sea surface. The outer surface of the cylindrical buoy of outer radius ρ_1' is specified by

$$x'^2 + y'^2 = \rho_1'^2 \tag{B-1}$$

It is noted that the primed and double-primed coordinate systems are obtained from the unprimed reference system by a simple rotation without translation. The origins of all three systems coincide.

The orientation of the buoy with respect to the sea surface is specified by the nine direction angles illustrated in Figure B2, only six of which are independent. Let the 3 x 3 matrix of direction cosines be defined by

$$\left[\gamma_{ij}\right] \triangleq \begin{bmatrix} \cos \alpha_1 & \cos \beta_1 & \cos \gamma_1 \\ \cos \alpha_2 & \cos \beta_2 & \cos \gamma_2 \\ \cos \alpha_3 & \cos \beta_3 & \cos \gamma_3 \end{bmatrix} \tag{B-2}$$
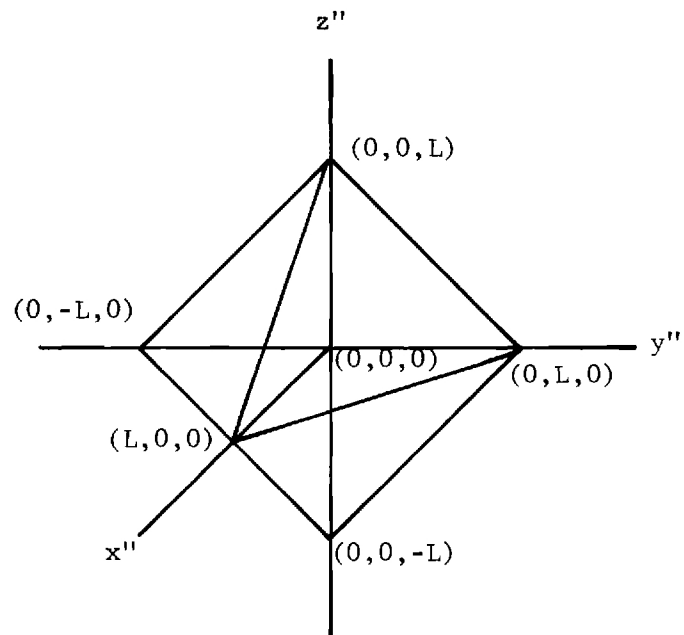
(a) Coordinate System for Corner Reflector Cluster
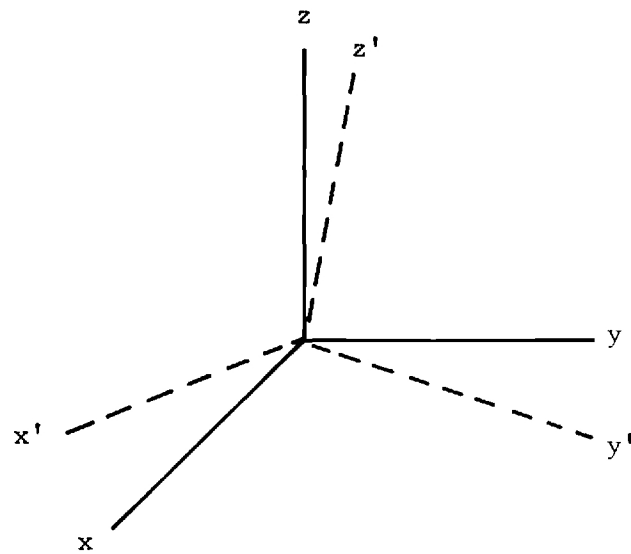
(b) Coordinate Systems for Sea Surface and Buoy

Figure B-1. Coordinate Systems of Interest.
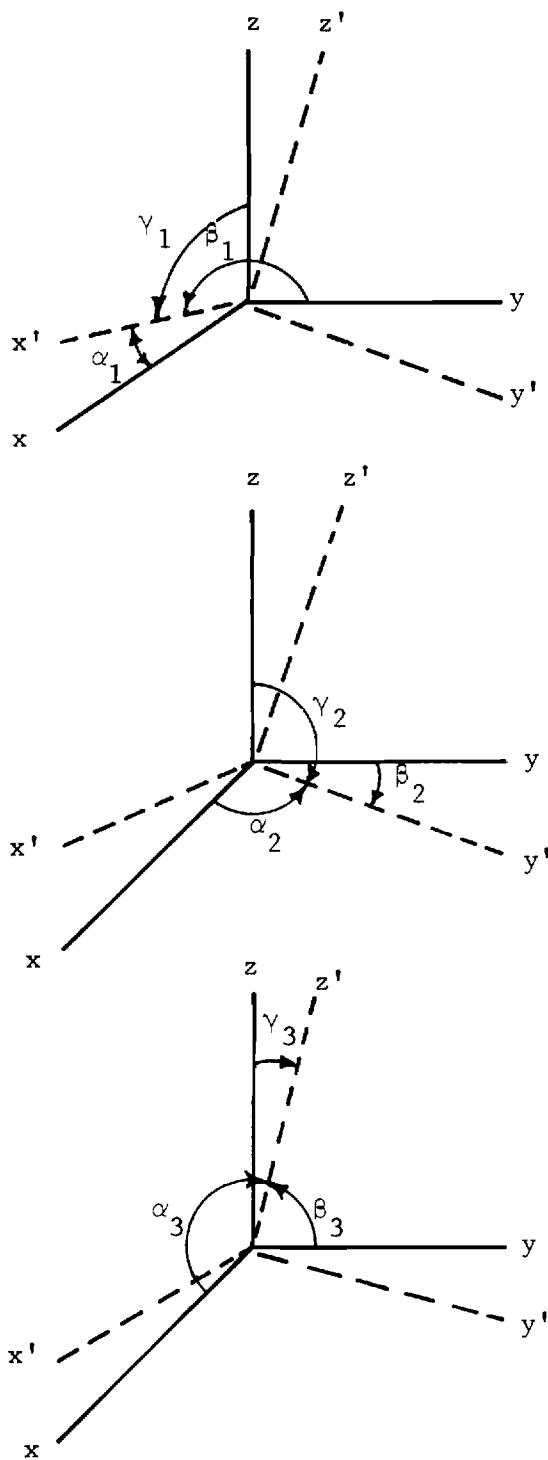
Figure B-2. Rotation of Coordinate Systems Showing
Direction Angles.

Then coordinate transformations between the primed and unprimed systems may be conveniently carried out using matrix algebra as follows where $\begin{bmatrix} & \end{bmatrix}^T$ denotes transpose:

$$\begin{bmatrix} x' \\ y' \\ z' \end{bmatrix} = \begin{bmatrix} \gamma_{ij} \end{bmatrix} \begin{bmatrix} x \\ y \\ z \end{bmatrix} \qquad (B-3)$$

$$\begin{bmatrix} x \\ y \\ z \end{bmatrix} = \begin{bmatrix} \gamma_{ij} \end{bmatrix}^T \begin{bmatrix} x' \\ y' \\ z' \end{bmatrix} \qquad (B-4)$$

Furthermore, if $(\hat{x},\hat{y},\hat{z})$ and $(\hat{x}',\hat{y}',\hat{z}')$ denote the unit vectors in the two systems, then the components of a vector

$$\underline{F} = \hat{x}F_x + \hat{y}F_y + \hat{z}F_z = \hat{x}'F_{x'} + \hat{y}'F_{y'} + \hat{z}'F_{z'} \qquad (B-5)$$

obey the transformation rules below:

$$\begin{bmatrix} F_{x'} \\ F_{y'} \\ F_{z'} \end{bmatrix} = \begin{bmatrix} \gamma_{ij} \end{bmatrix} \begin{bmatrix} F_x \\ F_y \\ F_z \end{bmatrix} \qquad (B-6)$$

$$\begin{bmatrix} F_x \\ F_y \\ F_z \end{bmatrix} = \begin{bmatrix} \gamma_{ij} \end{bmatrix}^T \begin{bmatrix} F_{x'} \\ F_{y'} \\ F_{z'} \end{bmatrix} \qquad (B-7)$$

The orientation of the corner reflector cluster in the cylindrical buoy is specified by the matrix of direction cosines

$$\left[\gamma'_{ij}\right] = \begin{bmatrix} \cos \alpha'_1 & \cos \beta'_1 & \cos \gamma'_1 \\ \cos \alpha'_2 & \cos \beta'_2 & \cos \gamma'_2 \\ \cos \alpha'_3 & \cos \beta'_3 & \cos \gamma'_3 \end{bmatrix} = \begin{bmatrix} \sqrt{1/2} & \sqrt{1/6} & -\sqrt{1/3} \\ -\sqrt{1/2} & \sqrt{1/6} & -\sqrt{1/3} \\ 0 & \sqrt{2/3} & \sqrt{1/3} \end{bmatrix} \qquad \text{(B-8)}$$

where the primed direction angles α'_1, β'_1, etc., define the rotation of the double-primed system with respect to the primed system of coordinates. Transformations between these two systems follow the rules given by Equations (B-3) through (B-7) when a prime is added throughout to the symbols shown there. Transformations between the unprimed system and the double-primed system obey the following rules:

$$\begin{bmatrix} x'' \\ y'' \\ z'' \end{bmatrix} = \left[\gamma'_{ij}\right] \left[\gamma_{ij}\right] \begin{bmatrix} x \\ y \\ z \end{bmatrix} \qquad \text{(B-9)}$$

$$\begin{bmatrix} x \\ y \\ z \end{bmatrix} = \left[\gamma_{ij}\right]^T \left[\gamma'_{ij}\right]^T \begin{bmatrix} x'' \\ y'' \\ z'' \end{bmatrix} \qquad \text{(B-10)}$$

The length L defined in Figure B1 is given by $L = (2\rho'_1 \sin(\frac{\pi}{3}))/\sqrt{2}$) in order for the cluster to fit snugly inside the cylindrical radome shell.

Let a monochromatic, linearly polarized, uniform plane wave traveling in the -x direction with phase constant $k_o = 2\pi/\lambda_o$ be incident on the cylindrical buoy. Such a wave is specified by

$$\underline{E}_i = \hat{y} E_o e^{+jk_o x} \qquad \text{(B-11)}$$

Further, let the direction angles α_1, β_1, etc. be chosen so that the x-axis is oriented in the quadrant of the double-primed system specified by $x'' \geqq 0$, $y'' \geqq 0$. Other orientations of the buoy in the reference system need not be considered since those orientations will produce duplications of the situations specified here.

78

First consider the retro-reflector action of the corner reflector cluster when no radome is present; i.e., when the cylindrical buoy shell is removed. Represent the incident plane wave as a system of parallel rays directed in the $-\hat{x}$ direction. For all practical purposes, only those rays which experience a "three-bounce" reflection will contribute to the radar cross-section of the cluster since it is these rays which are redirected along the $+\hat{x}$ direction; other rays either pass by the cluster with no contact or are scattered in directions other than the $+\hat{x}$ direction. The corner reflector cluster may be replaced then by an equivalent planar reflector which is oriented normal to the incident rays, the size and shape of which depends on the orientation and size of the cluster itself. Call the equivalent planar reflector the "active area" of the cluster. Note that since the incoming rays are $-\hat{x}$ directed, the active area is a planar region lying in the yz-plane.

It is a property of the corner reflector cluster that all retro-reflected rays travel the same distance while undergoing the three-bounce reflection. To clarify this statement, consider a plane erected at $x = x_0 > L$. An incident ray penetrating this plane at (x_0, y, z) is retro-reflected by the cluster and produces a reflected ray penetrating the plane at $(x_0, -y, -z)$. The distance traveled by this ray while going from (x_0, y, z) to $(x_0, -y, -z)$ is equal to the distance traveled by another ray going from (x_0, y_1, z_1) to $(x_0, -y_1, -z_1)$ via the three-bounce reflection of the cluster. This is true for all points (x_0, y_1, z_1) lying in the active area of the cluster. Hence, all retro-reflected rays arrive in phase on the plane $x = x_0$. The distance traveled by the ray which strikes the vertex of the cluster is clearly $2x_0$; hence, all retro-reflected rays travel a distance $2x_0$. These properties will be exploited below when the radome is placed over the cluster and the intervening void filled with a low dielectric foam material. In the latter case, the rays will travel the same physical distance but not the same electrical distance, and the retro-reflected rays will not arrive in phase on the plane $x = x_0$.

In general, the active area is a six-sided plane figure lying in the yz-plane. The vertices of the figure are found in the following way. First,

compute the direction cosines $(k_{x''}, k_{y''}, k_{z''})$ of the propagation vector, $\hat{k} = -\hat{x}$, in the double-primed coordinate system:

$$\begin{bmatrix} k_{x''} \\ k_{y''} \\ k_{z''} \end{bmatrix} = \begin{bmatrix} \gamma'_{ij} \end{bmatrix} \begin{bmatrix} \gamma_{ij} \end{bmatrix} \begin{bmatrix} -1 \\ 0 \\ 0 \end{bmatrix} \qquad \text{(B-12a)}$$

$$\hat{k} = -\hat{x} = \hat{x}''k_{x''} + \hat{y}''k_{y''} + \hat{z}''k_{z''} \qquad \text{(B-12b)}$$

Note that these direction cosines must all be negative for the three-bounce condition to hold. Next, compute the quantity

$$z''_1 = L \frac{-2k_{z''}}{k_{x''} + k_{y''} + k_{z''}} \qquad \text{(B-13)}$$

If $|z''_1| < L$, the figure is truly six-sided; if $|z''_1| \geqq L$, the six-sided figure degenerates into a four-sided figure. For notational convenience, let

$$A = k_{x''} \qquad \text{(B-14a)}$$

$$B = k_{y''} \qquad \text{(B-14b)}$$

$$C = k_{z''} \qquad \text{(B-14c)}$$

The vertices of the six-sided figure in the yz-plane are located at $(\pm y_i, \pm z_i)$, $i = 1,2,3$; the projections of these vertices onto the y''z''-plane are given by (letting SUM = A + B + C),

$$y''_1 = L \frac{C - A - B}{SUM} \quad , \qquad z''_1 = L \frac{-2C}{SUM} \qquad \text{(B-15a)}$$

$$y''_2 = L \frac{B}{A} \frac{A + B - C}{SUM} \quad , \qquad z''_2 = L \frac{C}{A} \frac{B - A - C}{SUM} \qquad \text{(B-15b)}$$

$$y''_3 = L \frac{-2B}{SUM} \quad , \qquad z''_3 = L \frac{B - A - C}{SUM} \qquad \text{(B-15c)}$$

80

If the figure is really four-sided, the vertices are located at $(\pm y_i, \pm z_i)$, $i = 1,2$; the projections of these vertices onto the $y''z''$-plane are given by

$$y''_1 = 0 \qquad , \qquad z''_1 = L \qquad \text{(B-16a)}$$

$$y''_2 = L \frac{2B}{SUM} \qquad , \qquad z''_2 = L \frac{A + C - B}{SUM} \qquad \text{(B-16b)}$$

The vertices of the figure in the yz-plane are then given by

$$\begin{bmatrix} x_i \\ y_i \\ z_i \end{bmatrix} = \left[\gamma_{jk} \right]^T \left[\gamma'_{jk} \right]^T \begin{bmatrix} 0 \\ y''_i \\ z''_i \end{bmatrix} \qquad \text{(B-17)}$$

where $i = 1,2,3$ for the six-sided figure (Equations (B-15) and $i = 1,2$ for the four-sided figure (Equation (B-16)).

The active area of the corner reflector cluster may be considered as a planar aperture antenna which radiates into the hemisphere $x > 0$. For no radome present, the field at all points in the aperture is $\hat{y}$-polarized and in phase. The far-zone field has maximum amplitude on the x-axis. The power received by the y-polarized ship antenna which originally transmitted the incident plane wave is given by

$$P_r = \left| C_1 \iint_S E_{y_{ap}} (0,y,z) dy dz \right|^2 \qquad \text{(B-18)}$$

where C_1 is a complex constant and $"| \quad |"$ denotes magnitude or absolute value. Equation (B-18) could be used to obtain a measure of the radar cross-section of the cluster; however, it will be used below to obtain a measure of the reduction in radar cross-section of the cluster due to the radome.

The effects of the radome on the retro-reflector action of the corner reflector cluster are such as to introduce phase and amplitude perturbations into the aperture field. Absorption losses in the thin outer cylindrical shell and in the low-dielectric constant foam core reduce the amplitude of the aperture field at various points in the active area. Reflections occurring at the air-dielectric interface (outer surface of the cylindrical shell) have the same effect. Phase perturbations in the aperture arise from the different electrical path lengths traveled by the incident rays in the core material and from the fact that the insertion phase delays of the parallel and perpendicular components of the incident wave are different in traversing the thin outer shell. This second effect also produces some depolarization of the incident wave so that the resulting aperture field has both y and z components. Note, however, that it is only the y-polarized component which contributes to the power received by the y-polarized (horizontal polarized) ship antenna.

To obtain a quantitative measure of the effects of the cylindrical shell and low dielectric constant foam core, the situation depicted in Figure B-3 is used. For simplicity, the buoy is shown tilted in the xz-plane, and the cross section is taken in a plane $y = y_0$ such that y_0 is greater than zero, yet not so large as to lie outside the active area. The planes x = X1MAX, x = X2MIN are used as reference planes. The incident plane wave is represented as a system of parallel rays. A typical ray is shown piercing the plane x = X1MAX at the point P_1. Taking this plane as the phase reference, the plane wave associated with this ray is given by

$$\underline{E}_i(P_1) = \hat{y}E_0 \quad , \quad E_0 \text{ real} \tag{B-19}$$

The effects of the shell and core on the field associated with the incident ray will now be obtained. The incident ray pierces the plane x = X1MAX at the point $P_1(\text{X1MAX}, y_0, z_0)$ and travels a distance (X1MAX - x_1) to the point $P_2(x_1, y_0, z_0)$ where it impinges on the outer surface of the shell. At this point, the field incident on the shell is given by
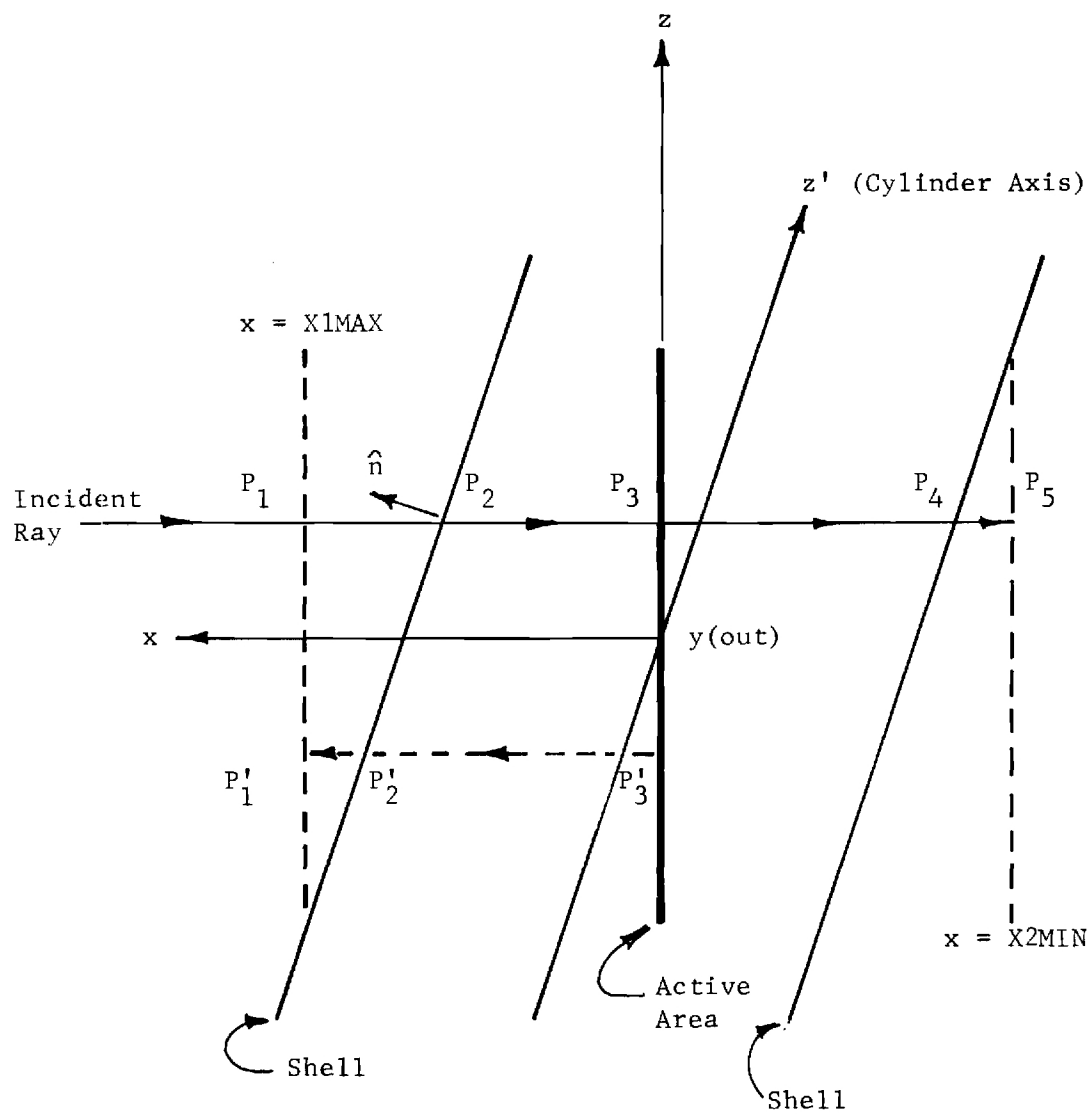
Figure B-3.   Cross Section of Cylindrical Shell.

$$E_i(P_2) = \hat{y}E_0 e^{-jk_0(X1MAX - x_1)} = \hat{y}E_0 e^{-j\Phi_1} \qquad (B\text{-}20)$$

The unit vector, $\hat{n}$, normal to the shell at P_2 and the unit vector, $\hat{x}$, define the plane of incidence and angle of incidence of the plane wave at P_2. The incident field at P_2 is resolved into two components: a component perpendicular to the plane of incidence and a component parallel to the plane of incidence; viz.,

$$E_i(P_2) = \hat{y}E_0 e^{-jk_0(X1MAX - x_1)} = \hat{a}_{\perp} E_{\perp}(P_2) + \hat{a}_{\parallel} E_{\parallel}(P_2) \qquad (B\text{-}21a)$$

$$E_i(P_2) = \hat{a}_{\perp} E_0 e^{-j\Phi_1} \sin \alpha p + \hat{a}_{\parallel} E_0 e^{-j\Phi_1} \cos \alpha p \qquad (B\text{-}21b)$$

where αp is the angle between the plane of incidence and $E_i(P_2)$, and $\hat{a}_{\perp}$, $\hat{a}_{\parallel}$ denote unit vectors perpendicular and parallel to the plane of incidence, respectively. Note that $(\hat{x}, \hat{a}_{\parallel}, \hat{a}_{\perp})$ are mutually orthogonal unit vectors. The field on the inner surface of the thin shell is given by

$$E(P_2) = E_0 e^{-j\Phi_1}(\hat{a}_{\perp} T_{\perp} \sin \alpha p + \hat{a}_{\parallel} T_{\parallel} \cos \alpha p) \qquad (B\text{-}22)$$

where $T_{\perp}$, $T_{\parallel}$ are the complex voltage transmission coefficients for a plane dielectric panel whose thickness and electrical properties are the same as those for the shell at P_2.

Once inside the shell, the ray travels in the core medium and undergoes a three-bounce reflection and emerges on the $x = X1MAX$ plane at the point $P_1(X1MAX, -y_0, -z_0)$. It can be shown that the path of the ray in going from P_2 to P_1' via the three-bounce reflection is the same as the ray path from P_2 to P_5 on the $x = X2MIN$ plane. Thus, at P_1' or at P_5, the field is

$$E(P_5) = E_0 e^{-j\Phi_1}(\hat{a}_{\perp} T_{\perp}^2 \sin \alpha p + \hat{a}_{\parallel} T_{\parallel}^2 \cos \alpha p) e^{-\Phi_2} e^{-j\Phi_3} \qquad (B\text{-}23)$$

where

$$\Phi_2 = (\alpha + j\beta)(x_1 - x_2) \tag{B-24}$$

$$\Phi_3 = k_0(x_2 - X2MIN) \tag{B-25}$$

The distance $(x_1 - x_2)$ is the distance from $P_2(x_1, y_0, z_0)$ to $P_4(x_2, y_0, z_0)$; α and β are the attenuation and phase constants associated with the (lossy) core dielectric given by

$$\begin{Bmatrix} \alpha \\ \beta \end{Bmatrix} = \frac{k_0}{\sqrt{2}} \sqrt{\sqrt{\epsilon_{rc}^2 - (\epsilon_{rc} \tan \delta_c)^2} \mp \epsilon_{rc}} \tag{B-26}$$

where ϵ_{rc}, $\tan \delta_c$ are the relative dielectric constant and loss tangent of the core material. It is noted that the transmission coefficients and geometry at P_4 are identical to those at P_2 so that the transmission coefficients are squared in Equation (B-23).

Equation (B-23) represents the aperture electric field at the point P_5 in the aperture. Because of the depolarization effect of the shell, the electric field at P_5 has a y-component and a z-component. Let

$$\Psi = j\Phi_1 + \Phi_2 + j\Phi_3 \tag{B-27a}$$

$$\hat{n} = \hat{x}n_x + \hat{y}n_y + \hat{z}n_z \tag{B-27b}$$

Then, the two components of the aperture field at P_5 are given by

$$E_y' = \frac{E_0 e^{-\Psi}}{n_y^2 + n_z^2} \left[n_z^2 T_-^2 + n_y^2 T_\perp^2 \right] \tag{B-28a}$$

$$E_z' = \frac{E_0 e^{-\Psi}}{n_y^2 + n_z^2} \left[- n_y n_z T_\perp^2 + n_y n_z T_\perp^2 \right] \tag{B-28b}$$

where the primes denote the aperture field with the radome present.

The power received by the y-polarized ship antenna is proportional to

$$P_r' = \left| C_1 \iint_S E_y' \ (X2MIN,y,z) dydz \right|^2 \tag{B-29}$$

where the integrand is given by Equation (B-28a) evaluated at each point $(0,y,z)$ in the active area. The ratio of the power received when the radome is present and the power received when the radome is removed gives a measure of the reduction, p_H, in the radar cross section of the corner reflector cluster, i.e.,

$$p_H = \frac{P_r'}{P_r} = \frac{\left| \iint_S \dfrac{(n_z^2 T^2 + n_y^2 T^2) e^{-\Psi}}{n_y^2 + n_z^2} dydz \right|^2}{\left| \iint_S dydz \right|^2} \tag{B-30}$$

where the subscript H denotes the case of a horizontally polarized ship antenna. A similar analysis shows that the reduction is radar cross section for a vertically polarized ship antenna is given by

$$p_V = \frac{\left| \iint_S \dfrac{(n_y^2 T^2 + n_z^2 T^2) e^{-\Psi}}{n_y^2 + n_z^2} dydz \right|^2}{\left| \iint_S dydz \right|^2} \tag{B-31}$$

To complete the analysis, the expressions for $\hat{n}$, x_1, and x_2 must be specified as functions of known quantities. For a point $(0,y_0,z_0)$ in the active area, x_1 and x_2 are given by

$$x_1 = \frac{-B + \sqrt{B^2 - 4AC}}{2A} \tag{B-32a}$$

86

$$x_2 = \frac{-B - \sqrt{B^2 - 4AC}}{2A} \qquad \text{(B-32b)}$$

where

$$A = \cos^2 \alpha_1 + \cos^2 \alpha_2 \qquad \text{(B-33a)}$$

$$B = 2y_0(\cos \alpha_1 \cos \beta_1 + \cos \alpha_2 \cos \beta_2) + 2z_0(\cos \alpha_1 \cos \gamma_1 + \cos \alpha_2 \cos \gamma_2) \qquad \text{(B-33b)}$$

$$C = (y_0 \cos \beta_1 + z_0 \cos \gamma_1)^2 + (y_0 \cos \beta_2 + z_0 \cos \gamma_2)^2 - \rho_i'^2 \qquad \text{(B-33c)}$$

The components (n_x, n_y, n_z) of the unit vector $\hat{n}$ are found through the following computations:

$$A = x_1 \cos \alpha_1 + y_0 \cos \beta_1 + z_0 \cos \gamma_1 \qquad \text{(B-34a)}$$

$$B = x_1 \cos \alpha_2 + y_0 \cos \beta_2 + z_0 \cos \gamma_2 \qquad \text{(B-34b)}$$

$$\frac{\partial f}{\partial x} = 2A\cos \alpha_1 + 2B\cos \alpha_2 \qquad \text{(B-34c)}$$

$$\frac{\partial f}{\partial y} = 2A\cos \beta_1 + 2B\cos \beta_2 \qquad \text{(B-34d)}$$

$$\frac{\partial f}{\partial z} = 2A\cos \gamma_1 + 2B\cos \gamma_2 \qquad \text{(B-34e)}$$

$$\text{RAD} = \sqrt{\left(\frac{\partial f}{\partial x}\right)^2 + \left(\frac{\partial f}{\partial y}\right)^2 + \left(\frac{\partial f}{\partial z}\right)^2} \qquad \text{(B-34f)}$$

$$\hat{n} = \frac{1}{\text{RAD}} \left[\hat{x} \frac{\partial f}{\partial x} + \hat{y}\frac{\partial f}{\partial y} + \hat{z}\frac{\partial f}{\partial z} \right] = \hat{x}n_x + \hat{y}n_y + \hat{z}n_z \qquad \text{(B-34g)}$$

The angle of incidence of the plane wave at the point $P_2(x_1, y_0, z_0)$ is given by

$$\theta_i = \cos^{-1}(n_x) = \cos^{-1}(\hat{n} \cdot \hat{x}) \qquad \text{(B-35)}$$

The unit vectors $\hat{a}_\perp$ and $\hat{a}_\parallel$ are given by

$$\hat{a}_\perp = \frac{\hat{n} \times \hat{x}}{|\hat{n} \times \hat{x}|} = \frac{\hat{y}n_z - \hat{z}n_y}{\sqrt{n_y^2 + n_z^2}} \qquad (B\text{-}36a)$$

$$\hat{a}_\parallel = \frac{\hat{a}_\perp \times \hat{x}}{|\hat{a}_\perp \times \hat{x}|} = \frac{-\hat{y}n_y - \hat{z}n_z}{\sqrt{n_y^2 + n_z^2}} \qquad (B\text{-}36b)$$

where "X" denotes vector cross product and "$|\ \ |$" denotes vector magnitude.

For comparison purposes, the reduction in radar cross section due to a flat dielectric panel placed parallel to the active area so that all incident rays are normally incident on the panel is of interest. The thickness and electrical properties of this flat panel are identical to those of the cylindrical shell. In this case, $T_\perp = T_\parallel$ so there is no depolarization of the incident wave; in addition, the effects of the core dielectric are ignored. Each ray is thus weighted by the square of the one-way complex transmission coefficient, $T_\perp (= T_\parallel)$, of the panel that the reduction in radar cross section is given by

$$P_0 = \frac{\left| \iint_S T_\perp^2 dydz \right|^2}{\left| \iint_S dydz \right|^2} = \left| T_\perp \right|^4 \qquad (B\text{-}37)$$

This parameter is of interest because it may give a good measure of the reduction in radar cross section due to the radome without having to go through the rather lengthy computations involved in the complete analysis which accounts for the geometry of the problem. It is noted that the quantity $|T_\perp|$ is derivable from the graphs of Appendix A for a number of dielectric constants, loss tangents and range of thicknesses (see Chapter III). Equation (B-37) applies to the case of a panel with air on both sides. For the radome composite of a panel with foam core on one side, see Chapter III.

DOCUMENT CONTROL DATA - R&D

(Security classification of title, body of abstract and indexing annotation must be entered when the overall report is classified)

1. ORIGINATING ACTIVITY (Corporate author)	2a. REPORT SECURITY CLASSIFICATION
Engineering Experiment Station Georgia Institute of Technology	Unclassified
	2b. GROUP

3. REPORT TITLE

ELECTRICAL DESIGN DATA FOR NAVIGATION BUOYS

4. DESCRIPTIVE NOTES *(Type of report and inclusive dates)*

Technical Report No. 2

5. AUTHOR(S) *(Last name, first name, initial)*

Huddleston, Gene K.
Rivers, Wayne

6. REPORT DATE	7a. TOTAL NO. OF PAGES	7b. NO. OF REFS
15 June 1971	88	6

8a. CONTRACT OR GRANT NO. DOT-CG-10657	9a. ORIGINATOR'S REPORT NUMBER(S) A-1277-TR-2
b. PROJECT NO.	
c.	9b. OTHER REPORT NO(S) *(Any other numbers that may be assigned this report)*
d.	

10. AVAILABILITY/LIMITATION NOTICES

11. SUPPLEMENTARY NOTES	12. SPONSORING MILITARY ACTIVITY
Georgia Tech Project A-1277	U.S. Coast Guard Headquarters

13. ABSTRACT

The electrical design of plastic buoys containing passive radar reflectors for use in radar navigation is discussed. The specific buoy configuration considered consists of a cylindrical homogeneous wall of uniform thickness (Radome) enclosing an octahedral radar reflector with the internal space filled with a low-density dielectric foam. Design data are presented to aid in the determination of optimum wall thicknesses and thickness tolerance for a number of candidate buoy wall materials. Computed performance data showing the reduction in radar cross section of the enclosed reflector due to the radome and filling for three orientations of the buoy are presented. A simplified flat-panel model of the radome/reflector system is developed which predicts with acceptable accuracy the wall transmission loss as a function of thickness and dielectric properties of the materials.

DD FORM 1 JAN 64 **1473**

/ £

14. KEY WORDS	LINK A		LINK B		LINK C	
	ROLE	WT	ROLE	WT	ROLE	WT
Design	2,8					
Navigation Aid	4					
Radar	4					
Plastics	9					
Radome	10					
Buoy	10					

INSTRUCTIONS

1. ORIGINATING ACTIVITY: Enter the name and address of the contractor, subcontractor, grantee, Department of Defense activity or other organization (corporate author) issuing the report.

2a. REPORT SECURITY CLASSIFICATION: Enter the overall security classification of the report. Indicate whether "Restricted Data" is included. Marking is to be in accordance with appropriate security regulations.

2b. GROUP: Automatic downgrading is specified in DoD Directive 5200.10 and Armed Forces Industrial Manual. Enter the group number. Also, when applicable, show that optional markings have been used for Group 3 and Group 4 as authorized.

3. REPORT TITLE: Enter the complete report title in all capital letters. Titles in all cases should be unclassified. If a meaningful title cannot be selected without classification, show title classification in all capitals in parenthesis immediately following the title.

4. DESCRIPTIVE NOTES: If appropriate, enter the type of report, e.g., interim, progress, summary, annual, or final. Give the inclusive dates when a specific reporting period is covered.

5. AUTHOR(S): Enter the name(s) of author(s) as shown on or in the report. Enter last name, first name, middle initial. If military, show rank and branch of service. The name of the principal author is an absolute minimum requirement.

6. REPORT DATE: Enter the date of the report as day, month, year; or month, year. If more than one date appears on the report, use date of publication.

7a. TOTAL NUMBER OF PAGES: The total page count should follow normal pagination procedures, i.e., enter the number of pages containing information.

7b. NUMBER OF REFERENCES: Enter the total number of references cited in the report.

8a. CONTRACT OR GRANT NUMBER: If appropriate, enter the applicable number of the contract or grant under which the report was written.

8b, 8c, & 8d. PROJECT NUMBER: Enter the appropriate military department identification, such as project number, subproject number, system numbers, task number, etc.

9a. ORIGINATOR'S REPORT NUMBER(S): Enter the official report number by which the document will be identified and controlled by the originating activity. This number must be unique to this report.

9b. OTHER REPORT NUMBER(S): If the report has been assigned any other report numbers (either by the originator or by the sponsor), also enter this number(s).

10. AVAILABILITY/LIMITATION NOTICES: Enter any limitations on further dissemination of the report, other than those imposed by security classification, using standard statements such as:

(1) "Qualified requesters may obtain copies of this report from DDC."

(2) "Foreign announcement and dissemination of this report by DDC is not authorized."

(3) "U. S. Government agencies may obtain copies of this report directly from DDC. Other qualified DDC users shall request through
_____ ."

(4) "U. S. military agencies may obtain copies of this report directly from DDC. Other qualified users shall request through
_____ ."

(5) "All distribution of this report is controlled. Qualified DDC users shall request through
_____ ."

If the report has been furnished to the Office of Technical Services, Department of Commerce, for sale to the public, indicate this fact and enter the price, if known.

11. SUPPLEMENTARY NOTES: Use for additional explanatory notes.

12. SPONSORING MILITARY ACTIVITY: Enter the name of the departmental project office or laboratory sponsoring (paying for) the research and development. Include address.

13. ABSTRACT: Enter an abstract giving a brief and factual summary of the document indicative of the report, even though it may also appear elsewhere in the body of the technical report. If additional space is required, a continuation sheet shall be attached.

It is highly desirable that the abstract of classified reports be unclassified. Each paragraph of the abstract shall end with an indication of the military security classification of the information in the paragraph, represented as (TS), (S), (C), or (U).

There is no limitation on the length of the abstract. However, the suggested length is from 150 to 225 words.

14. KEY WORDS: Key words are technically meaningful terms or short phrases that characterize a report and may be used as index entries for cataloging the report. Key words must be selected so that no security classification is required. Identifiers, such as equipment model designation, trade name, military project code name, geographic location, may be used as key words but will be followed by an indication of technical context. The assignment of links, roles, and weights is optional.

DD FORM 1473 (BACK)
1 JAN 64